An Investigation of the Photochemical and Spectroscopic Properties of Chromium, Molybdenum, Tungsten, and Rhodium Isocyanide Complexes

Thesis by

Kent Robert Mann

In Partial Fulfillment of the Requirements

for the Degree of

Doctor of Philosophy

California Institute of Technology

Pasadena, California

1977

(Submitted September 8, 1976)

ACKNOWLEDGMENT

I wish to acknowledge the help and tolerance of Chris, Harry, George, Nate, Greg, Mike, Bruce, Dave, Bill, Claude, and, aw hell, everybody.

I especially acknowledge the incredible amount of work done by Nate Lewis from whom we may all be taking orders someday.

Harry, I'll get right on it.

ABSTRACT

The X-ray crystal structure of $Cr(CNPh)_6$ has been determined. The complex crystallizes in the space group $R\bar{3}$ with one molecule in the unit cell $a = b = c = 10.628$ Å; $\alpha = \beta = \gamma = 111.17°$; $V = 861.1$ Å^3. The metal atom has crystallographic site symmetry S_6 with the MC_6 framework forming a perfect octahedron. The Cr-C-N bond angles are all 174.7°, the Cr-C bond lengths are 1.933(2) Å, and the C-N bond lengths are 1.168(2) Å.

Both infrared spectra, X-ray crystal structure data, and electronic absorption spectra are consistent with the operation of a second order Jahn Teller distortion of the ground state of $Cr(CNPh)_6$. Data obtained on the sterically hindered systems $Cr(CNDph)_6$ and $Cr(CNIph)_6$ [Dph = 2,6-dimethylphenyl and Iph = 2,6-diisopropylphenyl] also support the operation of a Jahn Teller effect. Similar considerations apply to the Mo and W systems.

The electronic absorption spectra of $M(CNAr)_6$ [M = Cr(0), Mo(0), W(0), Ar = phenyl, ph; 2,6-dimethylphenyl, Dph; and 2,6-diisopropylphenyl, Iph], $Mn(CNPh)_6Cl$ and $[Mn(CNPh)_6](PF_6)_2$ are reported. Each of the $M(CNAr)_6$ complexes exhibits intense allowed metal-to-ligand charge transfer (MLCT) absorption bands between 20.8 and 32.7 kK. The lowest MLCT bands are observed at 29.9 and 31.1 kK in the electronic spectrum of $Mn(CNPh)_6^+$. Low energy bands at 18.2 and 20.4 kK in $[Mn(CNPh)_6]^{2+}$ are assigned to vibronic components of a $\sigma(CNPh) \rightarrow d\pi$ charge transfer transition.

The unique electronic structural properties of arylisocyanide complexes are apparently related to the π conjugation of aromatic ring orbitals with the out-of-plane π^*(CN) function.

The emission and photochemical behavior of $M(CNPh)_6$ and $M(CNIph)_6$ complexes (M = Cr, Mo, W; Ph = phenyl, Iph = 2,6-diisopropylphenyl) has been studied. The complexes of Mo and W show emission attributable to an $L\pi^* \rightarrow d\pi$ process in a variety of solvents (2-methylpentane, 2-MeTHF, benzene, pyridine) at room temperature. Complexes of all three metals show emissions at 77 K in 2-MeTHF that overlap the MLCT absorption bands. The emission quantum yields for $Mo(CNIph)_6$ and $W(CNIph)_6$ in 2-MeTHF at 77 K are 0.78 ± 0.08 and 0.93 ± 0.07, respectively. The emission lifetimes at 77 K in 2-methylpentane for the $M(CNIph)_6$ complexes are: τ(Cr) < 10 nsec, τ(Mo) 40.2 ± 0.5 μsec (298 K, 43 ± 2 nsec), τ(W) 7.6 ± 0.5 μsec (298 K, 83 ± 2 nsec). Both $M(CNPh)_6$ and $M(CNIph)_6$ undergo photosubstitution reactions in pyridine solutions. Formation of $M(CNPh)_5py$ and $M(CNIph)_5py$ occurs upon irradiation at 436 nm, with quantum yields decreasing according to a regular pattern $[Cr(CNPh)_6]$ (0.23) ~ $[Cr(CNIph)_6]$ (0.23) > $[Mo(CNPh)_6]$ (0.055) > $[Mo(CNIph)_6]$ (0.022) > $[W(CNPh)_6]$ (0.011) >> $[W(CNIph)_6]$ (0.0003). The very small quantum yield for photosubstitution in the case of $W(CNIph)_6$ is interpreted as an indication that the mechanism of formation of $W(CNPh)_5py$ has associative character. Irradiation of $M(CNIph)_6$ at 436 nm in $CHCl_3$ yields the one-electron oxidation products $[M(CNIph)_6]Cl$. The quantum yield

in each case is 0.19 ± 0.01. Similar irradiation of $M(CNPh)_6$ in $CHCl_3$ gives two-electron oxidation products. For M = Mo, W, the products are identified as the seven-coordinate species $[M(CNPh)_6Cl]Cl$.

The room temperature UV-VIS solution spectra of $Rh(CNR)_4^+$ [R = aromatic or aliphatic] have been found not to follow Beer's law. This behavior has been attributed to complex oligomerization of the monomeric $Rh(CNR)_4^+$ units to form species of the type $[Rh(CNR)_4^+]_n$ (n = 1, 2, 3). The extinction coefficients and formation constants using the following expressions:

$$M + M \underset{K_1}{\rightleftharpoons} D$$

$$D + M \underset{K_2}{\rightleftharpoons} T$$

have been obtained for the systems R = phenyl in acetonitrile solution; and R = t-butyl in water solution. The values for the parameters used are for R = phenyl, $K_1 = 35\ M^{-1}$, $\epsilon_2 = 10{,}500$, $\epsilon_3 K_2 = 183{,}000\ M^{-1}$; for R = t-butyl, $K_1 = 251\ M^{-1}$, $\epsilon_2 = 16{,}900$.

The nature of the oligomerization is due to a direct metal-metal interaction of the d^8 Rh atoms. The band positions for the oligomeric species were found to conform to predictions made by simple Hückel theory.

The synthesis and characterization of a dimeric Rh(I) complex containing the bridging ligand 1,3-diisocyanopropane(bridge) is reported. In methanol solution, $[Rh_2(bridge)_4]^{2+}$ oligomerizes, and species containing four, six, and eight Rh atoms have been

identified spectroscopically. The dimer, $[Rh_2(bridge)_4]^{2+}$, undergoes two center oxidative addition reactions with I_2, Br_2, and CH_3I. The products, $[Rh_2(bridge)_4X_2]^{2+}$ (X = I, Br) which contain two strongly coupled Rh(II) atoms, possess trans stereochemistry. The mechanism of oxidative addition is thought to involve attack of the Rh(I) on the heavy atom of substrate molecule.

TABLE OF CONTENTS

CHAPTER	TITLE	PAGE
1	Preparation, Structural Characterization and Excited State Properties of Hexa-coordinate Aryl Isocyanide Complexes of Cr(0), Mo(0), and W(0)	1
2	Spectral Characterization of Rh(I) Isocyanide Complexes	169
3	The Preparation, Spectral Properties and Oxidative Addition Reactions of a Dimeric Rh(I) Isocyanide Complex $Rh_2(bridge)_4^{2+}$	197
	Propositions	209

CHAPTER I

PREPARATION, STRUCTURAL CHARACTERIZATION, AND EXCITED STATE PROPERTIES OF HEXACOORDINATE ARYL ISOCYANIDE COMPLEXES OF Cr(0), Mo(0), AND W(0)

Introduction

Surprisingly little is known about the electronic structure and photochemistry of isocyanide complexes, in spite of the strong current interest in the coordination chemistry of isocyanides and the obvious relationship of these ligands to cyanide ion and carbon monoxide.[1-12] Previous theoretical work on isocyanide complexes appears to be limited to a few semi-empirical molecular orbital calculations,[4-8] incomplete electronic spectral data,[4,7-11] and one photochemical study.[13]

The approach used in attacking this area was to obtain an overview of the complexes' electronic structure and to explore the photochemical reactions which were suggested by the nature of the excited states.

Low valent complexes containing only isocyanide ligands of Cr(0), Mo(0), W(0), and Mn(I) and (II) have been known for quite some time.[1] They are usually synthesized from simple metal complexes ($Cr_2(C_2H_3O_2)_4 \cdot 2H_2O$,[14] $Mo_2(C_2H_3O_2)_4$,[15] WCl_6[16], and MnI_2)[17] by addition of the appropriate isocyanide and in some cases a reducing agent such as magnesium. In Malatesta's and Bonati's book[1] and in several more recent reviews, the chemistry of isocyanide complexes of metals is reviewed.[1,3,4]

The $M(CNAr)_6$ complexes (where M = Cr(0), Mo(0), W(0)) are obtained as very thermally stable dark red to orange crystals that are stable to air in the solid state indefinitely (for M = Cr(0)) or for a few days (M = Mo(0) and W(0)). The Mn(I) complexes are air stable, being much more stable than the corresponding Mn(II) complexes

which under proper conditions are spontaneously reduced back to the Mn(I) complexes.[1]

Having low-spin d^6 configurations, one expects that thermal ligand exchange reactions would be rather slow. This is borne out by experiment,[14] the half life for exchange of C^{13} labeled phenyl isocyanide with $Cr(CNPh)_6$ being about 250 hours at 20°C. This rate is slower than the rate for the exchange of $C^{13}O$ with $Cr(CO)_6$.

Early in our work[15] on the electronic structure of $M(CNPh)_6$ complexes (where M = Cr(0), Mo(0), W(0)) it became obvious that an X-ray crystal structure would be needed to clarify the structural ambiguities suggested by the electronic spectra and the $\tilde{\nu}$(CN) region of the infrared spectra.[11,12,18]

X-ray Crystal Structure of $Cr(CNPh)_6$

Experimental Section

Red crystals of $Cr(CNPh)_6$ were obtained by slow cooling of a saturated toluene solution of the complex. The crystals were found to be rhombohedral in shape and of X-ray quality. A crystal, 0.24 mm on an edge, was selected and mounted so the spindle axis was perpendicular to the apparent three-fold symmetry axis of the crystal. Weissenberg photographs initially suggested that the space group was triclinic but a precession photograph showed the three-fold symmetry present in a hexagonal/rhombohedral unit cell. By fitting fifteen observed reflections with the program CELL[19] and examining the data set for absences, the space group was determined to be $[R\bar{3}; 148]$.

Data were collected on a Datex automated General Electric quarter circle diffractometer and the unit cell dimensions were determined by a least squares procedure program[19] using 2θ values measured for sixteen reflections. More information is given in Table 1.

Determination and Refinement of the Structure

Symmetry considerations require that the metal sit on the inversion center of the unit cell. This requires that all six ligands be equivalent. Thus only the positions of nine nonhydrogen atoms needed to be found. The program MULTAN[20] was used to solve the structure using 100 strong reflections.

Least squares[21] refinement of the structure anisotropically for all nine nonhydrogen atoms and isotropically for the five

Table 1. Experimental Data for the X-ray Diffraction Study of $Cr(CNPh)_6$

Space group [$R\bar{3}$; No. 148]

Rhombohedral Cell	Hexagonal Cell
a = b = c, Å 10.628	a = b = 17,535 Å
	c = 9.701 Å
$\alpha = \beta = \gamma$ 111.17°	$\alpha = \beta$ = 90°
	γ = 120°
V, Å^3 861.1	V = 2283.3
z = 1	z = 3

Mol. wt. 670.74

ρ calcd g cm^{-3} 1.294

ρ obsd (floatation in CCl_4/pentane) 1.3.

Radiation graphite-monochromatized MoKα (λ = 0.71069 Å)

Scan mode coupled θ - 2θ.

Scan speed 1°/min.

Range 1.5° < 2θ < 40°.

Background 20 sec at beginning and end of each scan.

Reflections collected: 2354 including equivalent forms to give 750 unique data reflections.

Absorption coeff: μ = 3.90 cm^{-1}.

hydrogen atoms yield R_1 and R_2 of 0.0311 and 0.0311 for $R_1 = \sum ||F_o| - |F_c|| / \sum |F_o|$ and $R_2 = (\sum w(|F_o| - |F_c|)^2 / \sum w|F_o|^2)^{\frac{1}{2}}$. The GOF parameter, GOF $= [\sum w(F_o^2 - F_c^2)^2/(m-s)]^{\frac{1}{2}}$ is 1.5215. A three dimensional difference Fourier synthesis[19] calculated at the conclusion of the refinement indicated no discrepancies greater than $\pm$ 0.21 Å^3.

Discussion

The metal atom sits on a site of S_6 symmetry, allowing a distortion along the three fold crystalographic axis such that the four-fold axis present in an octahedron vanishes. The distortion takes the form of a deviation from linearity of both the M-C-N angle and the C_{iso}-N-C_{ring} angle of about 7°. The two planes defined by these two sets of three atoms however do not coincide, the dihedral angle between the plane normals being 59.15°. The M-C_{iso}-N plane normal also makes an angle of 89.2° with the three fold symmetry axis. This can be visualized easily by taking the $M(CN)_6$ frame work and bending all of the MCN bond angles toward the plane perpendicular to the three fold axis of the complex, reducing the symmetry of the $M(CN)_6$ portion of the molecule from O_h to D_{3d}. Addition of the phenyl rings further reduces the symmetry of the molecule to that of the site symmetry, which is S_6. The phenyl rings are arranged in an almost perfect T_h fashion about the Cr atom. Each ring normal is tipped 6.86° away from one of the two fold axes of a T_h structure while it is nearly perpendicular (88.97°) to the other unique two-fold. (The angle made with the third two-fold is 90° + 6.86° = 96.86°.)

This reduction in the symmetry of the molecule from T_h to S_6 was predicted from the $\bar{\nu}$(CN) stretching region of the infrared spectrum.[15] Infrared data will be discussed in relation to structural considerations in a following section.

The bond lengths and angles are set out in Tables 2 and 3. The metal-carbon bond length of 1.933(2)Å is close to that found in $Cr(CO)_6$ where the M-C bond length is 1.92 ± 0.04Å.[25] The carbon-nitrogen triple bond is 1.168(2)Å which compares favorably to those found in other phenyl isocyanide structures.[26] The six carbon atoms of the phenyl rings form nearly perfect hexagons; the C-C bond lengths being (1.374 ± 0.018 Å); deviations from coplanarity being less than 0.007 Å.

Infrared Spectra

Symmetry considerations suggest that a $M(CN)_6$ fragment having perfect O_h symmetry should give rise to one infrared active T_{1u} $\bar{\nu}$(CN) stretching mode. If, however, one reduces the symmetry to D_{3d} by applying a trigonal distortion to the $M(CN)_6$ fragment, the triply degenerate T_{1u} $\bar{\nu}$(CN) mode is split into a singly degenerate A_{2u} and doubly degenerate E_u mode. Further lowering of the symmetry from D_{3d} to S_6 only changes the appropriate symmetry labels, maintaining the degeneracy of the E_u mode. (The new labels in S_6 are A_u and E_u.) Reduction of the $M(CN)_6$ fragment from O_h to T_h does <u>not</u> split the degeneracy of the triply degenerate T_{1u} $\bar{\nu}$(CN) mode (T_u in T_h). Interestingly, infrared spectra of

Table 2. Bond Distances[a] for $Cr(CNPh)_6$

CR - C(1)	1.933(2)	N - C(1)	1.168(2)
C(2) - C(3)	1.333(2)	C(2) - C(7)	1.384(2)
C(3) - C(4)	1.376(2)	C(3) - H(3)	C.991(16)
C(4) - H(4)	0.975(17)	C(5) - C(6)	1.366(2)
C(5) - H(6)	1.993(22)	C(6) - C(7)	1.386(2)
C(6) - H(7)	1.983(16)	C(7) - H(7)	0.852(16)
N - C(2)	1.381(2)	C(4) - C(5)	1.349(2)
C(2) - H(7)	1.935(16)	C(5) - H(5)	0.979(19)
		C(6) - H(6)	0.925(22)

[a] Numbering system is 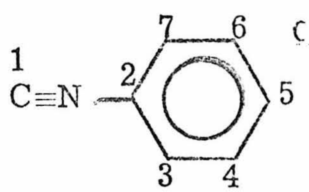

Table 3. Bond Angles[a] for $Cr(CNPh)_6$

CR - C(1) - N	174.73(15)	C(1) - N - C(2)	173.30(17)
N - C(2) - C(7)	121.09(15)	N - C(2) - H(7)	98.20(90)
C(2) - C(3) - H(3)	119.37(95)	C(3) - C(2) - C(7)	119.43(15)
C(2) - C(7) - H(7)	117.94(114)	C(3) - C(2) - H(7)	142.24(51)
C(3) - C(4) - C(5)	120.84(17)	C(3) - C(4) - H(4)	119.54(102)
C(4) - C(5) - C(6)	119.97(18)	C(4) - C(5) - H(5)	119.36(112)
C(5) - C(4) - H(4)	119.60(103)	C(5) - C(6) - C(7)	120.79(19)
C(5) - C(6) - H(7)	141.86(51)	C(6) - C(5) - H(5)	120.67(112)
C(6) - C(7) - H(7)	122.98(115)	C(7) - C(6) - H(6)	119.48(140)
N - C(2) - C(3)	119.45(14)	C(4) - C(5) - H(6)	143.69(66)
C(2) - C(3) - C(4)	119.91(15)	C(5) - C(6) - H(6)	119.60(140)
C(2) - C(7) - C(6)	119.04(17)	H(5) - C(5) - H(6)	96.93(129)
C(2) - H(7) - C(6)	75.07(60)	H(6) - C(6) - H(7)	98.37(148)
C(4) - C(3) - H(3)	120.44(95)		

[a] Number system is the same as for Table 2.

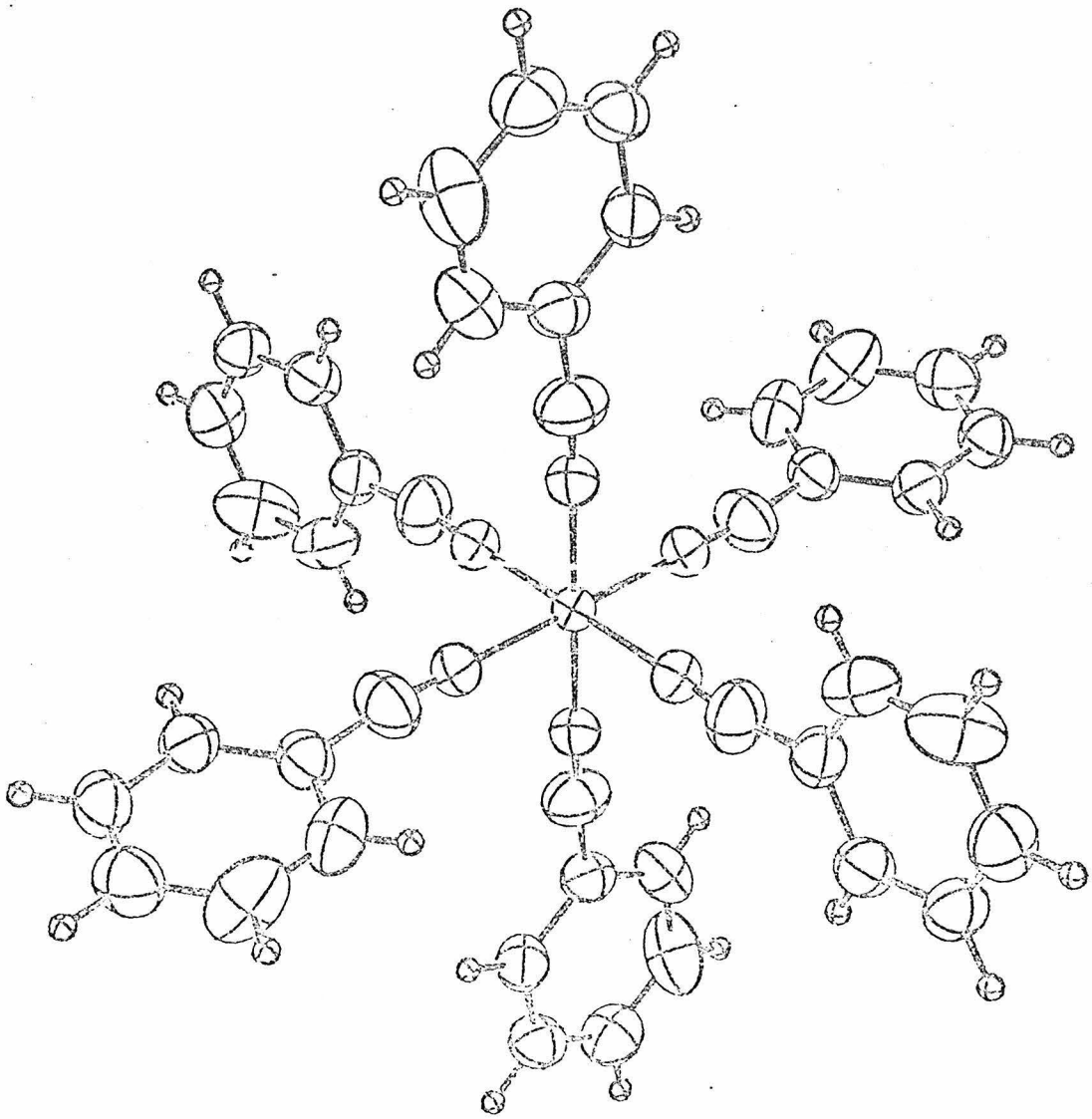

Figure 1. View of $Cr(CNPh)_6$ down the three-fold axis.

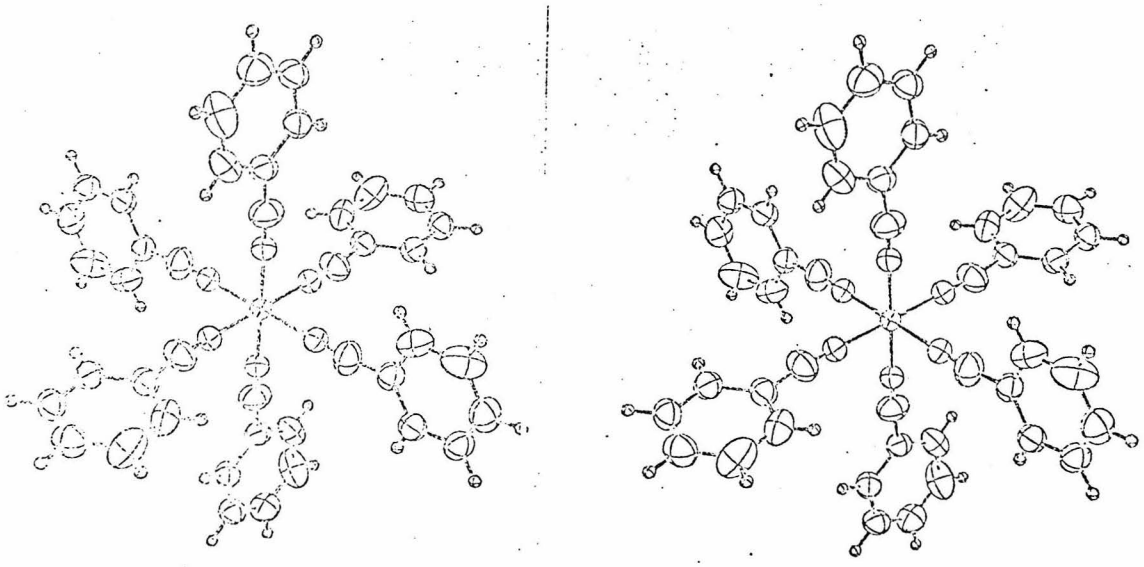

Figure 2. Stereoscopic view of $Cr(CNPh)_6$ down the three-fold axis.

Table 4. Atomic Coordinates in Terms of the Rhonbohedral Cell

Atom	X	Y	Z
CR	0.0 (30)	0.0 (28)	0.0 (28)
N	0.11769(30)	0.36113(28)	0.13648(28)
C(1)	0.06658(30)	0.22274(32)	0.07850(29)
C(2)	0.17730(32)	0.52185(30)	0.18869(29)
C(3)	0.07736(34)	0.57660(32)	0.18972(32)
C(4)	0.13269(36)	0.73416(32)	0.23257(32)
C(5)	0.28450(40)	0.83731(37)	0.27768(36)
C(6)	0.38540(41)	0.78570(41)	0.28009(40)
C(7)	0.33383(37)	0.62785(39)	0.23670(36)
H(3)	-0.03733(321)	0.49852(307)	0.14650(298)
H(4)	0.06022(339)	0.77079(335)	0.22839(328)
H(5)	0.32070(356)	0.94843(388)	0.30721(354)
H(6)	0.49175(441)	0.85893(426)	0.31772(409)
H(7)	0.39543(329)	0.59359(321)	0.24155(317)

Table 5. Atomic Coordinates in Terms of the Hexagonal Cell

Atom		X	Y	Z
COORD CR	CR	0.0	0.0	0.0
COORD N	N'	-0.087410	0.068620	0.205100
COORD C(1)	C'	-0.056027	0.044107	0.122607
COORD C(2)	C'	-0.118647	0.107257	0.295947
COORD C(3)	C'	-0.203533	0.092173	0.280893
COORD C(4)	C'	-0.233783	0.133903	0.366473
COORD C(5)	C'	-0.181997	0.188816	0.466496
COORD C(6)	C'	-0.098330	0.203640	0.483730
COORD C(7)	C'	-0.065630	0.162760	0.399460
COORD H(3)	HS	-0.239893	0.056063	0.202563
COORD H(4)	HS	-0.292913	0.124743	0.353133
COORD H(5)	HS	-0.204747	0.218237	0.525447
COORD H(6)	HS	-0.064383	0.238413	0.556133
COORD H(7)	HS	-0.014760	0.168640	0.410190

Table 6. Final Thermal Parameters for $Cr(CNPh)_6$

Atom	β_{11}	β_{22}	β_{33}	β_{12}	β_{13}	β_{23}
ANISO[a] CR	0.0026267	0.0026267	0.0108033	0.0026267	0.0	0.0
ANISO N	0.0062633	0.0061600	0.0150733	0.0084267	0.0049933	0.0015533
ANISO C(1)	0.0035011	0.0036578	0.0134044	0.0037511	-0.0000956	0.0015822
ANISO C(2)	0.0045433	0.0045267	0.0111133	0.0050600	0.0027133	0.0021400
ANISO C(3)	0.0043289	0.0043189	0.0114389	0.0038822	0.0008022	-0.0008022
ANISO C(4)	0.0046144	0.0053244	0.0124411	0.0055111	0.0030844	0.0017356
ANISO C(5)	0.0067489	0.0058222	0.0133789	0.0066489	0.0034022	-0.0009889
ANISO C(6)	0.0069511	0.0065611	0.0128244	0.0044778	-0.0025356	-0.0051644
ANISO C(7)	0.0040778	0.0070211	0.0143578	0.0051111	-0.0007356	0.0017689

Atom	B
ISO[b] H(3)	2.56851
ISO H(4)	3.764
ISO H(5)	4.4797
ISO H(6)	6.39606
ISO H(7)	3.15154

[a]The form of the anisotropic temperature factor is $\exp[-2\pi^2(h^2a^{*2}\beta_{11} + \ldots + 2Klb^*c^*\beta_{23})]$.

[b]The form of the isotropic temperature factor is of the form $\exp[-B(\sin^2\theta/\lambda^2)]$.

Table 7. Calculated and Observed Structure Factors

H	K	L	FOBS	FCAL	H	K	L	FOBS	FCAL
-13	-2	-5	16.50	15.07	-13	-1	0	43.38	44.06
-13	-3	-4	25.33	25.98	-13	-2	1	41.48	41.28
-13	-4	-3	15.20	14.26	-13	-3	2	10.19	10.53
-14	-1	-4	9.94	8.14	-13	-4	3	20.84	19.99
-14	-2	-3	14.21	11.76	-14	-1	2	24.36	22.59
-14	-3	-2	13.40	14.08	-14	-2	3	20.44	19.92
-15	-1	-2	10.46	10.07	-9	-1	-5	2.74	1.00
-15	-2	-1	14.59	14.20	-9	-2	-4	17.65	18.28
-11	-1	-7	4.46	1.82	-9	-3	-3	26.11	25.70
-11	-2	-6	35.64	36.84	-9	-4	-2	82.89	83.25
-11	-3	-5	17.72	17.59	-9	-5	-1	65.22	66.49
-11	-4	-4	8.08	8.48	-9	-6	0	4.01	3.06
-11	-5	-3	22.48	22.53	-9	-7	1	20.26	19.62
-11	-6	-2	47.56	49.49	-9	-8	2	8.11	7.28
-11	-7	-1	11.61	13.17	-9	-9	3	2.75	4.36
-12	-1	-5	49.00	51.08	-10	-1	-3	29.33	29.54
-12	-2	-4	42.19	42.73	-10	-2	-2	20.15	21.41
-12	-3	-3	29.29	30.52	-10	-3	-1	16.47	16.32
-12	-4	-2	7.83	4.80	-10	-4	0	23.63	23.93
-12	-5	-1	5.84	2.06	-10	-5	1	17.95	17.61
-12	-6	0	14.25	14.13	-10	-6	2	27.02	25.92
-13	-1	-3	0.71	0.70	-10	-7	3	6.16	3.51
-13	-2	-2	24.91	24.95	-11	-1	-1	46.79	44.27
-13	-3	-1	12.42	11.51	-11	-2	0	8.89	7.49
-13	-4	0	3.18	3.03	-11	-3	1	21.05	21.61
-13	-5	1	11.05	10.56	-11	-4	2	11.14	9.69
-14	-1	-1	7.30	9.37	-11	-5	3	7.65	9.02
-14	-2	0	6.97	6.19	-11	-6	4	22.59	23.17
-14	-3	1	3.31	3.85	-12	-1	1	12.08	12.20
-15	-1	1	25.94	25.65	-12	-2	2	39.84	38.39
-10	-1	-6	15.07	13.98	-12	-3	3	39.30	38.46
-10	-2	-5	37.33	38.47	-12	-4	4	4.71	4.24
-10	-3	-4	7.99	7.43	-13	-1	2	16.08	16.24
-10	-4	-3	15.41	13.56	-13	-2	4	35.58	37.22
-10	-5	-2	13.61	12.91	-8	-1	-4	74.14	73.69
-10	-6	-1	9.08	9.54	-8	-2	-3	44.04	42.30
-10	-7	0	1.49	4.40	-8	-3	-2	44.42	44.23
-10	-8	1	2.60	3.85	-8	-4	-1	13.13	12.02
-11	-1	-4	43.57	44.33	-8	-5	0	35.31	34.51
-11	-2	-3	5.75	6.97	-8	-6	1	19.87	19.42
-11	-3	-2	45.57	45.38	-8	-7	2	20.93	20.99
-11	-4	-1	2.16	2.61	-8	-8	3	17.69	17.00
-11	-5	0	35.43	33.51	-8	-9	4	21.44	21.12
-11	-6	1	35.41	33.94	-9	-1	-2	14.88	13.51
-11	-7	2	7.43	9.20	-9	-2	-1	10.18	8.45
-12	-1	-2	3.53	6.67	-9	-3	0	30.29	30.53
-12	-2	-1	13.40	14.07	-9	-4	1	26.09	25.59
-12	-3	0	36.43	35.98	-9	-5	2	28.87	29.32
-12	-4	1	13.33	13.64	-9	-6	3	26.96	26.85
-12	-5	2	35.72	35.08	-9	-7	4	11.80	10.82

H	K	L	FOBS	FCAL
-10	-1	0	34.32	35.25
-10	-2	1	48.45	46.38
-10	-3	2	29.70	29.55
-10	-4	3	35.85	34.00
-10	-5	4	2.69	1.77
-10	-6	5	14.32	14.55
-11	-1	2	29.85	30.72
-11	-2	3	24.04	23.21
-11	-3	4	46.52	46.78
-11	-4	5	6.12	5.91
-12	-1	4	13.85	13.39
-12	-2	5	7.57	9.35
-7	-1	-3	131.95	130.73
-7	-2	-2	66.52	68.80
-7	-3	-1	51.90	53.53
-7	-4	0	41.17	39.41
-7	-5	1	18.65	18.64
-7	-6	2	19.78	20.61
-7	-7	3	3.01	6.12
-7	-8	4	14.34	13.69
-7	-9	5	26.20	25.48
-8	-1	-1	6.44	8.02
-8	-2	0	1.85	0.60
-8	-3	1	31.48	30.74
-8	-4	2	40.92	41.45
-8	-5	3	48,02	49.23
-8	-6	4	7.72	9.37
-8	-7	5	3.23	0.54
-9	-1	1	49.71	51.02
-9	-2	2	24.42	24.28
-9	-3	3	6.20	7.01
-9	-4	4	45.18	45.83
-9	-5	5	12.87	11.97
-9	-6	6	10.33	10.19
-10	-1	3	40.40	40.79
-10	-2	4	8.65	8.27
-10	-3	5	13.56	11.61
-10	-4	6	17.17	17.20
-11	-1	5	26.58	26.51
-11	-2	6	4.58	4.06
-6	-1	-2	21.25	22.34
-6	-2	-1	59.49	57.53
-6	-3	0	55.17	53.99
-6	-4	1	40.64	42.56
-6	-5	2	11.19	10.86
-6	-6	3	21.12	20.16
-6	-7	4	11.74	10.46
-6	-8	5	19.24	19.61
-6	-9	6	8.33	9.18
-7	-1	0	17.17	14.58
-7	-2	1	31.20	26.95
-7	-3	2	50.00	48.75
-7	-4	3	49.22	48.44
-7	-5	4	32.97	32.53
-7	-6	5	3.27	0.93
-7	-7	6	12.40	12.09
-8	-1	2	32.90	33.23
-8	-2	3	35.75	37.28
-8	-3	4	10.19	9.16
-8	-4	5	17.35	16.08
-8	-5	6	22.40	21.36
-9	-1	4	36.93	35.13
-9	-2	5	33.04	33.22
-9	-3	6	6.08	8.59
-9	-4	7	4.03	2.68
-10	-1	6	24.81	24.81
-10	-2	7	4.55	3.61
-3	-3	-3	71.86	72.06
-5	-1	-1	10.33	12.92
-5	-2	0	51.21	52.34
-5	-3	1	48.33	48.67
-5	-4	2	13.70	12.56
-5	-5	3	5.64	2.79
-5	-6	4	32.32	31.93
-5	-7	5	2.20	0.89
-5	-8	6	4.73	3.16
-6	-1	1	23.63	23.72
-6	-2	2	54.44	55.09
-6	-3	3	16.13	18.92
-6	-4	4	6.26	5.08
-6	-5	5	13.34	11.69
-6	-6	6	12.45	11.32
-6	-7	7	34.38	35.19
-7	-1	3	23.37	22.47
-7	-2	4	18.71	20.20
-7	-3	5	50.25	49.80
-7	-4	6	18.47	18.77
-7	-5	7	22.56	23.46
-8	-1	5	8.76	8.39
-8	-2	6	49.78	50.11
-8	-3	7	29.86	29.12
-9	-1	7	23.77	24.60
-9	-2	8	23.09	23.80
-4	-1	0	54.41	53.92
-4	-2	1	34.77	31.43
-4	-3	2	21.90	20.83
-4	-4	3	5.62	7.00
-4	-5	4	34.97	33.97
-4	-6	5	35.11	34.87
-4	-7	6	44.44	43.32

H	K	L	FOBS	FCAL
-4	-8	7	20.15	21.37
-5	-1	2	15.73	13.69
-5	-2	3	75.63	73.81
-5	-3	4	50.32	49.63
-5	-4	5	55.54	56.10
-5	-5	6	21.20	21.72
-5	-6	7	23.77	23.29
-5	-7	8	7.84	6.81
-6	-1	4	59.80	58.03
-6	-2	5	38.69	36.75
-6	-3	6	71.11	71.42
-6	-4	7	4.17	3.68
-6	-5	8	4.85	1.38
-7	-1	6	24.57	25.14
-7	-2	7	25.01	25.49
-7	-3	8	11.46	13.50
-8	-1	8	10.11	10.28
-3	-1	1	41.94	38.56
-3	-2	2	90.53	90.94
-3	-3	3	84.41	83.57
-3	-4	4	27.39	31.07
-3	-5	5	53.65	52.93
-3	-6	6	13.76	13.36
-3	-7	7	7.69	7.23
-3	-8	8	21.23	22.57
-4	-1	3	50.44	52.94
-4	-2	4	43.68	44.10
-4	-3	5	28.54	28.59
-4	-4	6	46.23	47.41
-4	-5	7	15.98	17.15
-4	-6	8	17.54	16.13
-5	-1	5	79.30	80.39
-5	-2	6	15.60	15.26
-5	-3	7	10.49	12.23
-5	-4	8	32.05	31.80
-6	-1	7	57.53	57.88
-6	-2	8	5.24	3.64
-6	-3	9	4.66	6.86
-7	-1	9	3.16	2.20
-2	-1	2	165.60	165.76
-2	-2	3	65.60	65.78
-2	-3	4	47.05	45.96
-2	-4	5	29.00	29.49
-2	-5	6	34.12	33.65
-2	-6	7	8.21	7.35
-2	-7	8	9.85	9.23
-3	-1	4	81.49	79.38
-3	-2	5	24.34	26.68
-3	-3	6	8.52	9.27
-3	-4	7	10.72	10.86

H	K	L	FOBS	FCAL
-3	-5	8	16.77	16.86
-3	-6	9	4.82	6.36
-4	-1	8	8.88	9.12
-4	-2	7	23.07	23.52
-4	-3	8	17.53	18.20
-4	-4	9	15.83	16.32
-5	-1	8	46.64	47.60
-5	-2	9	3.97	4.24
0	0	0	0.0	1043.89
0	-1	1	127.94	133.20
0	-2	2	137.56	140.12
0	-3	3	18.70	14.71
0	-4	4	16.59	19.07
0	-5	5	34.93	34.90
0	-6	6	9.97	9.97
0	-7	7	3.79	0.57
0	-8	8	13.66	13.73
-1	-1	3	45.52	47.08
-1	-2	4	29.62	27.85
-1	-3	5	12.69	9.62
-1	-4	6	36.27	37.34
-1	-5	7	4.46	1.81
-1	-6	8	17.38	17.06
-1	-7	9	17.66	16.37
-2	-1	5	2.64	0.87
-2	-2	6	51.76	51.62
-2	-3	7	59.33	58.34
-2	-4	8	18.37	17.19
-2	-5	9	7.33	6.48
-3	-1	7	10.42	9.42
-3	-2	8	34.06	34.03
-3	-3	9	11.12	11.37
-4	-1	9	1.67	2.58
1	9	-8	7.81	9.04
1	8	-7	7.72	8.54
1	7	-6	6.27	4.27
1	6	-5	37.40	37.04
1	5	-4	74.21	75.65
1	4	-3	81.90	80.64
1	3	-2	51.45	51.15
1	2	-1	176.11	174.31
1	1	0	36.81	31.99
0	10	-7	30.09	30.00
0	9	-6	27.47	28.84
0	8	-5	2.52	1.88
0	7	-4	14.09	8.57
0	6	-3	32.13	33.60
0	5	-2	223.56	225.11
0	4	-1	173.02	172.91
0	3	0	68.03	69.20

H	K	L	FOBS	FCAL
0	-1	7	39.12	38.93
0	-2	8	15.07	14.61
0	-3	9	4.69	0.70
0	-4	10	22.22	22.09
-1	-1	9	29.03	28.31
-1	-2	10	7.21	8.02
3	10	-7	13.02	12.11
3	9	-6	42.23	43.25
3	8	-5	24.61	24.68
3	7	-4	12.79	12.82
3	6	-3	33.03	34.16
3	5	-2	11.87	7.88
3	4	-1	31.34	29.94
3	3	0	58.01	58.03
3	2	1	46.55	47.89
3	1	2	287.93	293.02
2	11	-6	34.26	36.03
2	10	-5	21.03	21.50
2	9	-4	20.47	20.49
2	8	-3	17.29	18.82
2	7	-2	26.09	27.57
2	6	-1	68.40	67.63
2	5	0	85.05	83.77
2	4	1	71.51	71.81
2	3	2	49.94	48.62
2	2	3	7.42	5.66
2	1	4	64.98	65.23
1	12	-5	34.25	34.06
1	11	-4	3.65	2.15
1	10	-3	24.88	23.82
1	9	-2	52.09	51.67
1	8	-1	7.20	2.52
1	7	0	34.82	34.53
1	6	1	41.88	42.64
1	5	2	22.54	21.24
1	4	3	86.72	84.90
1	3	4	38.75	40.30
1	2	5	15.63	16.46
1	1	6	21.72	23.59
0	14	-5	27.22	27.70
0	13	-4	19.18	18.01
0	12	-3	16.01	15.05
0	11	-2	34.57	34.46
0	10	-1	4.31	2.13
0	9	0	39.15	37.00
0	8	1	72.30	72.26
0	7	2	15.92	18.61
0	6	3	18.73	23.02
0	5	4	63.78	65.59
0	4	5	61.37	62.20

H	K	L	FOBS	FCAL
0	2	1	20.64	18.83
0	1	2	36.30	35.36
0	0	3	19.10	18.73
0	-1	4	28.35	27.98
0	-2	5	79.62	78.46
0	-3	6	11.13	12.66
0	-4	7	20.63	21.19
0	-5	8	5.20	1.89
0	-6	9	20.96	19.75
-1	-1	6	16.53	16.46
-1	-2	7	7.78	6.74
-1	-3	8	38.31	38.62
-1	-4	9	15.13	14.56
-2	-1	8	17.86	17.90
-2	-2	9	3.57	2.42
-2	-3	10	19.71	19.96
-3	-1	10	2.76	0.45
2	9	-7	18.22	18.39
2	8	-6	17.62	19.10
2	7	-5	30.93	31.79
2	6	-4	104.46	104.93
2	5	-3	13.32	10.53
2	4	-2	27.26	26.63
2	3	-1	86.78	86.65
2	2	0	215.58	218.60
2	1	1	211.04	212.82
1	11	-7	11.69	10.94
1	10	-6	26.43	28.06
1	9	-5	8.26	7.20
1	8	-4	18.71	17.66
1	7	-3	87.56	86.26
1	6	-2	162.61	159.21
1	5	-1	86.90	84.96
1	4	0	52.43	51.55
1	3	1	37.59	33.86
1	2	2	142.58	143.66
1	1	3	36.18	33.25
0	12	-6	5.22	9.45
0	11	-5	21.26	19.92
0	10	-4	91.70	92.29
0	9	-3	85.50	85.29
0	8	-2	20.91	20.66
0	7	-1	60.93	61.13
0	6	0	31.78	30.58
0	5	1	84.94	82.35
0	4	2	11.41	12.06
0	3	3	92.78	93.09
0	2	4	6.79	0.34
0	1	5	23.62	27.39
0	0	6	44.57	43.65

H	K	L	FOBS	FCAL
0	3	6	37.27	37.86
0	2	7	14.04	13.62
0	1	8	28.56	26.56
0	0	9	4.38	4.68
0	-1	10	21.51	20.59
4	10	-6	9.48	7.97
4	9	-5	8.25	11.63
4	8	-4	6.78	4.95
4	7	-3	21.22	21.59
4	6	-2	21.99	22.56
4	5	-1	126.70	126.10
4	4	0	43.84	42.59
4	3	1	53.08	52.25
4	2	2	61.22	57.83
4	1	3	126.23	127.26
3	11	-5	14.72	14.44
3	10	-4	4.84	1.99
3	9	-3	28.14	27.70
3	8	-2	58.24	56.29
3	7	-1	47.06	44.67
3	6	0	88.10	86.85
3	5	1	43.66	46.30
3	4	2	5.59	3.68
3	3	3	72.66	72.11
3	2	4	20.50	21.57
3	1	5	15.80	17.21
2	13	-5	6.39	4.93
2	12	-4	32.94	33.59
2	11	-3	23.37	22.90
2	10	-2	44.09	44.17
2	9	-1	62.37	61.87
2	8	0	7.74	8.48
2	7	1	42.40	36.65
2	6	2	32.80	33.94
2	5	3	79.89	80.34
2	4	4	51.96	51.15
2	3	5	32.81	28.85
2	2	6	37.03	37.75
2	1	7	18.40	19.75
1	14	-4	23.30	23.06
1	13	-3	26.56	27.42
1	12	-2	12.02	12.78
1	11	-1	9.31	10.33
1	10	0	30.52	31.25
1	9	1	34.48	33.88
1	8	2	24.95	26.10
1	7	3	12.97	12.69
1	6	4	61.61	61.55
1	5	5	25.63	24.91
1	4	6	8.17	6.28

H	K	L	FOBS	FCAL
1	3	7	53.06	52.17
1	2	8	27.86	28.26
1	1	9	31.44	29.18
0	15	-3	12.13	11.85
0	14	-2	11.07	9.34
0	13	-1	13.56	14.38
0	12	0	7.18	5.16
0	11	1	17.42	19.13
0	10	2	36.33	37.50
0	9	3	58.27	57.16
0	8	4	3.82	3.06
0	7	5	34.63	35.01
0	6	6	44.70	42.64
0	5	7	19.65	19.40
0	4	8	12.31	12.47
0	3	9	44.98	44.02
0	2	10	30.08	29.99
5	10	-5	18.90	18.53
5	9	-4	11.74	12.14
5	8	-3	10.57	9.45
5	7	-2	55.44	55.12
5	6	-1	3.98	4.10
5	5	0	47.17	49.65
5	4	1	70.64	70.33
5	3	2	86.28	84.37
5	2	3	66.84	66.85
5	1	4	73.58	70.25
4	11	-4	24.50	24.37
4	10	-3	6.08	5.82
4	9	-2	20.24	21.57
4	8	-1	50.71	51.35
4	7	0	80.27	79.68
4	6	1	48.76	47.32
4	5	2	13.80	12.16
4	4	3	25.03	19.69
4	3	4	90.32	88.66
4	2	5	60.39	61.23
4	1	6	33.97	32.60
3	13	-4	15.20	14.20
3	12	-3	17.31	15.83
3	11	-2	29.04	29.27
3	10	-1	42.21	43.86
3	9	0	13.19	13.86
3	8	1	31.20	29.34
3	7	2	36.61	35.94
3	6	3	20.17	20.64
3	5	4	34.36	35.23
3	4	5	59.51	60.20
3	3	6	33.77	34.47
3	2	7	40.24	39.56

H	K	L	FOBS	FCAL
3	1	8	30.19	29.26
2	14	-3	30.78	31.07
2	13	-2	4.63	1.31
2	12	-1	3.72	6.67
2	11	0	23.11	22.65
2	10	1	48.02	48.14
2	9	2	26.04	25.38
2	8	3	33.73	34.88
2	7	4	19.02	19.53
2	6	5	58.94	59.08
2	5	6	55.75	54.71
2	4	7	10.24	9.74
2	3	8	10.95	9.75
2	2	9	3.79	5.84
2	1	10	6.06	6.31
1	15	-2	16.30	15.11
1	14	-1	2.49	2.44
1	13	0	42.17	42.18
1	12	1	17.04	15.83
1	11	2	30.64	30.84
1	10	3	25.67	25.03
1	9	4	27.35	27.84
1	8	5	45.85	44.03
1	7	6	44.11	45.16
1	6	7	5.47	6.35
1	5	8	14.38	14.52
1	4	9	5.84	3.83
1	3	10	1.76	2.08
0	16	-1	12.75	11.99
0	15	0	4.31	4.38
0	14	1	38.28	36.63
0	13	2	30.84	30.10
0	12	3	38.10	37.10
0	11	4	35.83	34.41
0	10	5	6.75	6.15
0	9	6	23.60	23.51
0	8	7	32.12	32.44
0	7	8	13.60	12.10
0	6	9	3.96	3.16
6	10	-4	8.92	8.43
6	9	-3	3.59	3.32
6	8	-2	30.11	29.59
6	7	-1	52.86	52.21
6	6	0	54.21	56.72
6	5	1	42.42	42.73
6	4	2	49.43	49.32
6	3	3	31.05	30.40
6	2	4	111.78	111.89
6	1	5	4.49	0.39
5	11	-3	9.05	9.44
5	10	-2	22.97	23.42
5	9	-1	45.39	45.14
5	8	0	41.27	39.88
5	7	1	69.48	67.60
5	6	2	22.56	23.89
5	5	3	5.21	3.68
5	4	4	38.79	38.10
5	3	5	36.87	36.51
5	2	6	4.97	4.48
5	1	7	6.40	8.57
4	13	-3	24.03	23.83
4	12	-2	21.02	20.96
4	11	-1	41.27	40.84
4	10	0	21.02	20.77
4	9	1	8.36	8.04
4	8	2	37.66	37.61
4	7	3	29.68	28.38
4	6	4	8.04	6.23
4	5	5	33.95	33.77
4	4	6	16.91	18.48
4	3	7	12.15	11.65
4	2	8	5.84	4.56
4	1	9	11.76	10.07
3	14	-2	20.30	18.45
3	13	-1	3.11	1.79
3	12	0	36.32	36.05
3	11	1	22.87	22.26
3	10	2	26.02	23.33
3	9	3	5.47	3.63
3	8	4	13.71	13.74
3	7	5	46.74	47.32
3	6	6	23.77	23.65
3	5	7	9.30	7.69
3	4	8	17.96	18.10
3	3	9	6.98	5.62
3	2	10	21.33	20.96
2	15	-1	25.58	26.33
2	14	0	3.43	4.43
2	13	1	18.51	16.88
2	12	2	31.66	31.44
2	11	3	23.62	25.05
2	10	4	16.78	16.28
2	9	5	18.30	15.78
2	8	6	39.60	38.47
2	7	7	21.10	21.43
2	6	8	6.19	5.19
2	5	9	9.69	9.97
1	15	1	5.54	9.39
1	14	2	5.06	8.57
1	13	3	34.39	32.20

H	K	L	FOBS	FCAL	H	K	L	FOBS	FCAL
1	12	4	22.71	22.38	4	8	5	7.24	8.40
1	11	5	34.29	34.59	4	7	6	10.13	9.13
1	10	6	18.90	18.71	4	6	7	4.26	4.77
1	9	7	21.37	20.78	4	5	8	7.24	7.36
1	8	8	8.47	7.32	4	4	9	23.10	23.13
1	7	9	6.31	1.84	3	14	1	18.74	20.14
0	16	2	29.60	30.10	3	13	2	13.91	14.13
0	15	3	13.49	14.84	3	12	3	35.85	35.32
0	14	4	17.53	17.99	3	11	4	30.84	29.87
0	13	5	29.31	28.78	3	10	5	4.03	1.36
0	12	6	27.96	27.40	3	9	6	21.51	21.82
0	11	7	5.08	2.23	3	8	7	17.66	18.19
0	10	8	9.20	9.47	3	7	8	16.89	17.19
7	10	-3	10.75	11.46	3	6	9	5.55	7.09
7	9	-2	15.99	15.77	2	14	3	8.15	9.46
7	8	-1	27.95	29.13	2	13	4	19.73	20.65
7	7	0	35.79	34.69	2	12	5	4.79	0.62
7	6	1	56.56	57.82	2	11	6	8.48	10.74
7	5	2	13.70	11.59	2	10	7	4.57	5.56
7	4	3	37.03	36.45	2	9	8	17.93	16.68
7	3	4	27.16	27.20	8	10	-2	9.07	8.04
7	2	5	22.53	21.93	8	9	-1	26.46	26.70
7	1	6	17.09	16.49	8	8	0	55.68	55.94
6	11	-2	14.44	14.50	8	7	1	39.25	39.02
6	10	-1	22.60	22.56	8	6	2	41.77	41.54
6	9	0	39.68	38.62	8	5	3	7.31	6.66
6	8	1	16.45	16.57	8	4	4	2.65	0.98
6	7	2	18.68	19.18	8	3	5	25.93	26.22
6	6	3	42.80	42.55	8	2	6	24.73	24.39
6	5	4	31.65	31.29	8	1	7	11.41	10.85
6	4	5	30.88	28.97	7	11	-1	22.66	23.38
6	3	6	3.78	0.84	7	10	0	26.89	28.01
6	2	7	2.88	0.65	7	9	1	30.63	30.53
6	1	8	9.04	7.99	7	8	2	44.24	44.71
5	12	-1	1.71	4.40	7	7	3	6.99	3.82
5	11	0	22.51	22.06	7	6	4	31.82	32.13
5	10	1	23.30	22.24	7	5	5	3.56	0.14
5	9	2	21.02	20.71	7	4	6	22.56	22.06
5	8	3	33.69	33.56	7	3	7	3.29	3.07
5	7	4	32.21	32.39	7	2	8	27.70	26.69
5	6	5	10.48	12.93	7	1	9	19.87	20.14
5	5	6	18.29	17.45	6	12	0	19.24	19.67
5	4	7	7.72	6.11	6	11	1	17.53	17.41
5	3	8	11.09	10.78	6	10	2	18.86	18.04
5	2	9	5.18	2.09	6	9	3	7.56	6.14
4	13	0	4.52	0.62	6	8	4	24.69	25.59
4	12	1	31.49	29.79	6	7	5	16.45	16.30
4	11	2	24.51	25.22	6	6	6	28.07	28.49
4	10	3	32.13	32.52	6	5	7	31.36	32.48
4	9	4	39.74	40.41	6	4	8	17.58	17.55

H	K	L	FOBS	FCAL
6	3	9	14.32	13.46
5	13	1	13.20	12.07
5	12	2	5.18	2.11
5	11	3	3.75	3.13
5	10	4	11.06	10.57
5	9	5	19.23	19.63
5	8	6	20.61	19.73
5	7	7	17.80	15.90
5	6	8	25.75	23.93
4	13	3	4.47	7.98
4	12	4	4.11	3.22
4	11	5	3.10	0.87
4	10	6	22.33	21.93
4	9	7	30.63	31.09
9	9	0	26.64	27.23
9	8	1	24.22	23.25
9	7	2	7.05	6.35
9	6	3	7.39	7.16
9	5	4	30.54	30.96
9	4	5	21.73	20.83
9	3	6	44.06	44.47
9	2	7	16.42	16.77
9	1	8	3.91	3.61
8	10	1	8.16	9.13
8	9	2	6.31	6.25
8	8	3	20.64	19.33
8	7	4	25.11	24.12
8	6	5	12.55	13.13
8	5	6	21.63	20.94
8	4	7	21.14	19.32
8	3	8	8.62	7.79
7	11	2	5.31	6.00
7	10	3	12.37	9.85
7	9	4	21.85	21.74
7	8	5	16.76	16.60
7	7	6	11.24	10.88
7	6	7	29.54	30.57
7	5	8	9.28	10.81
6	11	4	19.18	19.35
6	10	5	21.93	22.77
6	9	6	9.00	8.47
10	8	2	6.55	6.84
10	7	3	26.39	27.96
10	6	4	14.00	13.48
10	5	5	13.08	12.47
10	4	6	15.02	14.40
10	3	7	10.32	10.13
9	9	3	11.60	13.47
9	8	4	13.75	12.63
9	7	5	17.81	17.17
9	6	6	8.80	9.00

$Cr(CNPh)_6$, determined as Nujol mulls or in $HCCl_3$ solution show a sharp band at about 2005 cm^{-1} and an extremely broad band at 1950 cm^{-1}.[15] Thus, although the precise value of the deviation of the MCN bond angle from 180° may be dependent on crystal packing forces, the fact that the bend is electronic in nature seems assured by the similarity between the solution and solid state spectra. The broadening of the $\bar{\nu}$(CN) band at 1950 cm^{-1} is also explainable in terms of the structure since pseudo rotations along the M-CN-C bonds should be of very low energies. In fact, a low temperature IR spectrum of $Cr(CNPh)_6$ in a KBr pellet shows the band at 1950 cm^{-1} sharpening considerably. Similar arguments obtain for the Mo and W complexes. The ramifications of this bending in terms of the electronic structure of the complex will not be discussed at this time, but will appear in a later section.

By changing the steric requirements of the phenyl rings by putting large alkyl groups in the two ortho ring positions, one should be able to perturb the M-C-N bonds back toward colinearity. Strong evidence suggests that this is the case for $Cr(CNIph)_6$ (CNIph = 2, 6-diisopropylphenylisocyanide). The IR spectrum of $Cr(CNIph)_6$ shows two bands in solution and in the solid state, but the bands are considerably sharper and the higher energy band is much weaker in intensity relative to the low energy band. The spectrum of $W(CNIph)_6$, which is almost identical, is shown in Figure 4. Molecular models show that the bulky R groups of $Cr(CNIph)_6$ should tend to push the structure band to T_h <u>via</u> nonbonding steric

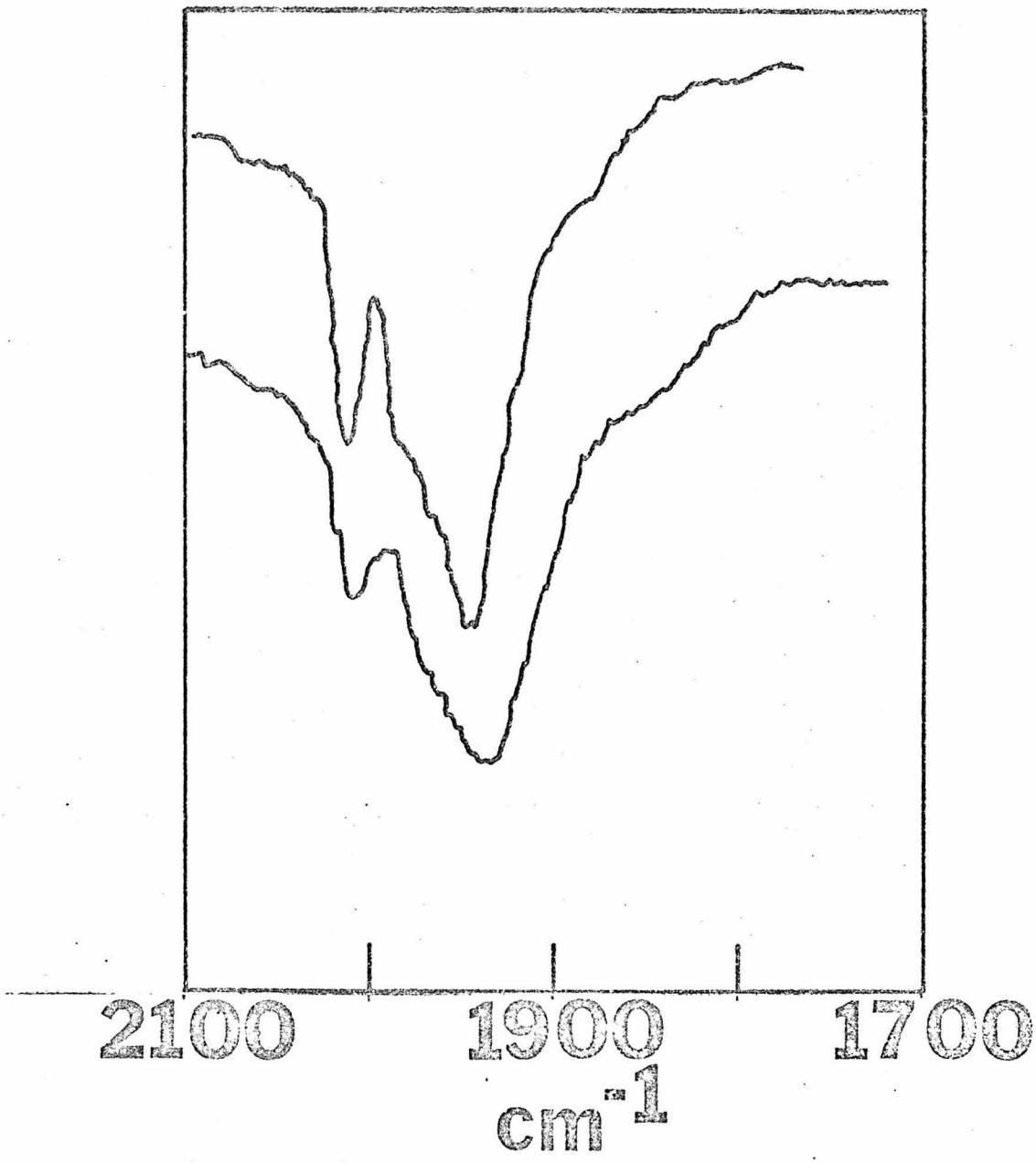

Figure 3. IR spectra of $Cr(CNPh)_6$ as a KBr pellet. Top curve T = 14 K; bottom curve T = 310 K.

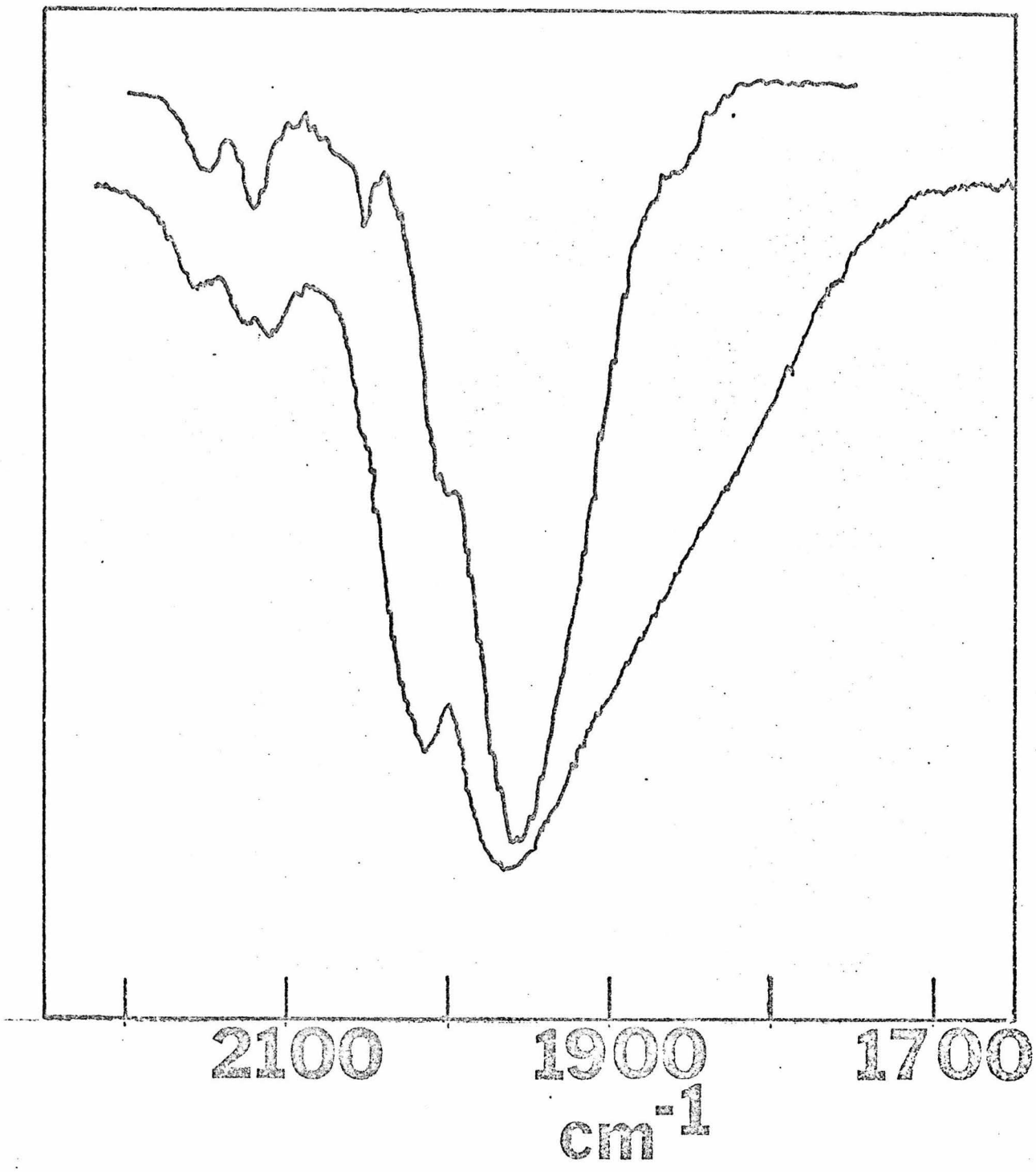

Figure 4. Upper curve, IR spectrum of $W(CNIph)_6$ in $HCCl_3$.
Lower curve, IR spectrum of $W(CNPh)_6$ in $HCCl_3$.

interactions among the i-propyl groups. The idea that $Cr(CNIph)_6$ is closer to T_h symmetry is also supported by the simpler appearance of its electronic spectrum compared to $CrCNPh)_6$. Useful correlations of the appearance of the $\bar{\nu}$(CN) region of the IR spectrum of $M(CNAr)_6$ complexes with the microsymmetry at the metal are apparent.

In Figure 5, the infrared spectra of $Cr(CNPh)_6^{0,+1,+2}$ are shown, and in Figure 6 are spectra for $Cr(CNPh)_6$, $Mn(CNPhCH_3)_6^{+}$, and $Mn(CNPhCH_3)_6^{2+}$. Other IR spectral data are given in Table 8. Thus it appears from the data presented that for a given metal, oxidation results in a sharpening of the $\bar{\nu}$(CN) stretch, an increase in energy, and a lessening of distortions away from T_h symmetry. For the isoelectronic d^6 metals (Cr(0), Mn(I), Re(I), Mo(0), W(0), Fe(II)) it is seen that moving to the right and down in the periodic table, the $M(CNR)_6$ complexes tend to deviate more from T_h symmetry. This is consistent with an increasing propensity of the metal toward distortion to relieve the instability caused by increased electron density at the metal which is caused by a gradual saturation of the CNAr π^* orbitals' ability to accept electron density through π donation from the metal.

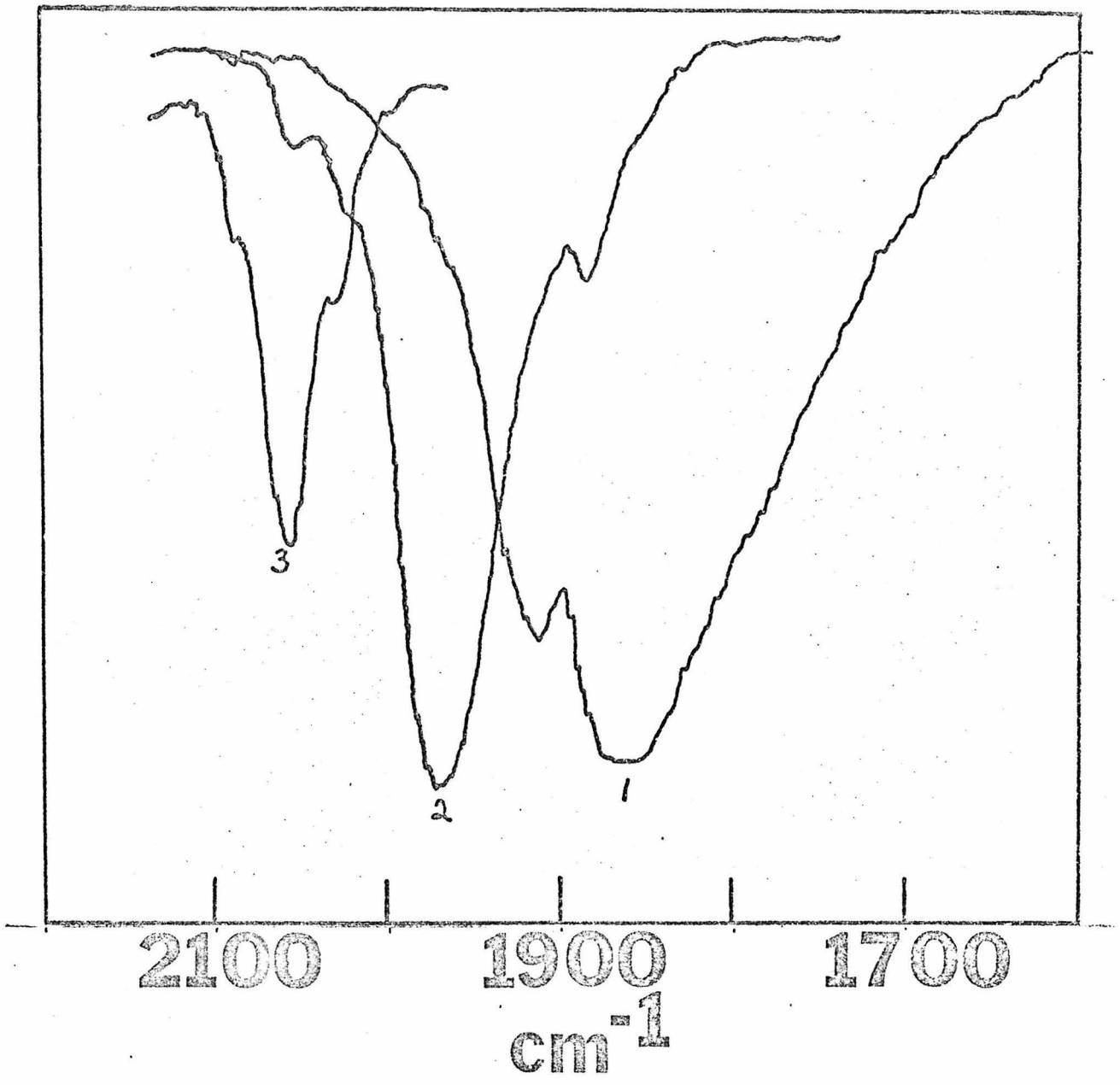

Figure 5. Curve 1: IR spectrum of $Cr(CNPh)_6$ in $HCCl_3$;

Curve 2: IR spectrum of $Cr(CNPh)_6^+$ in $HCCl_3$;

Curve 3: IR spectrum of $Cr(CNPh)_6^{2+}$ in $HCCl_3$.

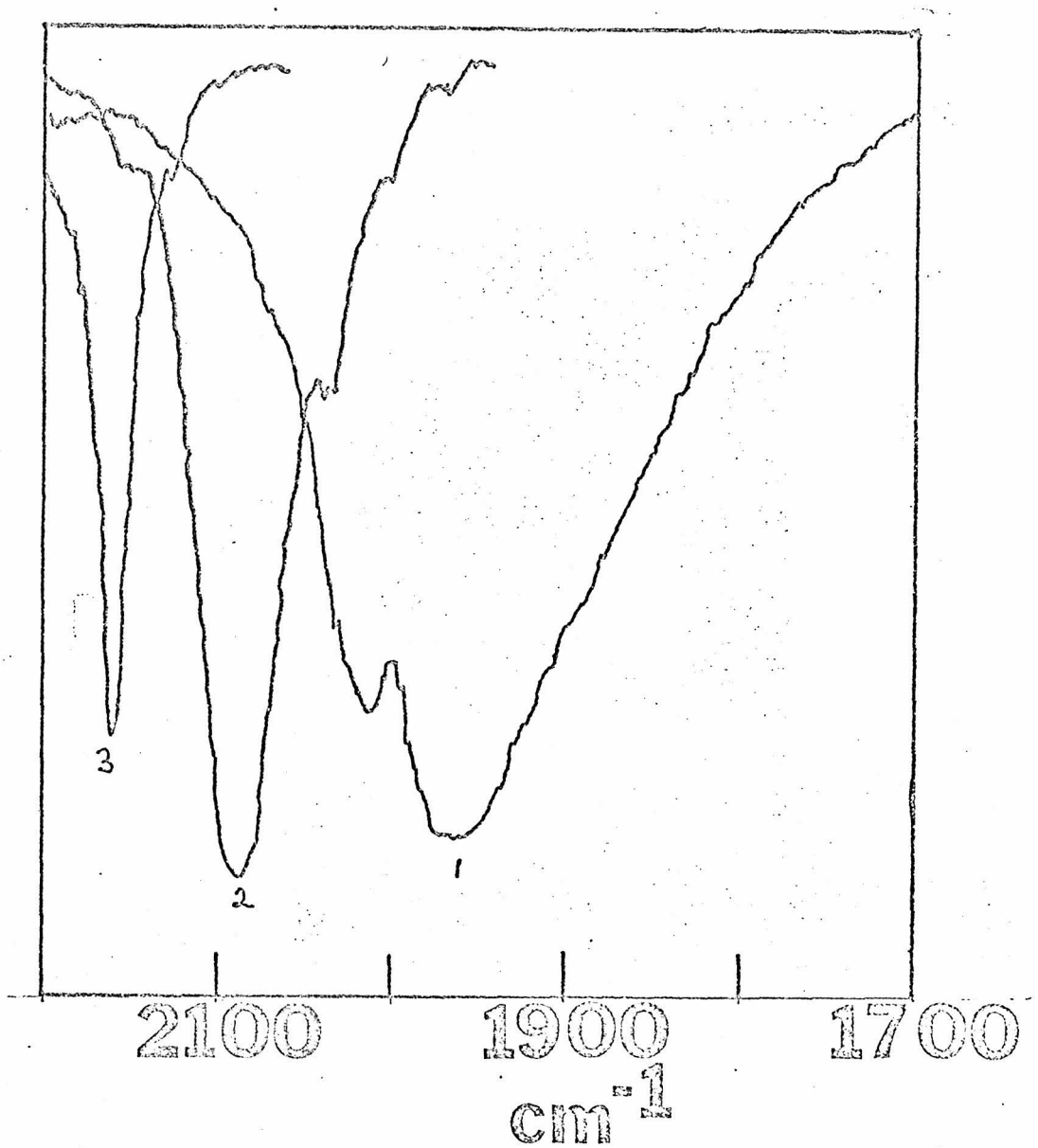

Figure 6. Curve 1: IR spectrum of $Cr(CNPh)_6$ in $HCCl_3$;

Curve 2: IR spectrum of $Mn(pCNPhCH_3)_6$ in $HCCl_3$;

Curve 3: IR spectrum of $Mn(pCNPhCH_3)_6^{2+}$ in $HCCl_3$.

Table 8. Positions[a] of $\bar{\nu}$(CN) for Several Six Coordinate Aryl Isocyanide Complexes

d^6 Complexes	$\bar{\nu}$(CN) in cm^{-1}
$Cr(CNPh)_6$	2012 s, 1965 vs
$Mo(CNPh)_6$	2012 s, 1960 vs
$W(CNPh)_6$	2013 s, 1962 vs
$Mn(pCNPhCH_3)_6^+$	2038 vs, 1990 wk
$Re(pCNPhCH_3)_6^+$ [b]	2070, 2040 wk
$Cr(CNIph)_6$	2005 m, 1962 vs
$Mo(CNIph)_6$	2000 m, 1960 vs
$W(CNIph)_6$	2000 m, 1960 vs
d^5 Complexes	$\bar{\nu}$(CN) in cm^{-1}
$Mn(pCNPhCH_3)_6^{2+}$	2160 s
$Cr(CNIph)_6^+$	2065 vs
$Mo(CNIph)_6^+$	2050 vs
$W(CNIph)_6^+$	2040 vs

[a] This work, unless otherwise noted.

[b] M. Fremi and V. Valenti, Gazz. Chim. Ital., 91, 1352 (1961).

Electronic Structure

The Electronic Structure of the Ligands

Simple molecular orbital calculations[5,23] have been carried out on methyl, vinyl, and phenyl isocyanides. The important aspects of the electronic structure of these molecules are that they contain a lone pair of electrons localized on the carbon atom which can form a strong σ bond to a transition metal and that they all contain two CN π^* molecular orbitals which can be potentially useful in forming $d\pi$-$p\pi^*$ π bonds. The calculations[5] show that for alkyl isocyanides, which have cylindrical symmetry about the C≡N bond, the two π^* levels are degenerate as in cyanide ion. In vinyl and phenyl isocyanide however, the planarity of these groups splits the degeneracy of the π^* levels so as to stabilize one (π^* vertical) through interaction with other p orbitals of π symmetry relative to the other (π^* horizontal). Thus in qualitative terms, taking phenyl isocyanide as an example, π^*_v should be a much better acceptor than π^*_h since it should be able to allow electron density to escape into the phenyl ring. This is in agreement with Horrocks' work[24] which puts p-tolyl isocyanide above t-butyl isocyanide in respect to forming π bonds. This effect will be quite important in the discussion of the complexes which contain phenyl isocyanide.

The Electronic Spectra of the d^6 Systems

Each of the complexes $M(CNAr)_6$ [M = Cr(0), Mo(0), W(0)] exhibits strong electronic absorption bands above 300 nm. The bands below 300 nm are attributable to $\pi \rightarrow \pi^*$ transitions localized primarily in the ligand system[25] and are not of primary interest. Spectral data for the observed bands of $M(CNAr)_6$ (M = Cr(0), Mo(0), W(0))and Ar = Ph, 2,6-dimethylphenyl = Dph, 2,6-diisopropylphenyl = Iph; and 4-chlorophenyl are set out in Table 10.

In Figure 12 , a molecular orbital diagram was constructed assuming the idealized T_h symmetry for $M(CNAr)_6$ complexes. This diagram was constructed by estimating the interaction of the highest occupied and lowest unoccupied molecular orbitals of six CNPh ligands with the central metal.

The ground state for each complex has the $(t_g)^6\ ^1A_g$ configuration. As is the case with the related $M(CO)_6$ complexes,[26] the lowest energy excited states are derived from either d-d ($d\pi \rightarrow d\sigma^*$) or metal-to-ligand charge transfer (MLCT) transitions. It can reasonably be assumed that the d-d states lie above 25,000 cm^{-1}, and transitions to them should give rise to relatively weak bands. Therefore, it is not likely that any of the intense bands in the $M(CNPh)_6$ complexes are due to d-d transitions.

The situation regarding MLCT transitions is more complicated than for the $M(CO)_6$ complexes. As has been previously discussed, molecular orbital calculations[5] suggest that there are two low-lying

Table 9a. Electronic Absorption Spectra[a] of $M(CNAr)_6$ Complexes

Complex	λ_{max}, nm	$\bar{\nu}_{max}$, kK	$\epsilon \times 10^{-3}$	Assignment
$Cr(CNPh)_6$	476	21.0	40.1	$d\pi \rightarrow \pi_v^*L$
	397	25.2	65.6	$d\pi \rightarrow \pi_v^*L$
	321	31.1	35.5	$d\pi \rightarrow \pi_h^*L$
	230	43.5	65.6	intraligand
$Mo(CNPh)_6$	475	21.0	35.0	$d\pi \rightarrow \pi_v^*L$
	382	26.2	76.2	$d\pi \rightarrow \pi_v^*L$
	311	32.2	46.0	$d\pi \rightarrow \pi_h^*L$
	250	40.0	55.8	intraligand
	234	42.7	57.6	intraligand
$W(CNPh)_6$	466	21.5	31.5	$d\pi \rightarrow \pi_v^*L$
	368	27.2	81.0	$d\pi \rightarrow \pi_v^*L$
	315	31.7	55.6	$d\pi \rightarrow \pi_h^*L$
	250	40.0	54.8	intraligand
	234	42.7	55.6	intraligand

Table 9a (Continued)

Complex	λ_{max}, nm	$\bar{\nu}_{max}$, kK	$\epsilon \times 10^{-3}$	Assignment
$Cr(CNDph)_6$	465	21.5	48.0	$d\pi \rightarrow \pi_v^*L$
	405	24.7	66.6	$d\pi \rightarrow \pi_v^*L$
	317	31.5	37.0	$d\pi \rightarrow \pi_h^*L$
	244	41.0	47.0	intraligand
$Mo(CNDph)_6$	454	22.0	39.7	$d\pi \rightarrow \pi_v^*L$
	387	25.8	73.9	$d\pi \rightarrow \pi_v^*L$
	313	31.9	42.6	$d\pi \rightarrow \pi_h^*L$
	257	38.9	55.9	intraligand
$W(CNDph)_6$	457	21.9	39.9	$d\pi \rightarrow \pi_v^*L$
	381	26.2	85.6	$d\pi \rightarrow \pi_v^*L$
	318	31.4	54.8	$d\pi \rightarrow \pi_h^*L$
	260	38.5	61.7	intraligand
$Cr(CNIph)_6$	475	21.0	76.0	$d\pi \rightarrow \pi_v^*L$
	402	24.9	26.1	$d\pi \rightarrow \pi_h^*L$
	312	32.0	64.1	$d\pi \rightarrow \pi_h^*L$
	242	41.3	47.6	intraligand

Table 9a (Continued)

Complex	λ_{max}, nm	$\bar{\nu}_{max}$, kK	$\epsilon \times 10^{-3}$	Assignment
$Mo(CNIph)_6$	475	21.0	71.6	$d\pi \rightarrow \pi_v^*L$
	435	23.0	51.3	$d\pi \rightarrow \pi_v^*L$
	384	26.0	34.1	$d\pi \rightarrow \pi_v^*L$
	310	32.3	79.0	$d\pi \rightarrow \pi_h^*L$
	245	40.8	48.6	intraligand
$W(CNIph)_6$	521	19.2	74.5	$d\pi \rightarrow \pi_v^*L$
	463	21.6	60.0	$d\pi \rightarrow \pi_v^*L$
	434	23.0	44.3	$d\pi \rightarrow \pi_v^*L$
	373	26.8	37.0	$d\pi \rightarrow \pi_v^*L$
	310	32.2	85.7	$d\pi \rightarrow \pi_h^*L$
	283	35.3	44.3	intraligand
	250	40.0	58.0	intraligand
$Cr(pNPhCl)_6$	484	20.7	41.8	$d\pi \rightarrow \pi_v^*L$
	408	24.5	66.0	$d\pi \rightarrow \pi_v^*L$
	325	30.8	36.4	$d\pi \rightarrow \pi_h^*L$
	242	41.3	68.1	intraligand

Table 9a (Continued)

Complex	λ_{max}, nm	$\bar{\nu}_{max}$, kK	$\epsilon \times 10^{-3}$	Assignment
$Mo(pCNPhCl)_6$	479	20.9	42.6	$d\pi \rightarrow \pi_v^*L$
	389	25.7	81.2	$d\pi \rightarrow \pi_v^*L$
	321	31.2	50.6	$d\pi \rightarrow \pi_h^*L$
	254	39.4	66.8	intraligand
$W(pCNPhCl)_6$	471	21.2	36.6	$d\pi \rightarrow \pi_v^*L$
	378	26.5	80.1	$d\pi \rightarrow \pi_v^*L$
	316	31.6	53.9	$d\pi \rightarrow \pi_h^*L$
	254	39.4	63.4	intraligand

[a] Extinction coefficients measured in THF at 25°C in a 0.2 nm cell ($\epsilon \pm 10\%$).

Table 9b. Electronic Absorption Spectra of $M(CNPh)_6^Z$ Complexes

Complex	300° K			77° K[a]			Assignment
	λ_{max}, nm	$\tilde{\nu}_{max}$, kK	$\varepsilon_{max} \times 10^{-3}$	λ_{max}, nm	$\tilde{\nu}_{max}$, kK	$\varepsilon_{max} \times 10^{-3}$	
$Cr(CNPh)_6$[b]	458 sh	21.8	46.0	480	20.8	36.0	$d\pi \rightarrow \pi_v^*$ (CNPh)
	394	25.4	73.0	419	23.9	61.0	$d\pi \rightarrow \pi_v^*$ (CNPh)
	310	32.3	36.0	307	32.6	23.0	$d\pi \rightarrow \pi_h^*$ (CNPh)
$Mo(CNPh)_6$[c]	453 sh	22.1	d	470	21.3	42.0	$d\pi \rightarrow \pi_v^*$ (CNPh)
	378	26.5	d	396	25.3	78.0	$d\pi \rightarrow \pi_v^*$ (CNPh)
	313 sh	31.9	d	307	32.6	53.0	$d\pi \rightarrow \pi_h^*$ (CNPh)
	255 sh	39.2	d	250	40.0	81.0	intraligand
$W(CNPh)_6$[c]	446	22.4	44.0	467	21.4	35.0	$d\pi \rightarrow \pi_v^*$ (CNPh)
				405	24.7		
	367	27.2	58.0	380	26.3		$d\pi \rightarrow \pi_v^*$ (CNPh)
	320	81.3	41.0	306	32.7	46.0	$d\pi \rightarrow \pi_h^*$ (CNPh)
	250	40.0	–	250	40.0	–	intraligand
$[Mn(CNPh)_6]Cl$[c]	340 sh	29.4	61.0	345	29.0	46.0	$d\pi \rightarrow \pi_v^*$ (CNPh)
	322	31.1	66.0	325	30.8	46.0	$d\pi \rightarrow \pi_v^*$ (CNPh)
	249 sh	40.2	51.0	250	40.0	–	intraligand
	234 sh	42.7	71.0	235	42.6	–	
	225	44.4	75.0	–	–	–	
$[Mn(CNPh)_6][PF_6]_2$[c,f]	–	–	–	548	18.2	5.3	$\sigma(CNPh) \rightarrow d\pi$
	490	20.4	4.6	490	20.4	6.4	

[a] Spectra corrected for solvent contraction. [b] 1:1 isopentane/diethylether solution. [c] 8:2:1 ethanol/methanol/diethyl ether solution. [d] Solutions were too photosensitive to allow measurement. [e] EPA solution. [f] Ultraviolet spectra are not reported, owing to interfering absorption of the nitric acid added to the solutions.

Table 9c. Electronic Absorption Spectra[a] of $M(CNAr)_6$ Complexes

Complex	λ_{max}, nm	$\bar{\nu}_{max}$, kK	Relative Absorbance
$Cr(CNPh)_6$	469	21.3	0.71
	420	23.8	1.00
$Mo(CNPh)_6$	474	21.1	0.66
	408	24.5	1.00
	385	26.0	0.87
$W(CNPh)_6$	540	18.5 (triplet)	0.08
	425 sh	21.0	0.59
	470	21.3	0.63
	459 sh	21.8	0.59
	402	24.9	1.00
	379 sh	26.4	0.92
$Cr(CNDph)_6$	470 sh	21.3	0.27
	410	24.4	1.00
$W(CNDph)_6$	510	19.6 (triplet)	0.05
	460	21.7	0.19
	387	25.8	1.00
$Cr(CNIph)_6$	482	20.7	1.00
	422	23.7	0.57
$W(CNIph)_6$	508	19.7 (triplet)	0.35
	469 sh	21.3	0.99
	461	21.7	1.00
	432 sh	23.2	0.77
	360	27.8	0.53

Table 9c (Continued)

Complex	λ_{max}, nm	$\bar{\nu}_{max}$, kK	Relative Absorbance
$Cr(pCNPhCl)_6$	488	20.5	0.70
	435	23.0	1.00
$Mo(pCNPhCl)_6$	483	20.7	0.63
	420	23.8	1.00
	391	25.6	0.76
$W(pCNPhCl)_6$	552	18.1 (triplet)	0.11
	494 sh	20.2	0.74
	480	20.8	0.80
	470 sh	21.3	0.78
	414 sh	24.2	--
	380	26.3	1.00

Figure 7. Electronic absorption spectra of $Cr(CNPh)_6$ in 1:1 isopentane/diethyl ether (——), $Mo(CNPh)_6$ in 8:2:1 ethanol/methanol/diethyl ether (---), and $W(CNPh)_6$ in EPA (···) at 77 K.

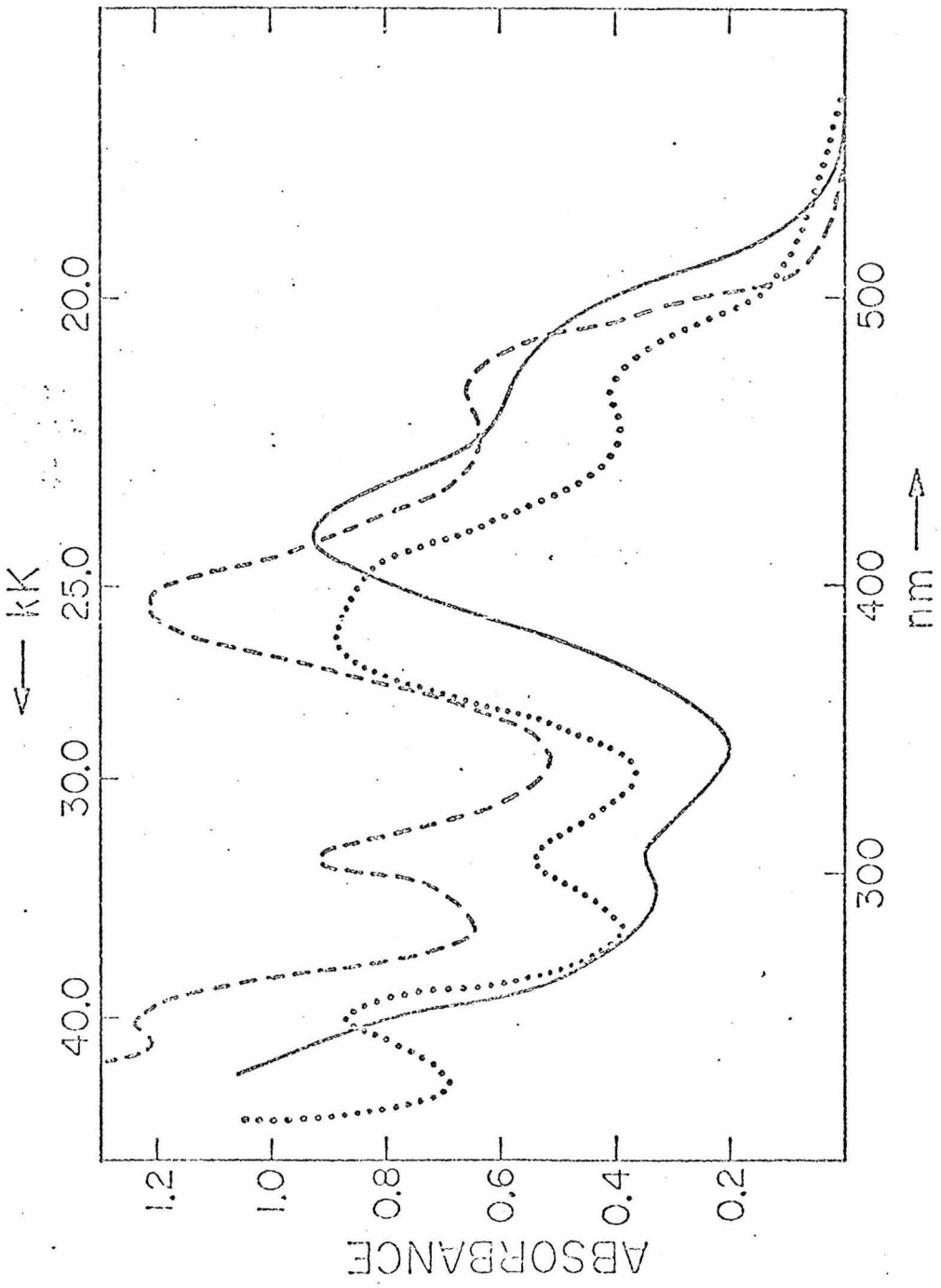
ABSORBANCE
1.2
1.0
0.8
0.6
0.4
0.2
40.0
30.0
25.0
20.0
kK
300
400
500
nm

Figure 8. Electronic absorption spectra of $Cr(CNPh)_6$ (——), $Mo(CNPh)_6$ (- - -), and $W(CNPh)_6$ (· · ·) in degassed THF (—·—·—) at 298 K.

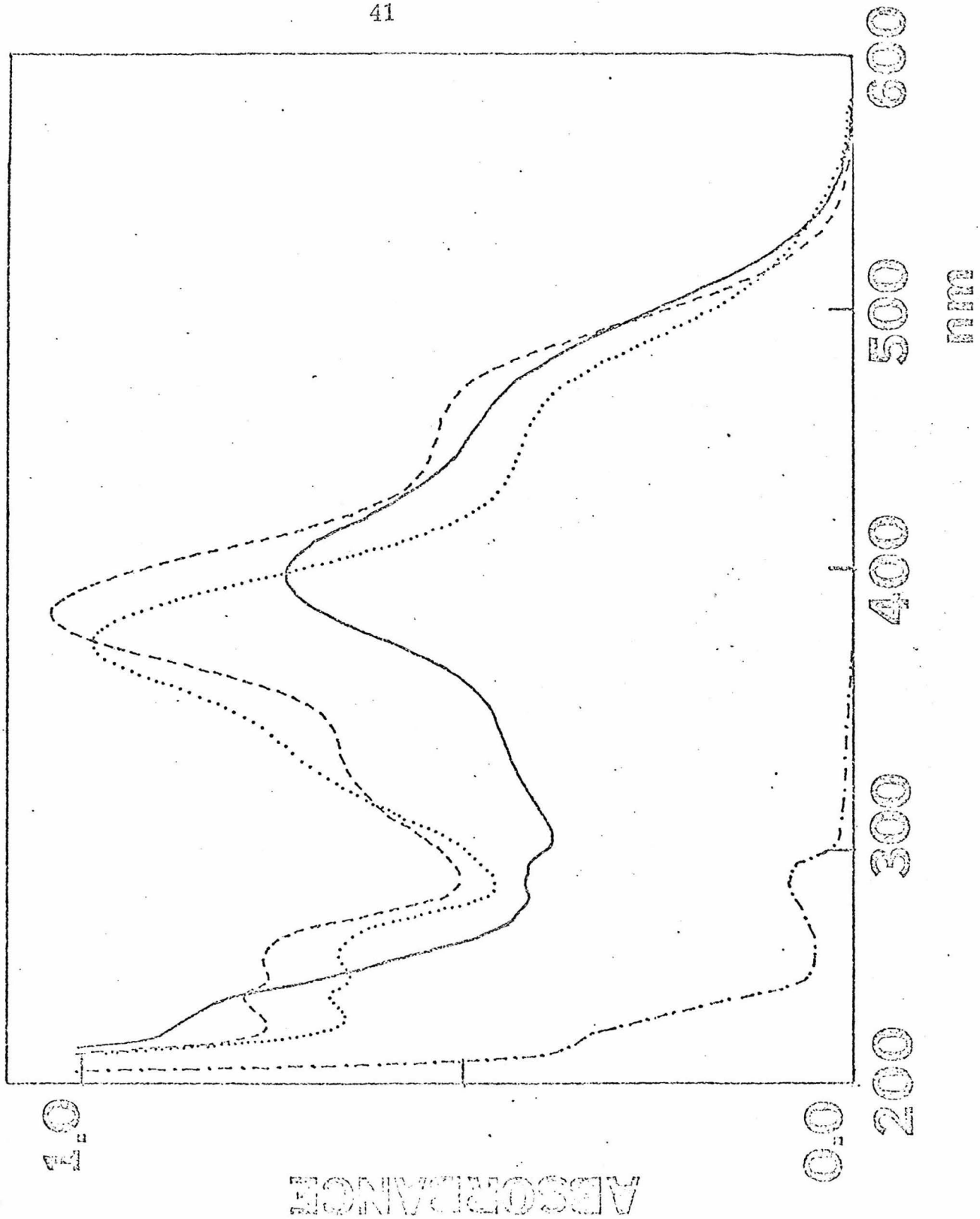
ABSORBANCE
0.0
2.0
200
300
400
500
600
nm

Figure 9. Electronic absorption spectra of $Cr(CNDph)_6$ (——), $Mo(CNDph)_6$ (---), and $W(CNDph)_6$ (···) in degassed THF (·—·—·) at 298 K.

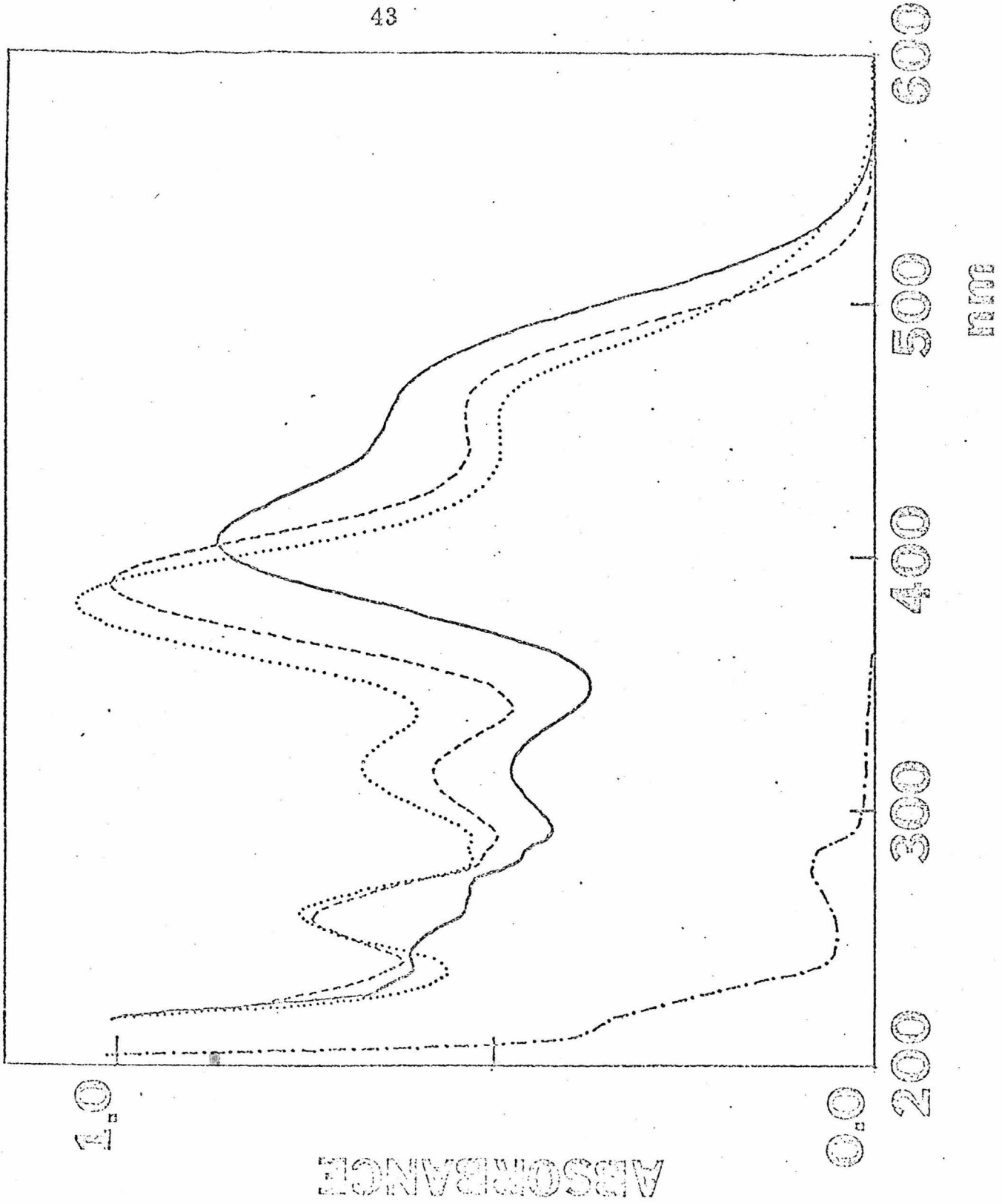
ABSORBANCE
0.0
200
300
400
500
600
nm

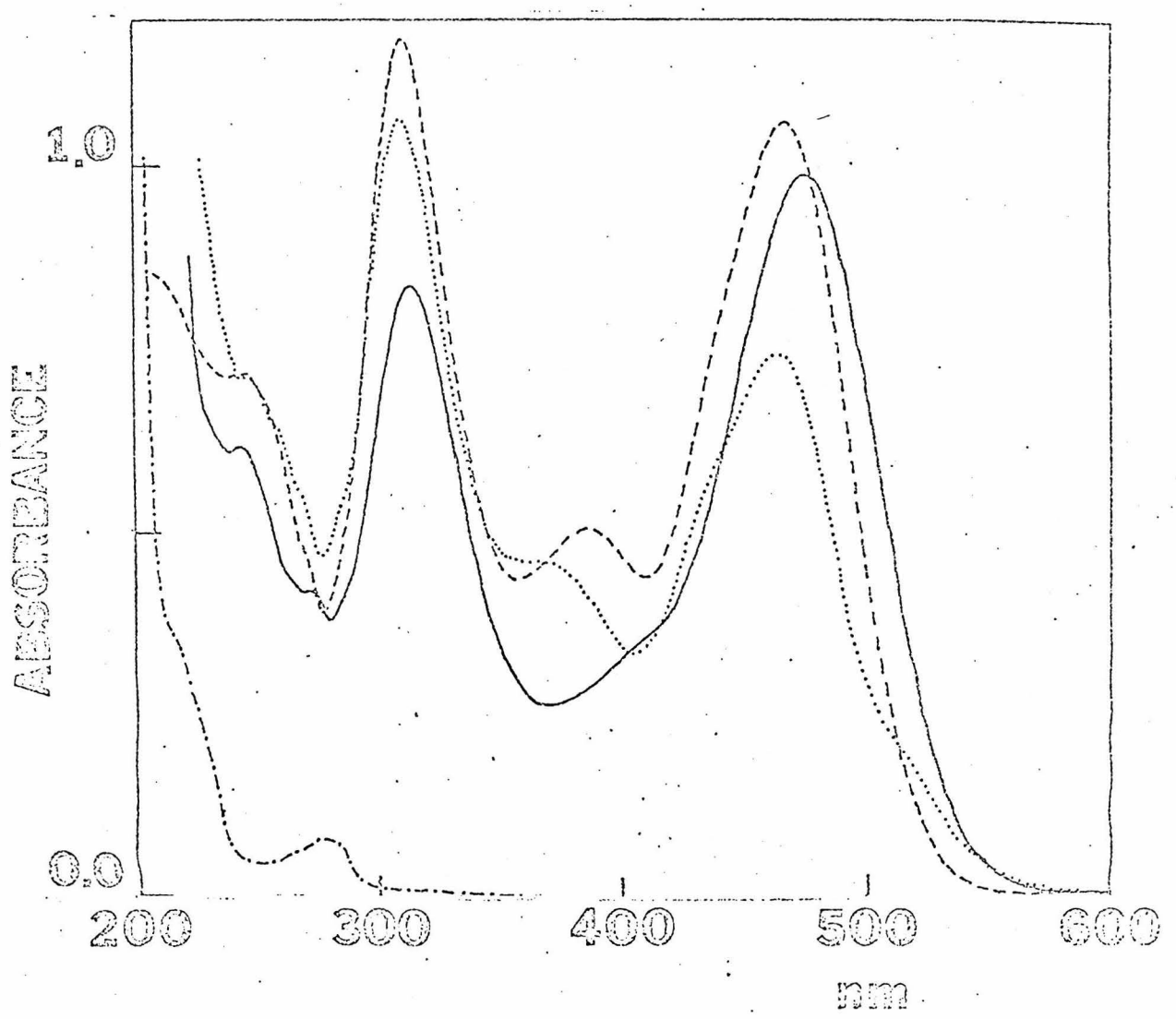

Figure 10. Electronic absorption spectra of $Cr(CNIph)_6$ (——), $Mo(CNIph)_6$ (---), and $W(CNIph)_6$ (···) in degassed (—·—·—) at 298 K.

Figure 11. Electronic absorption spectra of $Cr(pCNPhCl)_6$(——), Mo(pCNPhCl) (---), and $W(pCNPhCl)_6$ (· · ·) in degassed THF (·—·—·) at 298 K.

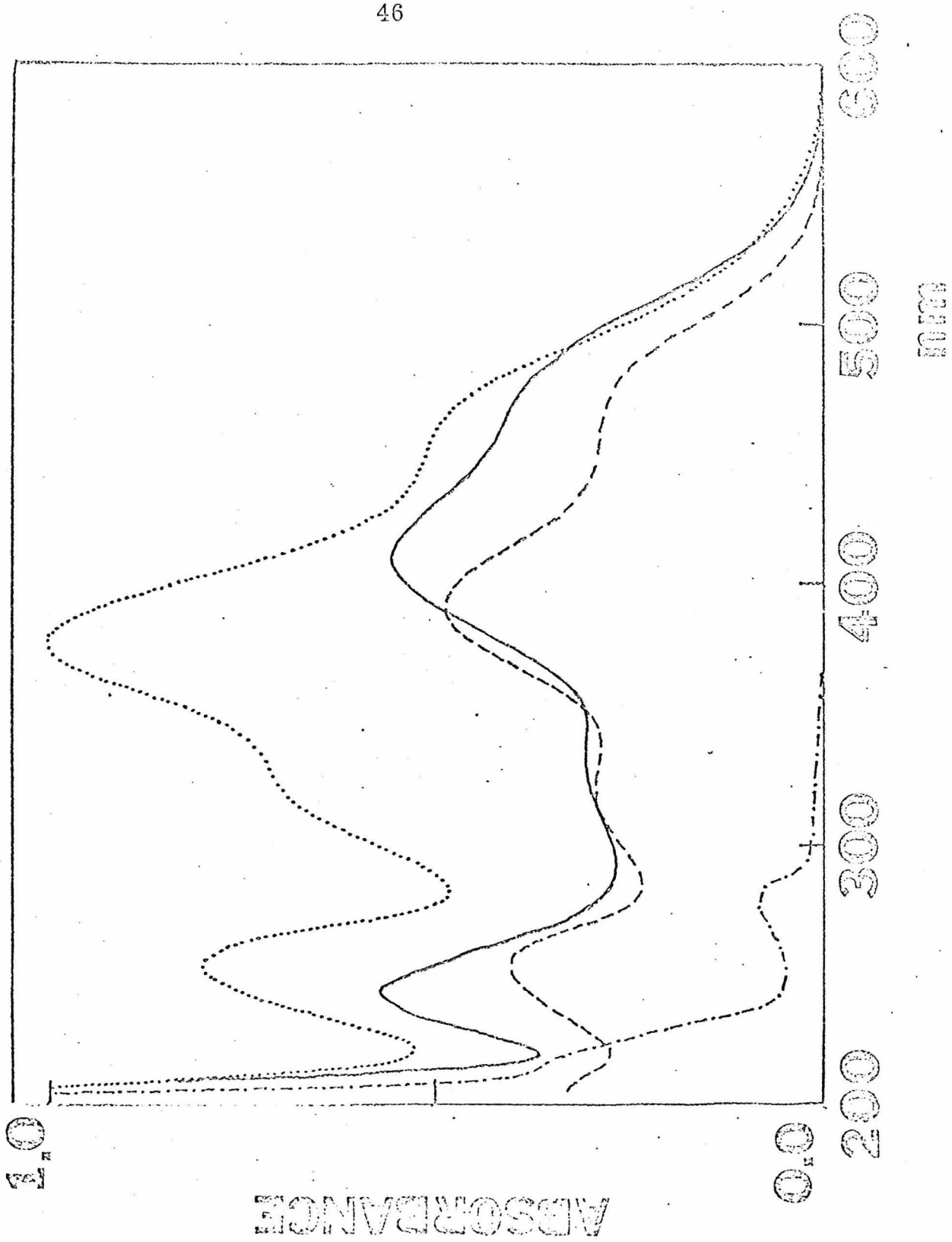
ABSORBANCE
200
300
400
500
600
nm

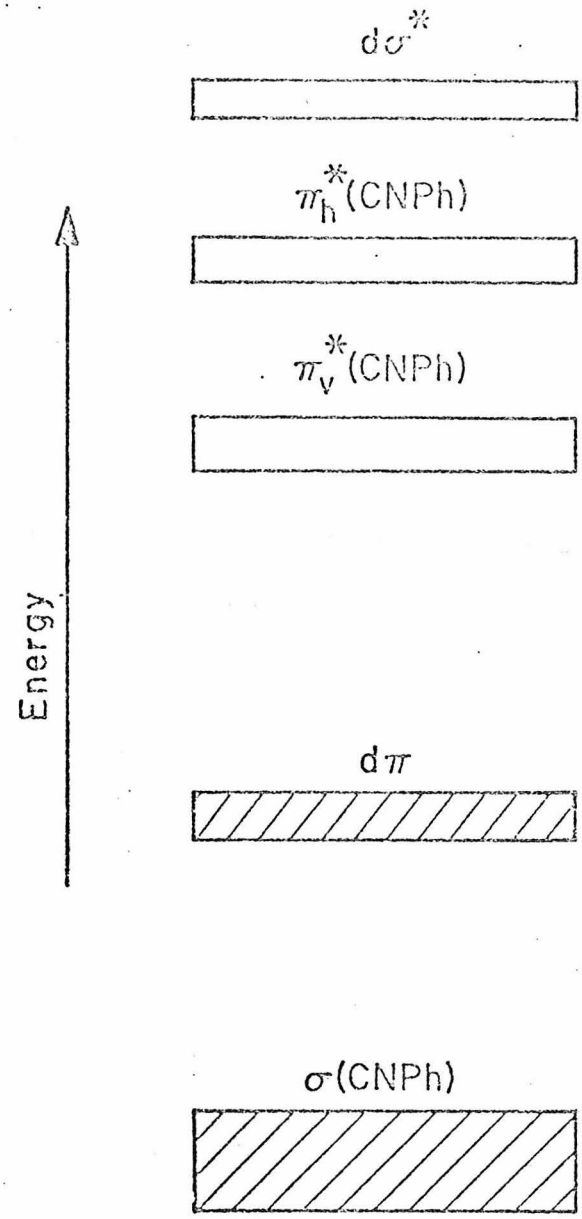

Figure 12. General classification and estimated relative energies of the molecular orbitals in $M(CNPh)_6$ complexes; $d\pi$ and σ(CNPh) levels are occupied in the ground state.

π^* levels in CNPh. The out-of-plane π^*(CN) function is involved in the lower level, which is designated π_v^* in Figure 12. The π_v^* MO, therefore, is stabilized by conjugation with the π orbitals on the aromatic ring, whereas the in-plane orbital, π_h^*, is localized on the cyano group.

The two lowest bands above 300 nm in each of the $M(CNPh)_6$ complexes may be assigned to allowed components of the $t_g \rightarrow tu\pi_v^*$ (CNPh) one electron transition. The fact that these transitions are substantially blue-shifted in the electronic spectrum of the $(d\pi)^6$ complex $Mn(CNPh)_6^+$ confirms the MLCT interpretation. The lowest $d\pi \rightarrow \pi_v^*$ (CNPh) band, for example, is 8kK higher in $Mn(CNPh)_6^+$ than in $Cr(CNPh)_6$. The magnitude of the shift is very nearly the same as that observed for the lowest $^1A_{1g} \rightarrow {}^1T_{1u}$ transitions in $Cr(CO)_6$ (35.7 kK) and $Mn(CO)_6^+$ (44.5 kK).[26]

The 33 kK band present in the zero valent complexes could be assigned as a higher energy component of the $t_g \rightarrow t_u \pi_v^*$CN transition but is more logically assigned to an excitation to $t_u\pi_h^*$CN based on the following argument. Comparing the position of the lowest MLCT bands[8] in $Mn(CNMe)_6^+$[8] to $Mn(CNPh)_6^+$, one finds a red shift of about 10 kK (43.1 kK vs. 33.0 kK). Attributing the entire shift in the MLCT band to the position of π^*CN and assuming that the π^*CN orbitals of methylisocyanide are good models for π_h^*CN of phenylisocyanide, one predicts the $t_g \rightarrow t_u\pi_h^*$ transitions of $Cr(CNPh)_6$ to be located at or above 31.8 kK, which is very close to the 33 kK band found in all the $M(CNAr)_6$ (M = Cr(0), Mo(0), W(0))

complexes. This view is further strengthened by the spectrum of $Cr(CNvinyl)_6$[27] which is similar to $Cr(CNPh)_6$ except that the two lowest bands are shifted to higher energy while the highest band is again found at about 33 kK. This is exactly as expected since the stabilization of π_v^*CN conjugated to a vinyl group has been shown[5] in calculations to be less than that conjugated to a phenyl ring.

The spectra of the W(0) complexes show more complexities, containing several additional weak bands not found in the corresponding Cr(0) and Mo(0) complexes. It is perfectly reasonable to assign these bands to transitions which have increased in allowedness via the increase in the spin orbit coupling in W vs Mo and Cr. To call the transitions singlet triplet transitions though seems rather dangerous in view of the work of Crosby, et al.[28,29] on $Ru(bipy)_3^{2+}$. They have developed a model which treats MLCT transitions in d^6 systems by weakly coupling a d^5 low spin core to the excited electron which is placed in the appropriate ligand orbital. In its limits, this model predicts that the singlet and triplet MLCT transitions are degenerate when e^2/r_{ij} and π are zero. Crosby's analysis of the luminescence arising from $Ru(bipy)_3^{2+}$ suggests that off-diagonal matrix elements due to spin orbit coupling are larger ($\sim 1000\ cm^{-1}$) than those due to the e^2/r_{ij} elements ($100\ cm^{-1}$) involving an electron on the ligands and the d^5 core. Thus assigning spin labels to the various states arising from this analysis has little justification except for determining the allowedness of the transition. A more complete discussion of the comparison between the $M(CNAr)_6$ (M = Cr, Mo, W)

and $M(bipy)_3^{2+}$ (M = Fe, Ru, Os) is included in the section discussing the emission results.

Up to this point, the electronic structure of the $M(CNAr)_6$ complexes has been discussed in terms of idealized T_h symmetry. Crystallographic and infrared data show however that the M-CN linkage in $Cr(CNPh)_6$ is bent to 173° lowering the symmetry of the complex to S_6 symmetry. The data suggest that the distortion is also present in solution since solid state and solution IR spectra are identical and consistent with S_6 symmetry. The observed distortion can be rationalized in terms of a second order Jahn-Teller distortion[30-32] of the ground state which can be formulated as follows. The second order Jahn-Teller effect states that the energy of the ground electronic state is given by

$$E = E_0 + f_{oo}Q_i^2 + f_{ok}Q_i^2$$

where E_0 is the energy of the unperturbed wavefunction ψ_0, Q_i is the normal vibrational coordinate and f_{oo} and f_{ok} contribute to the force constant of the normal mode. The constant f_{oo} consists of matrix elements containing ψ_0 only, but f_{ok} is of the form

$$\sum_k [< \psi_0 | \frac{\partial u}{\partial Q_i} | \psi_k >]^2 / (E_o - E_k)$$

Consequently, for matrix elements of this form to be non-zero, the direct product of $\Gamma_o\Gamma_k$ must contain Γ_Q. Thus a normal vibrational mode of proper symmetry Γ_Q can mix the excited state ψ_k into the ground state ψ_o, causing a ground state distortion in the normal

coordinate Γ_{Q_i} provided that the energy gap $E_o - E_k$ is small (less than 30,000 cm^{-1} and that the excited state which is coupled to the ground state via this mechanism is distorted. MLCT excited states can be expected to be substantially via bending of the M-CN bond angle to relieve the electron density build up.

For a molecule $M(CNPh)_6$ constrained to have perfect Th symmetry, the ground state will be $(t_g)^6 = {}^1A_g$ the lowest excited states are MLCT states $(t_g)^5(t_u)^1$ and $(t_g)^5(t_g)^1$ ($2\,{}^1T_u + {}^1A_u + {}^1E_u$ and $2\,{}^1T_g + {}^1A_g + {}^1E_g$), respectively. Since the $(t_g)^5(t_g)^1$ one electron excitation corresponds to exciting an electron from the metal t_g orbitals (which are bonding) to the t_g π^* orbitals (the antibonding analog of the metal t_g) a distortion along a t_g, a_g, or e_g normal mode is parity allowed. The mode along which the ground state is distorted is the t_g symmetric bending mode which simultaneously reduces all the M-C≡N bond angles. Thus the data are clearly consistent with the operation of this mechanism.

Further evidence for the occurrence of a second order Jahn-Teller distorted ground state is obtained from the temperature dependence of the uv-vis spectra of $M(CNIph)_6$ and $M(CNDph)_6$ which are shown in Figures 13-16 . The spectra of these complexes in 2 MeTHF or 2 Me pentane show drastic changes in intensity in cooling to 77 K,suggestive of some sort of gross structural changes. As has been previously noted in the systems,[32,33] changes in the

Figure 13. Electronic absorption spectra of $Cr(CNIph)_6$ in 2-Methylpentane at 77 K (upper curve) and 298 K (lower curve).

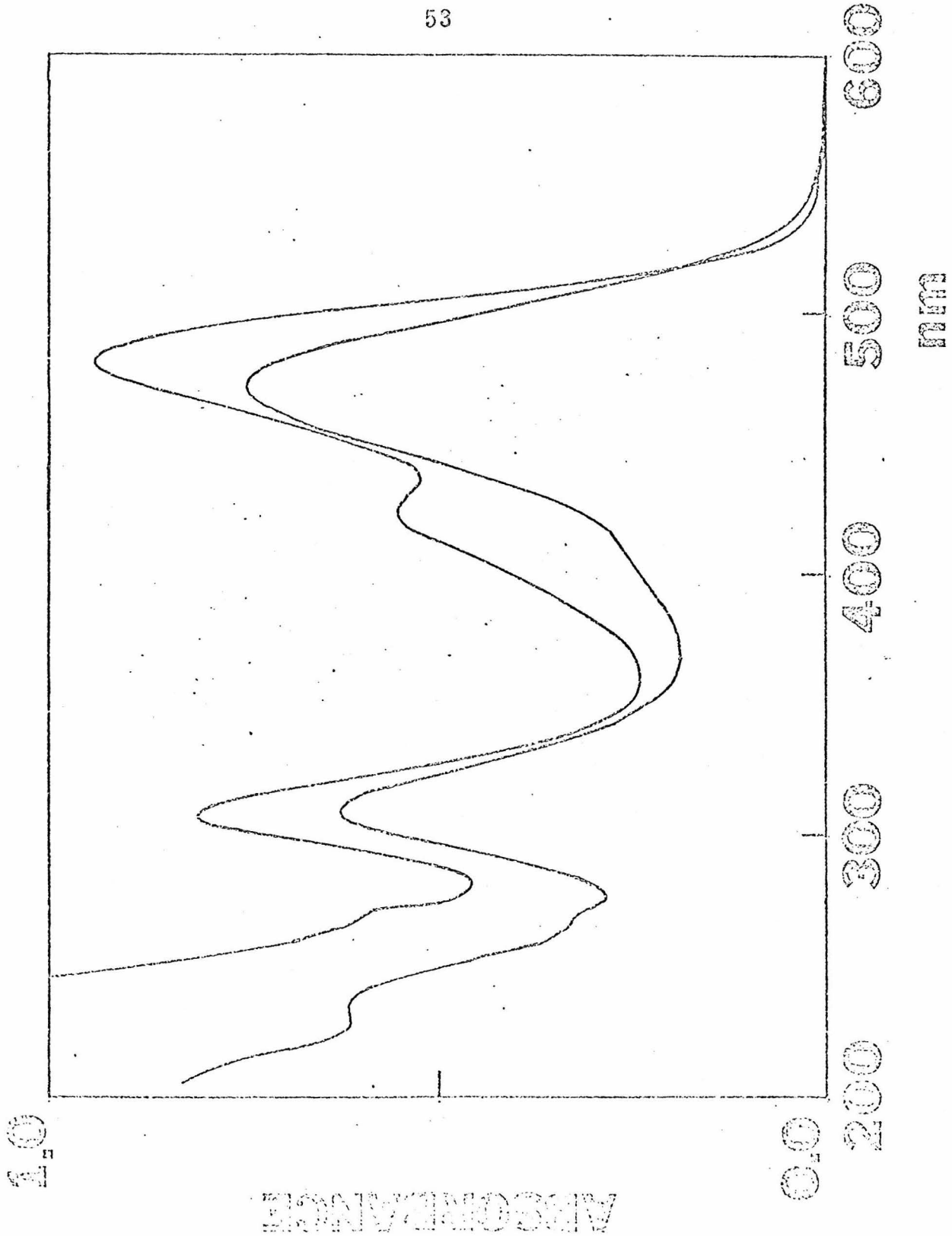
ABSORBANCE
1.0
0.0
2000
3000
400
500
600
nm

Figure 14. Electronic absorption spectra of $Mo(CNIph)_6$ in 2-Methylpentane at 77 K (upper curve) and 298 K (lower curve).

3500
3000
2500
2000
1500
1000
500
WAVENUMBERS (CM-1)
ABSORBANCE
100%
0%

spectra with temperature such as these are also consistent with second order Jahn-Teller distorted ground state. Based on simplistic arguments from the spectra in Figure 15 it appears that the structure of the complexes containing CNDph become less distorted on cooling while those of CNIph become more distorted. Both of these cases as well as the case where no change is observed (Ar =Ph) have previously been observed in other systems.[31-33] Low temperature solution infrared data would be especially helpful in accessing the structural changes which are occurring on cooling in these $M(CNAr)_6$ systems.

In view of the complicated nature of the spectral details involved in assigning more specific labels to the various electronic transitions present in these systems it would not be warranted to pursue assignments further without data of more detailed nature. Of major importance here is that these ambiguities are recognized and could be resolved by expanding the simplified model presented. Further experiments designed to elucidate the electronic structure of these complexes are in progress.

The Electronic Spectra of the d^5 Systems

The spectral data for $Mn(CNPh)_6^{2+}$ and $Cr(CNIph)_6^{+}$ are given in Table 11. The ground state of both of these complexes has been shown[5,12] to be low spin $(t_g)^5$. The low temperature spectrum of $[Mn(CNPh)_6](PF_6)_2$ exhibits a structured low energy system (18.2, 20.4 kK) attributable to the LMCT transition $\sigma(CNPh) \rightarrow t_g$. Similar

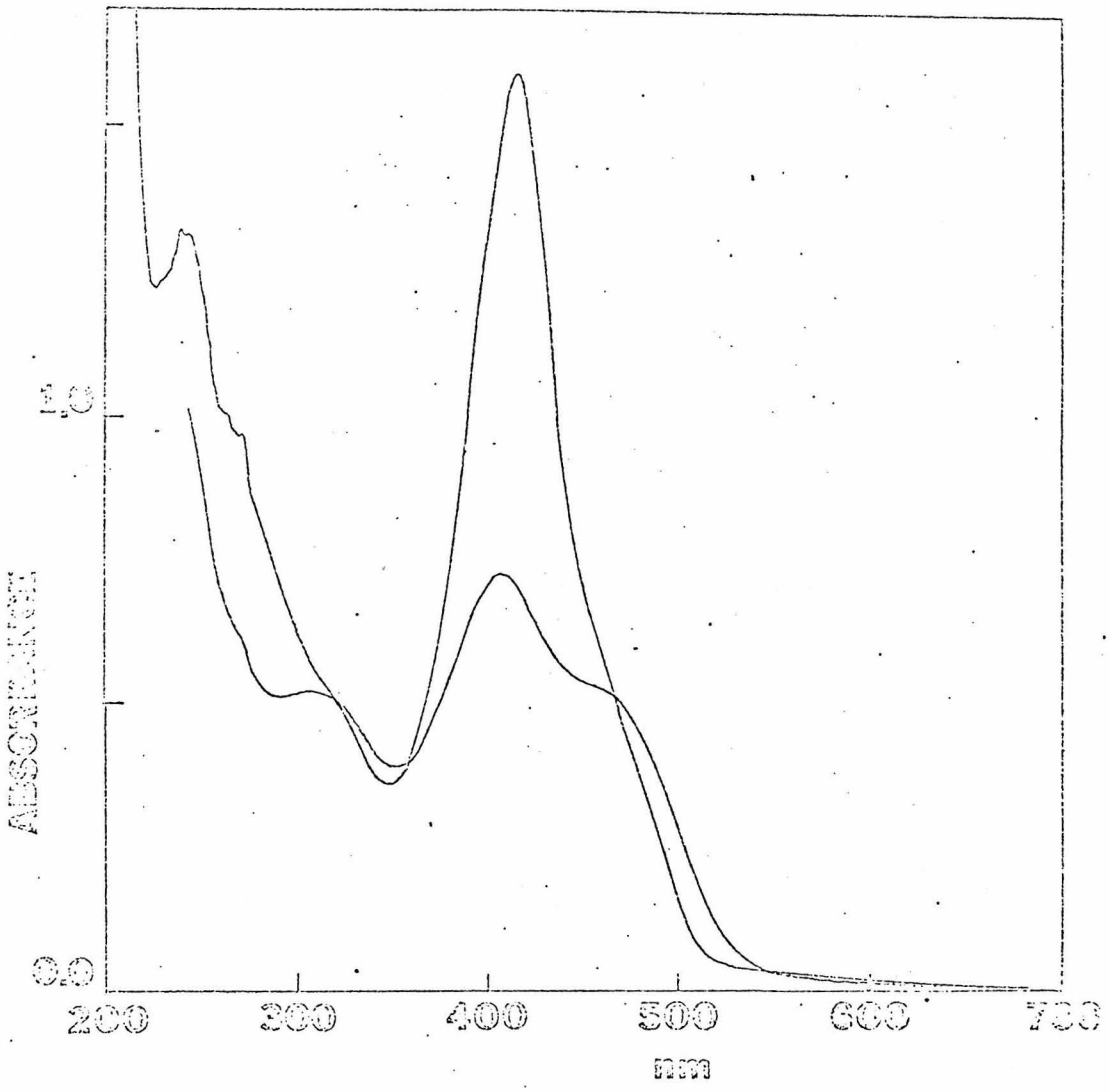

Figure 15. Electronic absorption spectra of $Cr(CNDPh)_6$ in 2-Methylpentane at 77 K (upper curve) and 298 K (lower curve).

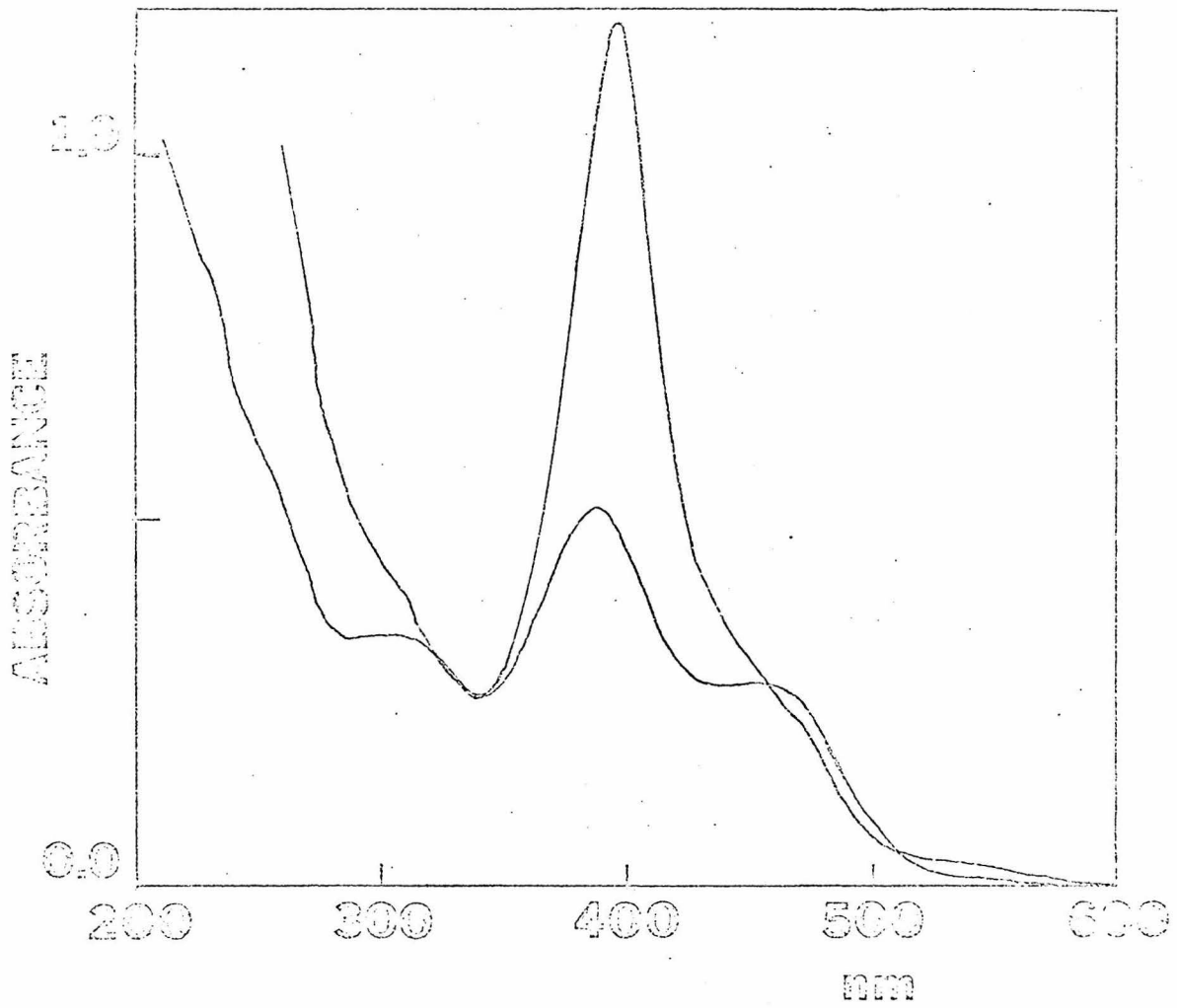

Figure 16. Electronic absorption spectra of $Mo(CNDph)_6$ in 2-Methylpentane at 77 K (upper curve) and 298 K (lower curve).

Table 11. Electronic Absorption Spectra of $M(CNAr)_6^z$ Complexes

Complex	λ_{max}, nm	$\bar{\nu}_{max}$, kK	$\epsilon_{max} \times 10^{-3}$	Assignment
$Cr(CNIph)_6^+$ [a]	440	22.7	41.9	$d\pi \rightarrow \pi_v^*L$
	371	27.0	42.7	$\sigma(CNIph) \rightarrow d\pi^*$
	355	28.2	45.0	
	320	31.3	45.8	$d\pi \rightarrow \pi_h^*L$
$Mn(CNPh)_6[PF_6]$ [b]	490	20.4	4.6	$\sigma(CNPh) \rightarrow d\pi^*$
	293	34.1	31.0	$d\pi \rightarrow \pi_v^*L$
	273	36.6	43.0	$d\pi \rightarrow \pi_v^*L$

[a] Acetonitrile.

[b] 8:2:1 ethanol/methanol/diethylether.

low energy LMCT bands have been observed in $Fe(CN)_6^{3-}$ and $Mn(CN)_6^{4-}$.[34] The two observed peaks in the $\sigma(CNPh) \rightarrow t_g$ system may be assigned to components of a vibrational progression in the symmetrical C≡N stretching motion. The excited state value of about 2200 cm^{-1} for this vibration is reasonable.

The spectrum of $Cr(CNIph)_6^+$ is similar to the Mn(II) spectrum showing allowed MLCT bands at 36.2kK and 22.75 kK very close to the values for $Cr(CNIph)_6$. In addition the LMCT band which occurs at 18.2 and 20.4 kK in the Mn(II) system is observed at 28.2, 27.0 kK in the Cr(I) system. This substantial blue shift (8.6 kK) is in line with a net destabilization of the t_g level in Cr(I) relative to Mn(II) making the Cr(I) complex harder to reduce. Electrochemical redox potentials[12,35,36] are in line with this argument predicting a shift of about 5.5 kK in the LMCT band.

It is of some interest that the MLCT bands in the $(d\pi)^6$ $M(CNPh)_6^Z$ complexes are substantially lower in energy than corresponding peaks in $M(CO)_6^Z$ analogs (Table 12). The lower energies of $d\pi \rightarrow \pi^*$ transitions are probably due in part to the effects of enhanced σ donation in the CNPh complexes, which would tend to increase the electron density on the central metal, thereby raising the energies of both $d\pi$ and $d\sigma^*$ levels relative to carbonyl analogs. The splitting of $\pi^*CN(\pi_v^* < \pi_h^*)$ by interaction with aromatic ring orbitals must also play an important role, as judged by the high energy of the observed $d\pi \rightarrow \pi^*$ band in $Mn(CNMe)_6^+$ (43.1 kK).[8] Preferential stabilization of π_v^*, of course, is not

Table 12. Energies of MLCT Transitions in $M(CO)_6^z$ and $M(CNPh)_6^z$ Complexes

M	$d\pi \rightarrow \pi^*(CO)$, kK[a]	$d\pi \rightarrow \pi^*(CNPh)$, kK[b]
Cr(0)	35.7	21.8
	43.6	25.4
Mo(0)	34.6	22.1
	42.8	26.5
W(0)	34.7	22.4
	43.8	27.2
Mn(I)	44.5	29.4
	49.9	31.1

[a] Acetonitrile solution, 300 K; Ref. 34.

[b] This work.

available to alkylisocyanide ligands. It follows that stabilization of low-oxidation ground states of metals through $d\pi$ back donation to π_v^* should be much more pronounced in aryl- than in alkylisocyanide complexes.

Emission Properties

Introduction

The complexes $M(CNAr)_6$ where M = Cr, Mo, W and Ar = Ph, DPh, Iph, 4-ClPh were all found to show unstructured emission at 77 K in 2-MeTHF glass. The peak positions, width at half height, and excitation wavelengths are given in Table 13. Complexes of all three metals were also found to luminesce in fluid solutions of pyridine, Xylene, 2 MeTHF, 2 Me pentane, and Me cyclohexane. The emission maxima of $W(CNPh)_6$ and $W(CNIph)_6$ at 298 K were found to be only slightly solvent dependent (the values are given in Table 14). No emission at 298 K was observed from the Cr(I), Cr(II), Mn(I), Mn(II), Mo(I), Mo(II), W(I), W(II) complexes. The emission from the Cr(0) complexes at room temperature was extremely weak. Information regarding the room temperature emission properties of the complexes in pyridine are reported in Table 13 . The emission quantum yields for some selected complexes of Mo and W at 77 K are given in Table 15. The lifetimes of several of the complexes at 77 and 298 K in 2-Me-pentane are given in

Table 13. Emission Data[a] $M(CNAr)_6$ Complexes

	77 K			298 K[b]	
	Cr	Mo	W	Mo	W
Ph	590	559	571	613	638
	16,900 (1800)	17,900 (1100)	17,500 (900)	16,300 (2700)	15,700 (3200)
	400	450	450	420	420
Dph	579	548	563	619	613
	17,300 (2900)	18,200 (1400)	17,800 (1400)	16,200 (1600)	16,600 (1900)
	400	450	400	450	420
Iph	583	568	578	579	578
	17,200 (2100)	17,600 (1200)	17,300 (1150)	17,300 (2000)	17,300 (1800)
	380	450	400	450	420
p-PhCl	618	568	580	617	683
	16,200 (2400)	17,600 (800)	17,200 (810)	16,200 (3100)	15,800 (3000)
	400	450	450	450	420

[a] All spectra were corrected for phototube and monochromator response; maxima given in nm; energies are given in cm^{-1} (width at half-height); excitation wavelength in nm.

[b] Determined in pyridine solution.

Table 14. Emission Maxima[a] as a Function of Solvent at 298 K

	Iso-octane	p-Xylene	Pyridine
$W(Iph)_6$	571	576	581
$W(CNPh)_6$	--	591	603

[a] In nm.

Table 15. Emission Quantum Yields[a] at 77 K

$W(CNPh)_6$	0.93 ± 0.07
$W(pCNPhCl)_6$	0.68 ± 0.08
$W(CNDph)_6$	0.67 ± 0.10
$Mo(CNPh)_6$	0.78 ± 0.08
$Mo(pCNPhCl)_6$	0.71 ± 0.08

[a] Excitation wavelength 450 nm, $Ru(bipyridine)_3Cl_2$ (ϕ = 0.376 ± 0.037) optical densities were matched under the conditions of the measurements.

Table 16. EmissionLifetime Data for Selected $M(CNAr)_6$ Complexes

	τ Observed[a,b,c]	
	278 K	77 K
$Cr(CNIph)_6$	--	< 10 nanosec
$Mo(CNIph)_6$	43 ± 2 nanosec	40.2 ± 0.5 microsec
$W(CNIph)_6$	83 ± 2 nanosec	7.6 ± 0.5 microsec
$Cr(CNDph)_6$	--	<10 nanosec
$Mo(CNDph)_6$	21 ± 2 nanosec	22.8 ± 0.5 microsec

[a] Monitored at 580 nm.

[b] Measured by Steve Milder, California Institute of Technology.

[c] In 2-methylpentane.

Table 16. Typical emission spectra at 77 K are shown for $M(CNPh)_6$ (M = Cr, Mo, W) in Figures 17, 18, and 19.

Discussion

In view of the similarities in the absorption spectra and the gross similarities of the emission spectra, the luminescence observed in the complexes of all three metals is reasonably assigned to a ligand to metal charge transfer. The differences in the emission properties place the Mo and W complexes together while the Cr emissions have the more unique characters. The Stoke's shifts observed for the Cr complexes are larger than in the corresponding Mo and W complexes, suggesting that the excited state geometry in the Cr complexes is more distorted relative to the ground state. The emission half-widths for the Cr complexes are about a factor of two broader than the Mo or W complexes. The lifetimes of the Cr complexes' emission are much shorter ($<$ 10 msec vs. 50 μ sec at 77 K) than the Mo and W complexes.

The quantum efficiency at 77 K for the Mo and W complexes measured were all quite high while the Cr complexes were estimated to be at least a factor of 10 smaller. Thus in many aspects the emission arising from the Cr complexes is significantly different from that arising from the Mo and W complexes. Any model describing the nature of the emitting excited states must be able to account for these differences.

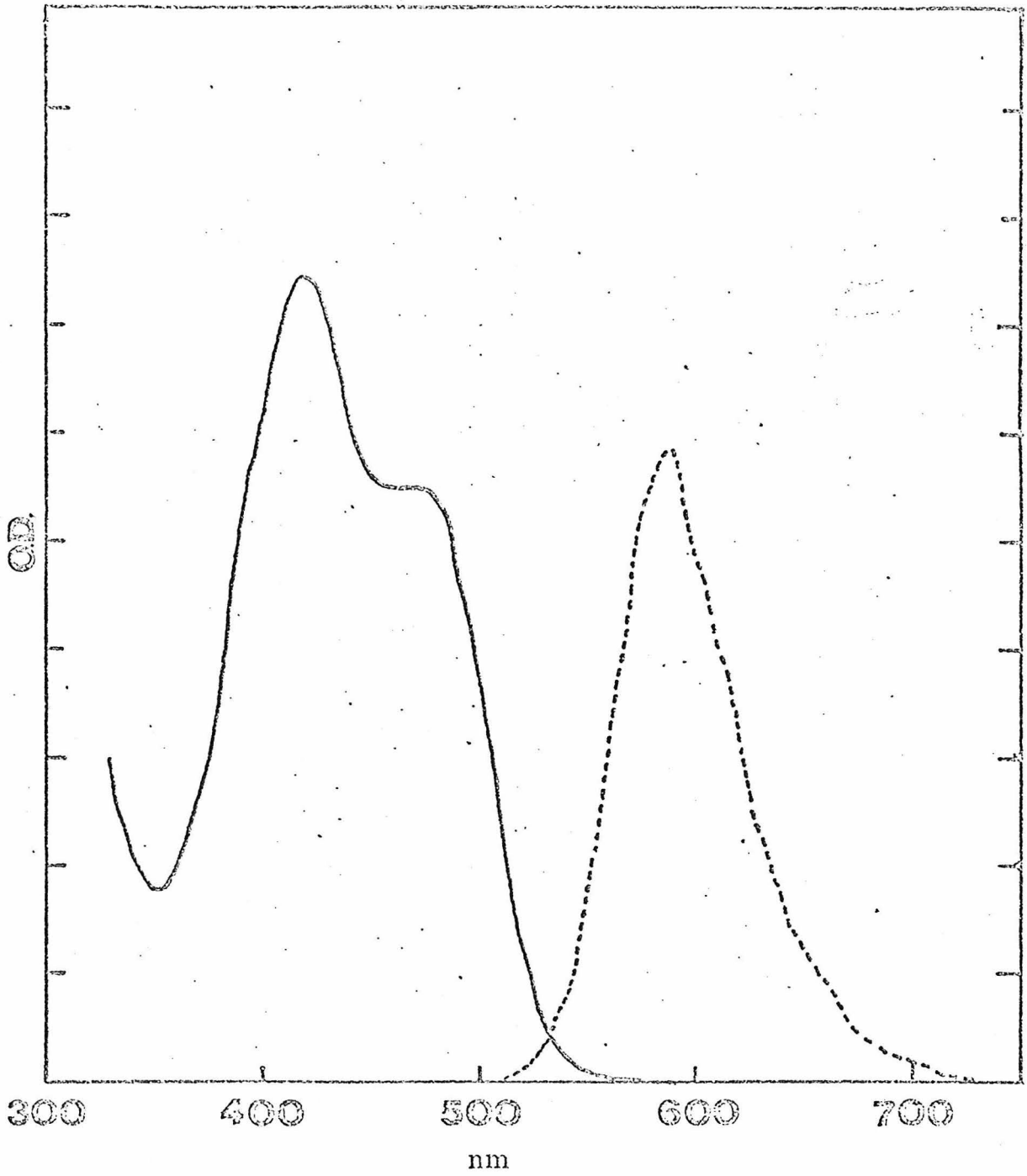

Figure 17. Absorption spectrum (——) and emission spectrum (---) of $Cr(CNPh)_6$ at 77 K in 2-methylTHF glass.

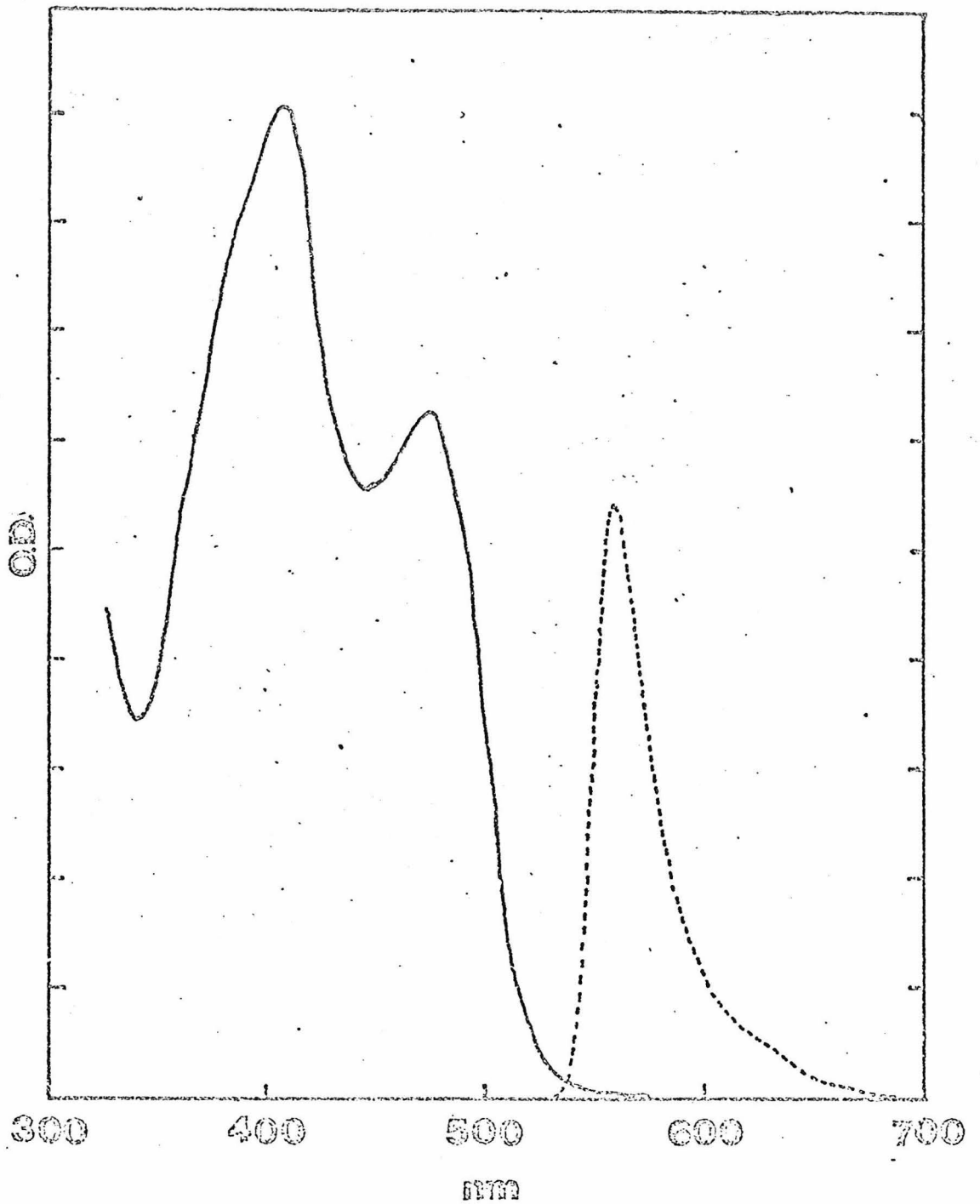

Figure 18. Absorption spectrum (——) and emission spectrum (---) of $Mo(CNPh)_6$ at 77 K in 2-methylTHF glass.

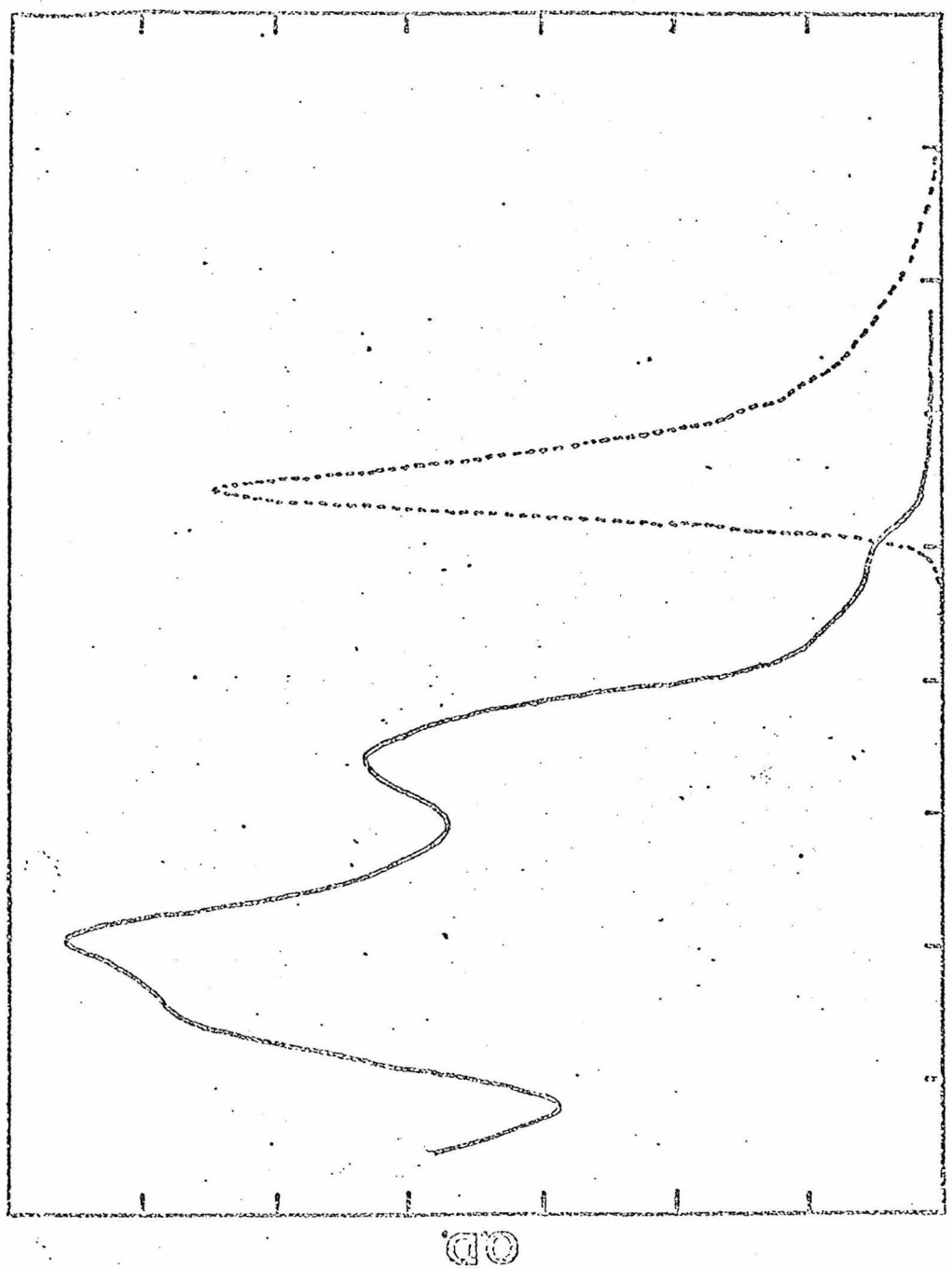

Figure 18. Electronic absorption spectra of $Mo(CNDph)_6$ in 2-Methylpentane at 77 K (upper curve) and 298 K (lower curve).

Characterization of the emitting states in terms of a good working model is also important in describing their photochemical properties. Since excitation spectra are similar to the absorption spectra in all cases, rapid relaxation to the lowest emitting state(s) is suggested. This suggests that excitations into the bands at $\lambda > 300$ nm will populate the emitting state(s) which are also responsible for the observed photochemistry. Thus by studying the nature of the emitting state(s) in these complexes, one most likely is studying the states responsible for the observed photochemistry.

The model which best seems to explain the limited emission results here is the model of Crosby,[28,29] et al. which has been developed to explain the emission spectra of $Ru(bipy)_3^{2+}$ complexes. The results are so strikingly similar for the $M(CNAr)_6$ (M = Cr, Mo, W) and $M(bipy)_3^{2+}$ (M = Fe, Ru, Os) that a common model is literally demanded. First, a short review of the absorption emission properties of $M(bipy)_3^{2+}$ complexes is in order.

The absorption spectra of the low spin d^6 complexes of the form $M(bipy)_3^{2+}$ where M = Fe, Ru, Os are extremely similar to one another,[37-43] showing intense ($\epsilon \sim 10,000 - 20,000$) MLCT bands of virtually identical energy and band shape. The spectrum of the Os complex,[40] however, has some additional bands of moderate intensity ($\epsilon \sim 4000$) at lower energy. Spectra are reproduced here from references 37 and 40 (Figure 20).

Figure 20. Spectral data for $M(bipy)_3^{2+}$ (M = Fe, Ru, Os); (A) from ref. 37; (B) from ref. 40; (C) from ref. 40.

A

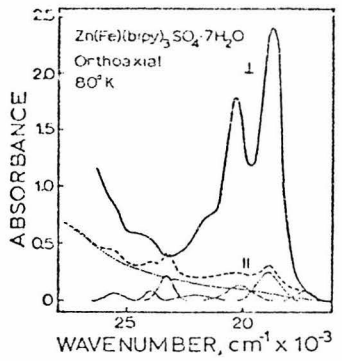

Figure 16.—Crystal thickness, 1.9 mm; approximately 4×10^{-3} mole % iron. Dotted curves are analysis of parallel spectrum only.

B

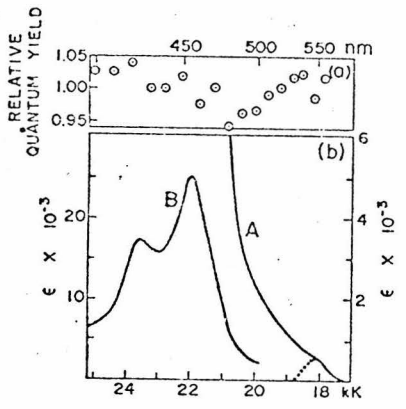

Figure 2. Relative quantum yield (a) and absorption spectrum (b) of tris(2,2′-bipyridine)ruthenium(II) chloride in an ethanol–methanol glass (4:1, v/v) at 77°K: (a) 3.4×10^{-7} *M* in a 1.76-cm cell; (b) curve A (right-hand scale), 1.32×10^{-4} *M* in a 1.76-cm cell; curve B (left-hand scale), 2.65×10^{-5} *M* in a 1.76-cm cell. Dotted curve is the estimated contribution of the singlet-triplet absorption.

C

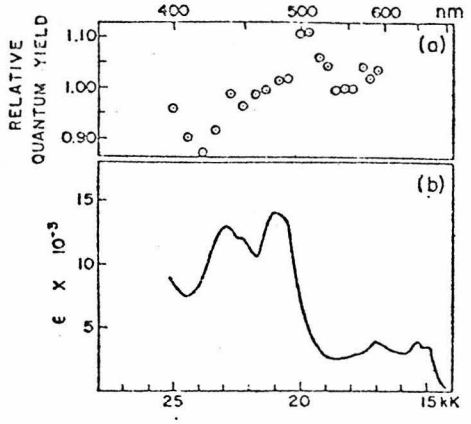

Figure 5. Relative quantum yield (a) and absorption spectrum (b) of tris(2,2′-bipyridine)osmium(II) iodide in an ethanol–methanol glass (4:1, v/v) at 77°K: (a) 7.2×10^{-7} *M* in a 1.76-cm cell, (b) 6.73×10^{-5} *M* and 1.35×10^{-5} *M* in 1.76-cm cells.

The gross emission characteristics of these systems are that no emission is observed for the Fe system while intense emission is observed for the Ru[44] and Os[40] systems.

In the case of the Os complex, the emission band is found to show good overlap with the low intensity absorption peaks, while the emission spectrum of the Ru complex barely overlaps the higher intensity absorption band.[40] That the Fe complex shows no CT emission is supported by the work of Piper, et al.,[37] who have shown that a weak d-d band is probably present on the low energy absorption tail of the intense charge transfer transition.

The emission lifetimes and quantum yields (at 77 K) are similar for the Ru and Os complexes but show some differences. Both the quantum yield and the lifetime are smaller in the Os complex (discussions of this are in references 40 and 45).

In Table 17 the data available on the emission properties of the isocyanides and the bipyridine complexes are compared. The similarities are striking.

The detailed work on the emission spectrum of $Ru(bipy)_3^{2+}$ and related complexes has led to the formulation of a weak coupling model[28,29] which explains all the experimental results for the Ru complexes. In simple terms the model for MLCT transitions couples the d^5 low spin core levels with the excited electron placed in an appropriate ligand orbital. Since the excited electron is localized mostly on the ligands, electron repulsion terms between it and the core electron are much smaller than those found in normal d-d

Table 17. Comparison of $M(CNAr)_6$ (M = Cr, Mo, W) and $M(bipy)_3^{2+}$ (M = Fe, Ru, Os) Complexes

	$M(CNAr)_6$		
	ϕ 77 K	τ 77 K	τ 298 K
Cr	<0.07	<10nsec	--
Mo	~ 0.7	40.2 μsec	43 nsec
W	~ 0.7	7.6 μsec	83 nsec
	$M(bipy)_3^{2+}$		
Fe	--	--	--
Ru	0.376	5.21 μsec	0.6 nsec
Os	0.0348	0.89 μsec	19.2 nsec

transitions (100 cm^{-1} vs.>1000 cm^{-1}). Since the spin orbit coupling in Ru is several thousand cm^{-1}, the spin orbit perturbation terms are far more important than the terms arising from the electron repulsion. Thus the emission from the lowest excited states of $Ru(bipy)_3^{2+}$ has been shown to possess both singlet and triplet-character. Since both types of states can be thermally populated, at appropriate temperatures, the spin allowedness of the emission is a strong function of temperature.

This model, when applied to the isocyanides of Cr(0), Mo(0), W(0) gives the following results consistent with the data. As one goes to the heavier metals, the spin orbit coupling and the crystal field splitting should increase. Thus in the Cr complexes where the spin orbit coupling and the crystal field splittings are smaller, the lowest CT excited states will have a small amount of d-d character mixed into them and the energy differences between "singlet" and "triplet" spin orbit states will be small. The emission bands arising from such a "CT singlet with some d-d character" should have: 1) a very short lifetime since it is mainly spin allowed due to the small value of λ; 2) good overlap with the CT "singlet" absorption band; 3) show a fair Stoke's shift and 4) be reasonably broad. This description fits the emission spectra observed for the Cr complexes very well.

The heavier metals (Mo and W) where the spin orbit coupling is quite large and the crystal field splitting is also large, should show: 2) lessened d-d character in the emission band(s) resulting

in narrower emission band(s) and a smaller Stoke's shift; 2) longer lifetimes reflecting the increasing "forbiddeness" of the emission modified to account for the exact thermal population of the spin orbit states populated and 3) enhanced absorption due to the spin orbit allowed transitions like those seen in the low energy region of $Os(bipy)_3^{2+}$. (These are observed in the W spectra, see Figure 19 .)

Since only detailed lifetime and quantum yield measurements as a function of temperature can sort out the exact disposition of states contributing to the emission spectra, further discussion at this time seems unwarranted. It will be interesting to see if the model (which works very well in describing the properties of $Ru(bipy)_3^{2+}$) stands up under close scrutiny for the isocyanide complexes of Cr, Mo, W. Clearly the model should work even better for the isocyanide complexes since the absorption bands are much more intense (ϵ = 70,000 vs. 11,000) suggesting that they are much purer MLCT in character than even the MLCT transitions in $M(bipy)_3^{2+}$.

One other experimental result of interest is the very small shift in the emission peak in the 77 K vs. 298 K data for the complexes of CNIph (Table 18). Usually emission maxima determined in a low temperature matrix will be at higher energy than when they are determined in fluid solution since the relaxation of the excited state geometry is not as complete in the "hard" matrix obtained in a

glassing solvent. The fact that all the complexes show a red shift in the absorption spectra at 298 K except complexes of CNIph suggests that complexes of this ligand are much less subject to excited state geometry changes probably a consequence of the increased steric requirements of the ligand.

The solution emission maximum for $W(CNPh)_6$ and $W(CNIph)_6$ vary only slightly with solvent (see Table 14) suggesting that the emitting state(s) is not perturbed to the extent of forming an exiplex in the better donor solvent. The smaller shifts found in $W(CNIph)_6$ compared to $W(CNPh)_6$ suggest that interaction of the solvent with $W(CNAr)_6$ occurs to a greater extent in the complex of the less hindered ligand.

Table 18. Shift in Emission Maxima from 77 K Measurements in 2-Methyl THF and 298 K Measurements in Pyridine

CNAr	Mo	W
Ph	1600 cm^{-1}	1800 cm^{-1}
Dph	2000 cm^{-1}	1200 cm^{-1}
Iph	300 cm^{-1}	0 cm^{-1}
pPhCl	1400 cm^{-1}	1400 cm^{-1}

Photochemistry

The photochemical behavior of $M(CNAr)_6$ complexes (M = Cr(0), Mo(0), W(0); Ar = Ph, IPh) has been studied. Two major reaction pathways were discovered: substitution and electron transfer.

Substitutional Photochemistry

The Photochemistry of the Cr(0), Mo(0), and W(0) Complexes. When $M(CNAr)_6$ complexes are irradiated in neat pyridine, spectral changes occur which suggest the following reaction:

$$M(CNAr)_6 + py \xrightarrow{h\nu} M(CNAr)_5py + CNAr$$

In Figures 21-23, the infrared spectral changes upon irradiating $M(CNAr)_6$ are shown. The UV-VIS spectral changes are shown in Figures 24-29 . It is immediately noticed that for complexes of a given ligand, the spectral changes are very similar for all three metals. The infrared spectra show $\bar{\nu}$(CN) for the liberated isocyanide occurring at 2115 cm^{-1} for Ar = Iph and 2125 cm^{-1} for Ar = Ph. Most easily interpreted is the infrared spectrum shown in Figure 22 which shows the photolysis of $Cr(CNIph)_6$ in neat pyridine. The two bands at 2002 cm^{-1} and 1960 cm^{-1} due to $Cr(CNIph)_6$ decrease in intensity on photolysis while three major bands grow in at 1930, 2030, and 2115 cm^{-1}. (The last of which is $\bar{\nu}$(CN) of free CNIph.) From their relative positions and band shapes, it is likely that the 1930 cm^{-1} band is due to an E stretching mode of a $M(CN)_5L$ C_{4v} fragment, involving mainly the four planar CN groups while the 2030 cm^{-1} band

is one of the two allowed A_1 modes, probably due to the unique CNR ligand. The other allowed A_1 mode may be weak or obscured by the broad E mode. Spectra of the corresponding carbonyl complexes $M(CO)_5L$ have been studied.[46] Although the spectra are similar, they differ enough that the assignments presented here should by no means be taken as conclusive. Further irradiation of this $Cr(CNIph)_5py$ complex shows the 2030 cm^{-1} band decreasing in intensity while the 1930 cm^{-1} band remains virtually unchanged with (Figure 23) the peak at 2115 also increasing in intensity suggesting further release of CNIph with the formation of trans $Cr(CNIph)_4py_2$ which from symmetry considerations should have a single IR active E mode in nearly the same position as the E mode of $Cr(CNIph)_5py$.

The structural information obtained from the IR of the photolysis product of $Cr(CNPh)_6$ in pyridine is much harder to interpret (Figure 21). Interpretation of this spectrum is complicated by the ability of the M-CN linkage to be extremely bent since the ligands' steric requirements do not force linearity upon the M-CN units as does the CNIph ligand. Uv-vis spectral changes are also consistent with this notion since the spectrum of $Cr(CNPh)_5py$ consists of one peak at 410 nm with a long tail extending out to 600 nm (Figure 24). This might be due to gross distortion of the $M(CNAr)_5$ portion of the molecule since the $M(CNIph)_5py$ spectra are "normal" having a low energy peak in each case in the same region where the tail for $M(CNPh)_5py$ occurs (Figure 27). Similar spectra (uv-vis and IR) are obtained in all cases for the Mo and W complexes (Table 19).

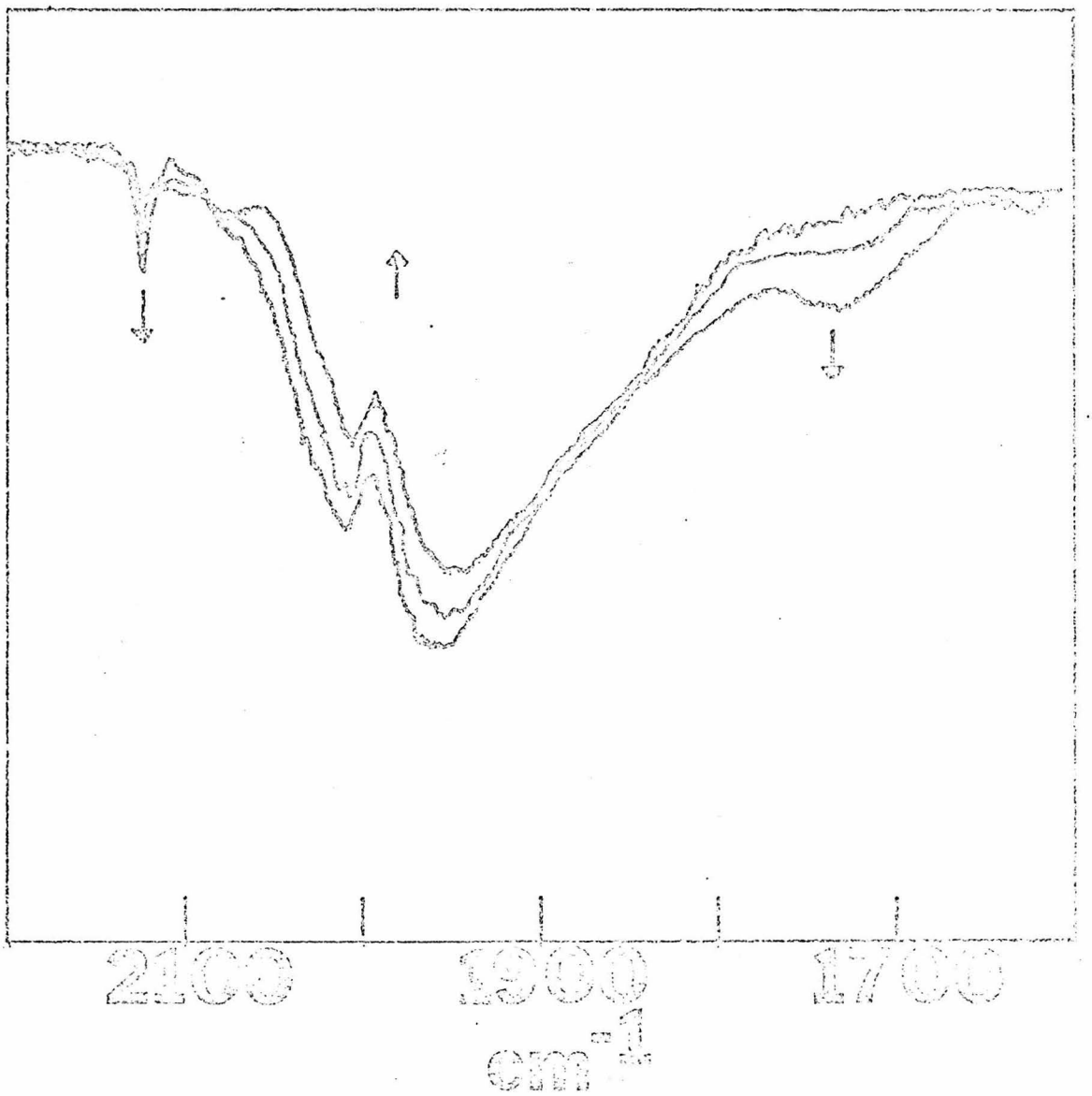

Figure 21. The photolysis of $Cr(CNPh)_6$ in neat pyridine ($\lambda > 313$ nm). Spectra are about 1 min. apart.

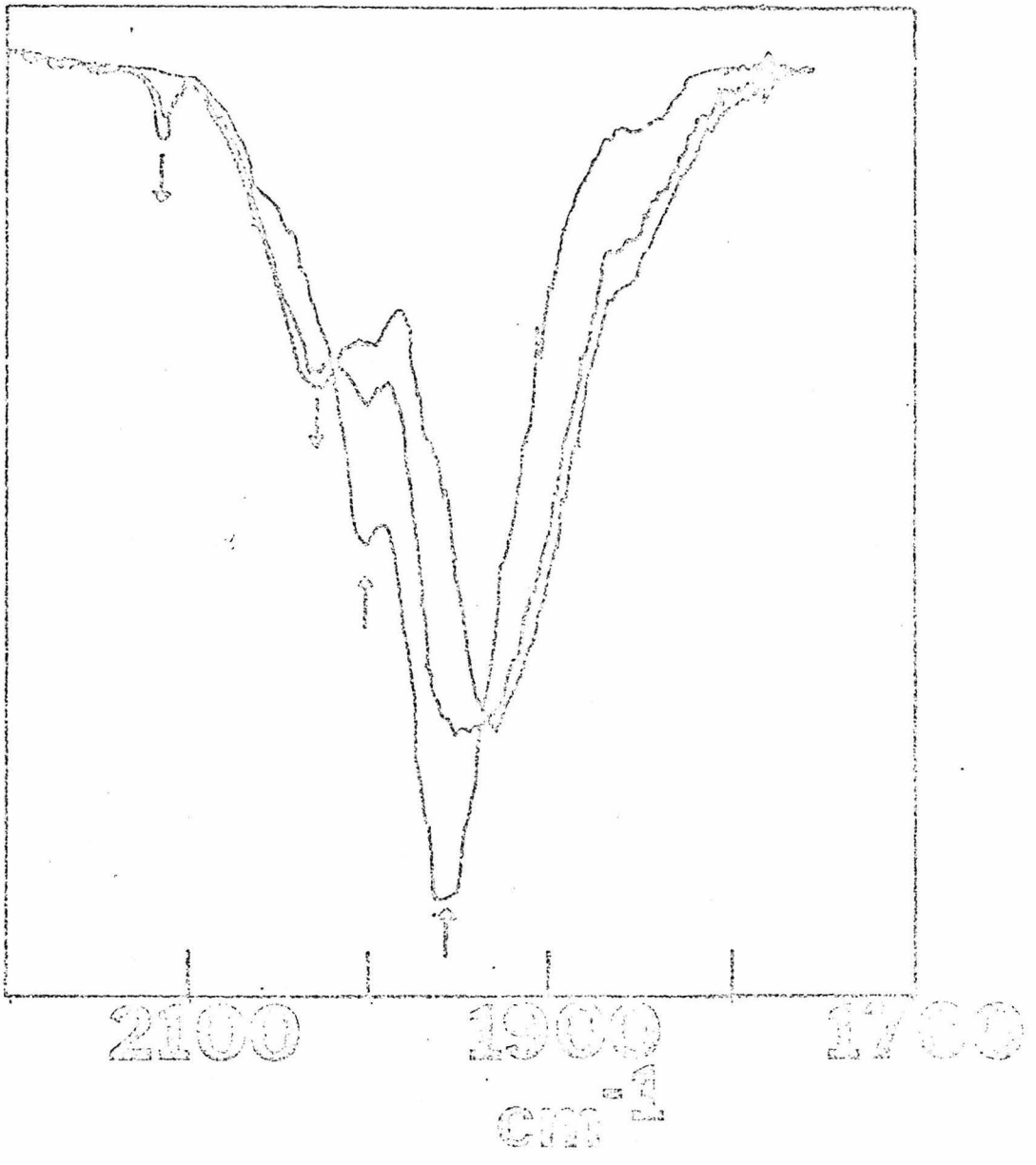

Figure 22. The photolysis of $Cr(CNIph)_6$ in neat pyridine ($\lambda > 313$ nm). Spectra are about 1 min. apart.

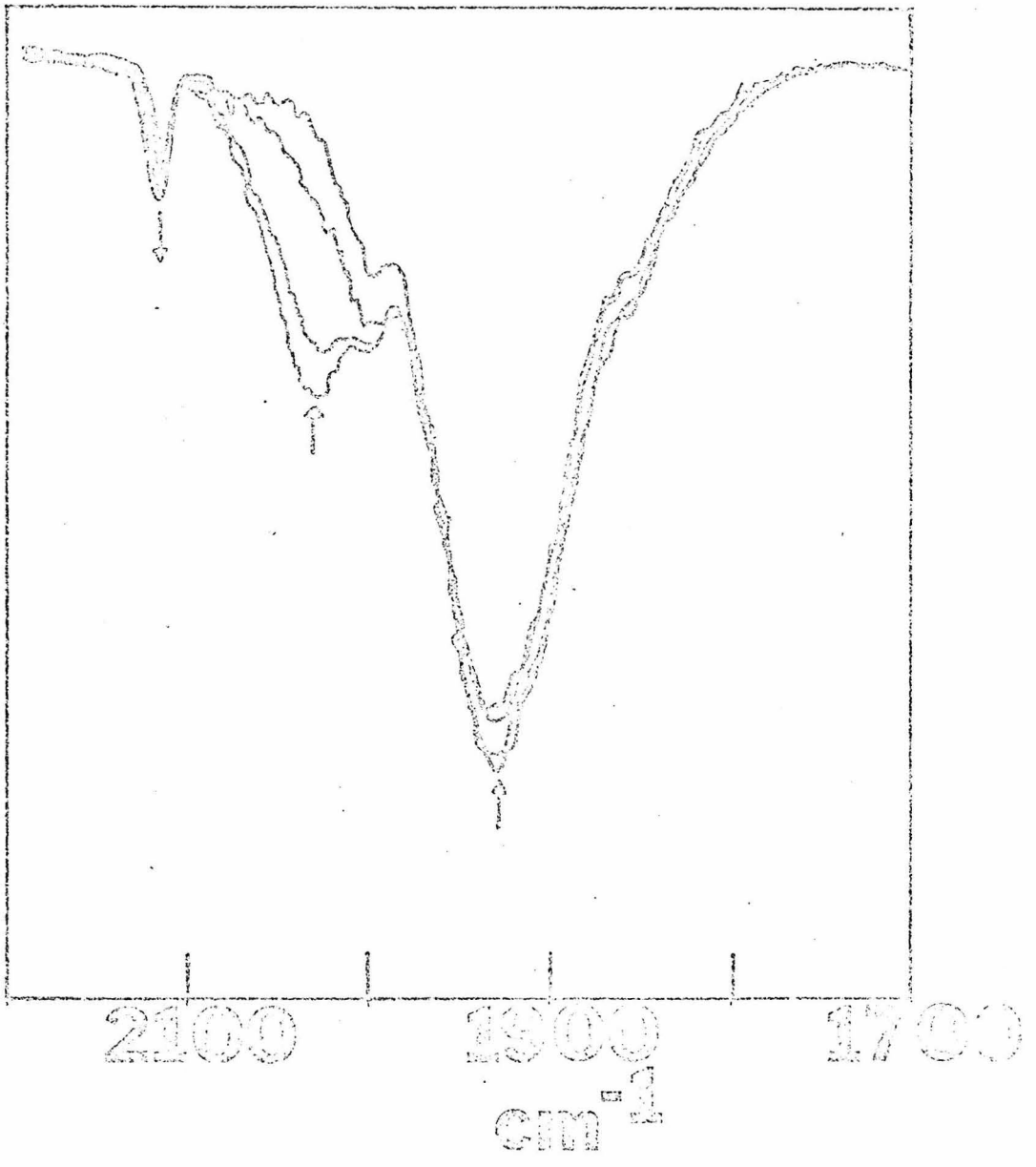

Figure 23. Continuation of the photolysis in Figure 22.

Figure 24. The photolysis of $Cr(CNPh)_6$ in neat pyridine by room light. About 10 sec. between spectra.

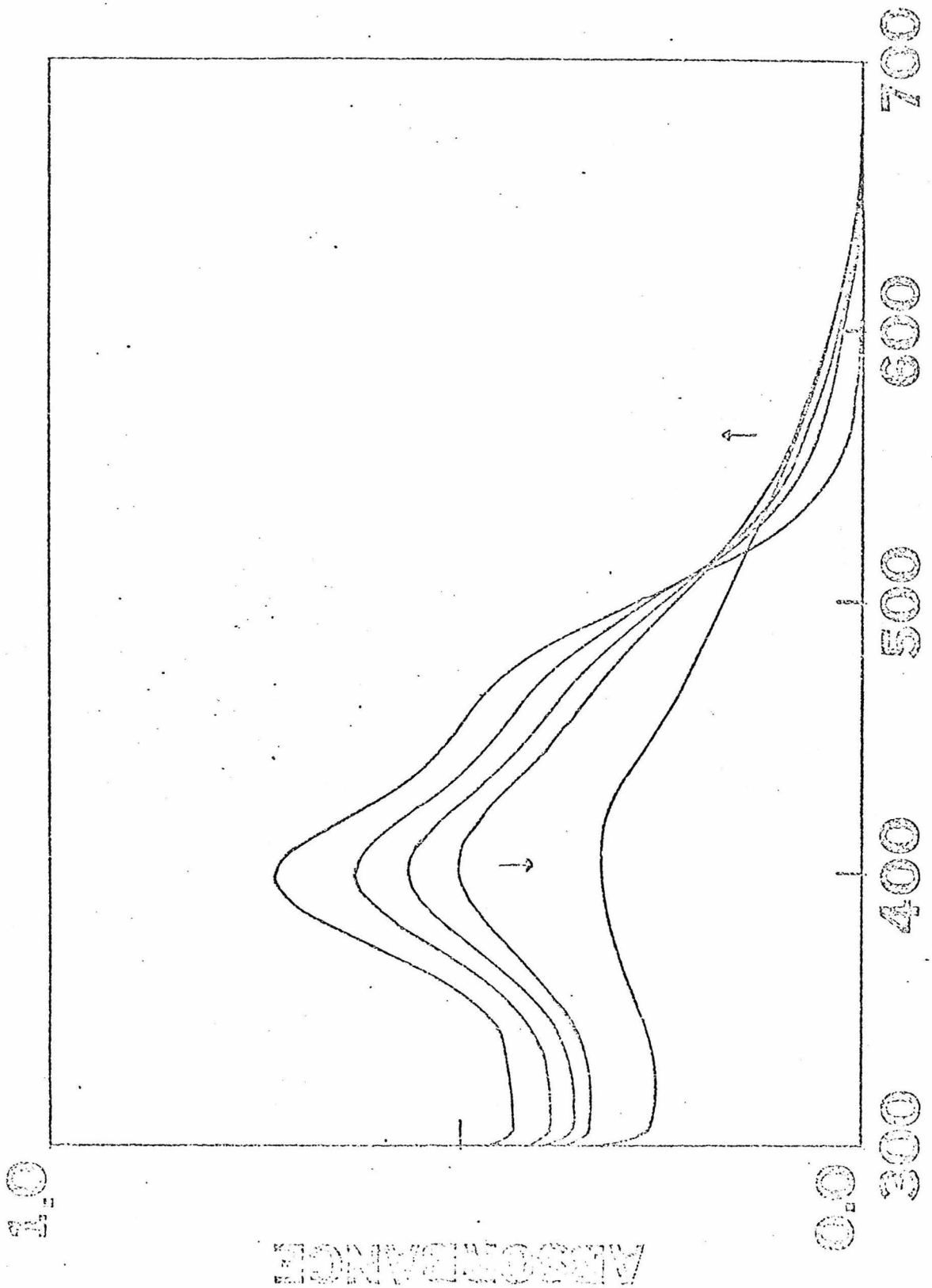
ABSORBANCE
0.0
300
400
500
600
700
nm

Figure 25. The photlysis of $Mo(CNPh)_6$ in neat degassed pyridine ($\lambda > 313$ nm). Spectra are ~30 sec. apart.

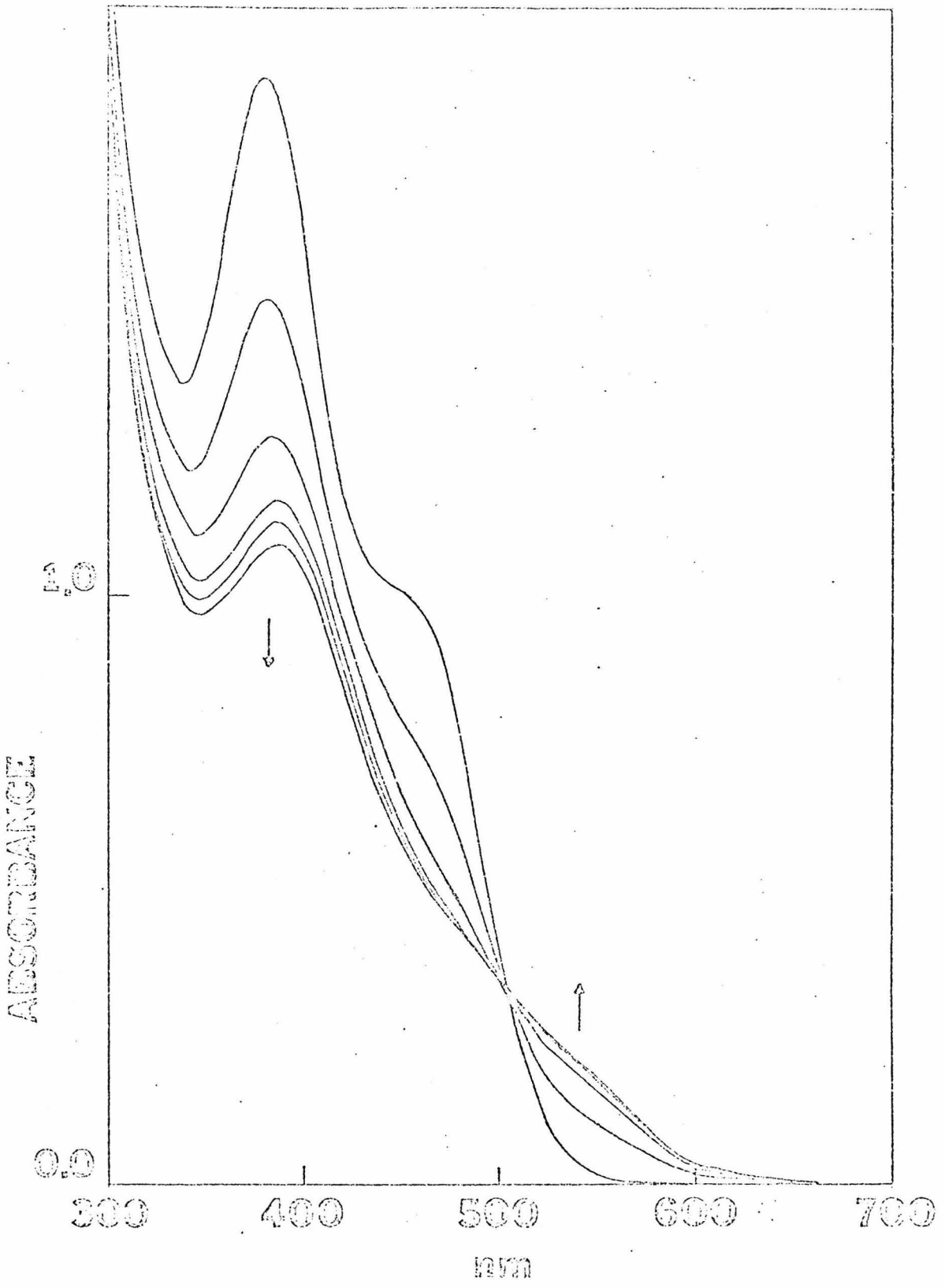
ABSORBANCE
1.0
0.0
300
400
500
600
700
nm

Figure 26. The photolysis of $W(CNPh)_6$ in neat, degassed pyridine ($\lambda > 313$ nm). Spectra are several minutes apart.

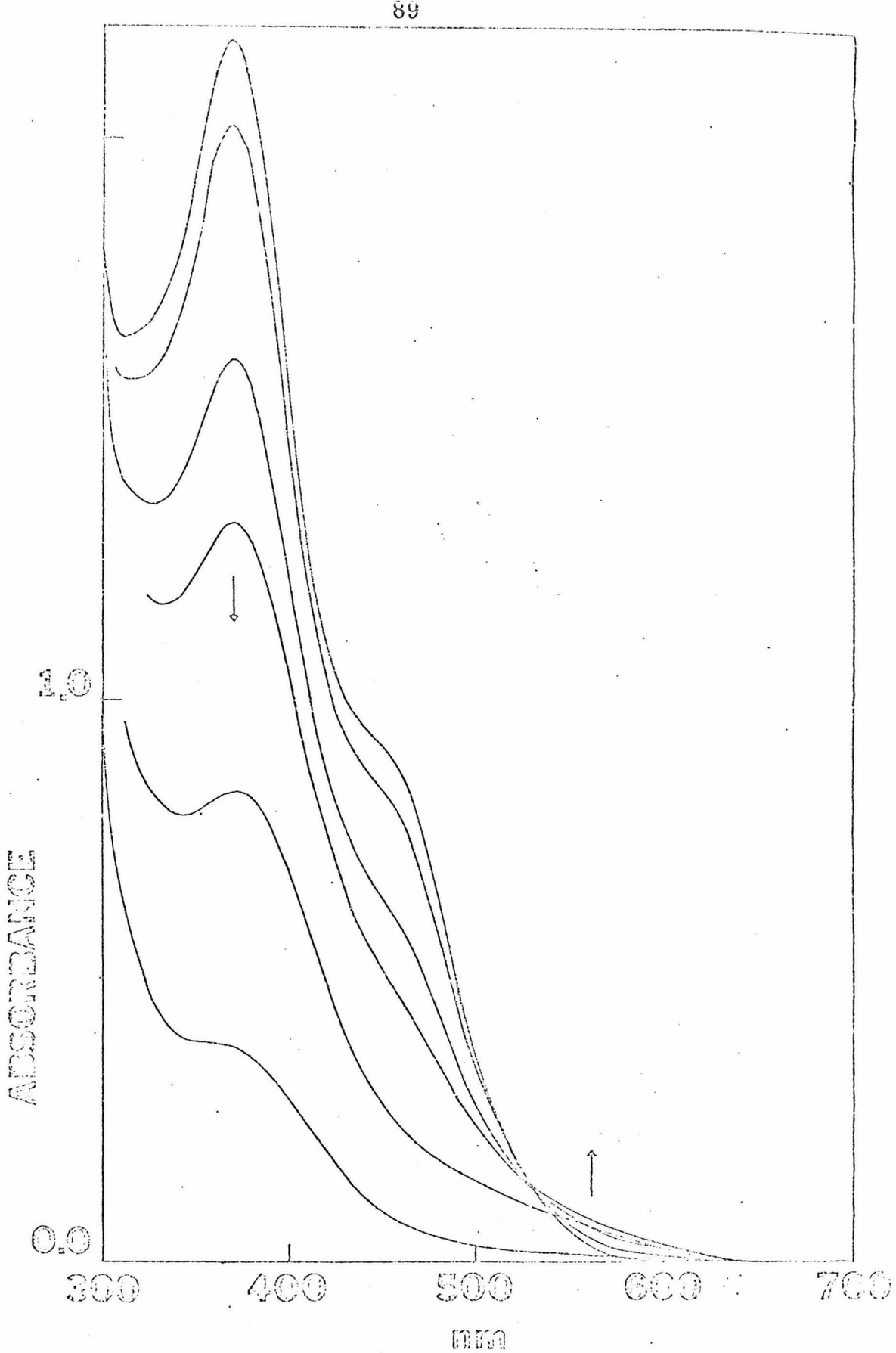
ABSORBANCE
1.0
0.0
300
400
500
600
700
nm

Figure 27. The photolysis of $Cr(CNIph)_6$ in neat pyridine by room lights. About 10 sec between spectra.

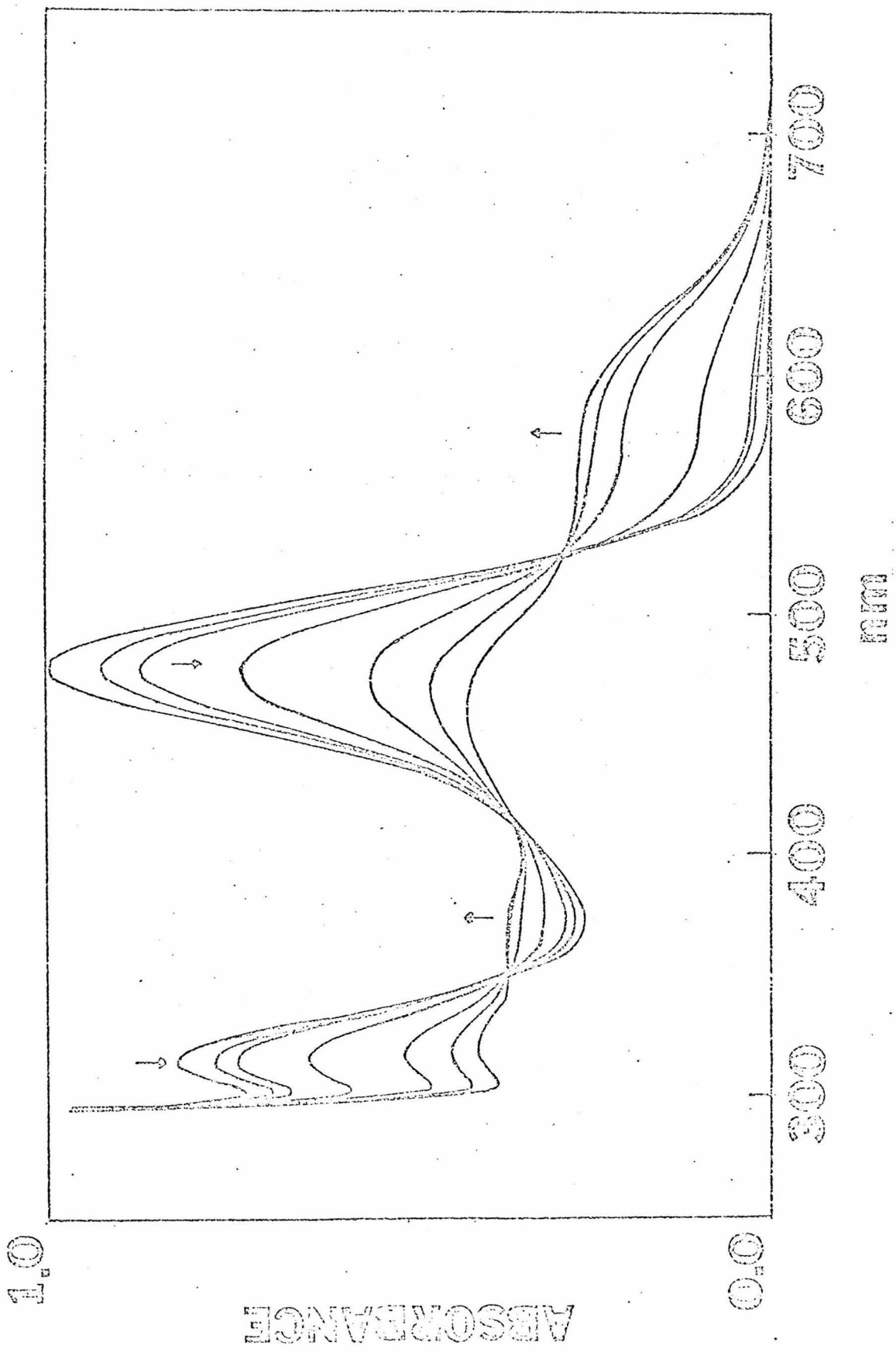
1.0
0.0
ABSORBANCE
300
400
500
600
700
nm

Figure 28. The photolysis of $Mo(CNIph)_6$ in neat, degassed pyridine ($\lambda > 313$ nm). About 2 min. between spectra.

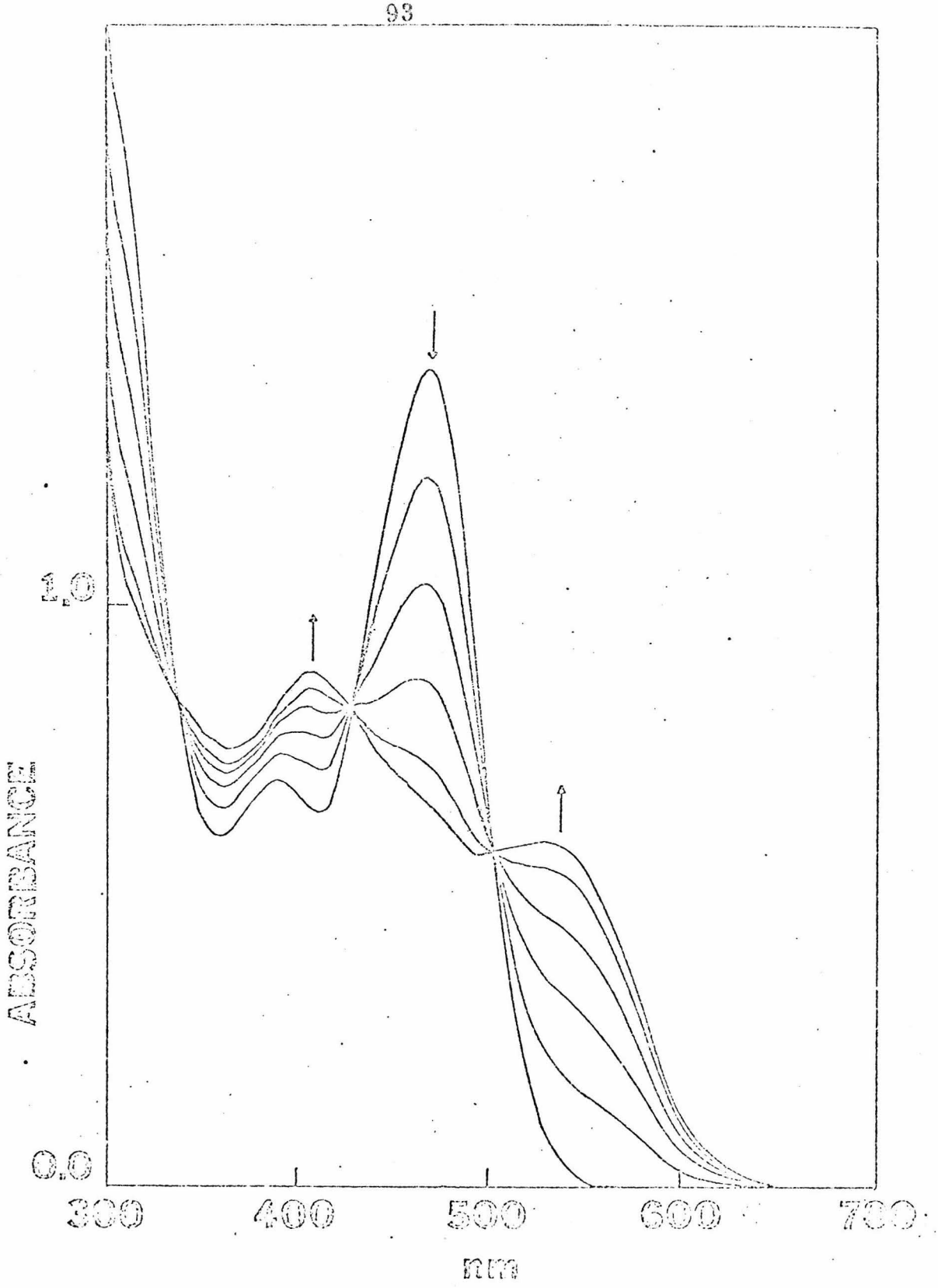
ABSORBANCE
1.0
0.0
300
400
500
600
700
nm

Figure 29. The photolysis of $W(CNIph)_6$ in neat, degassed pyridine ($\lambda > 313$ nm). About 5 min. between spectra.

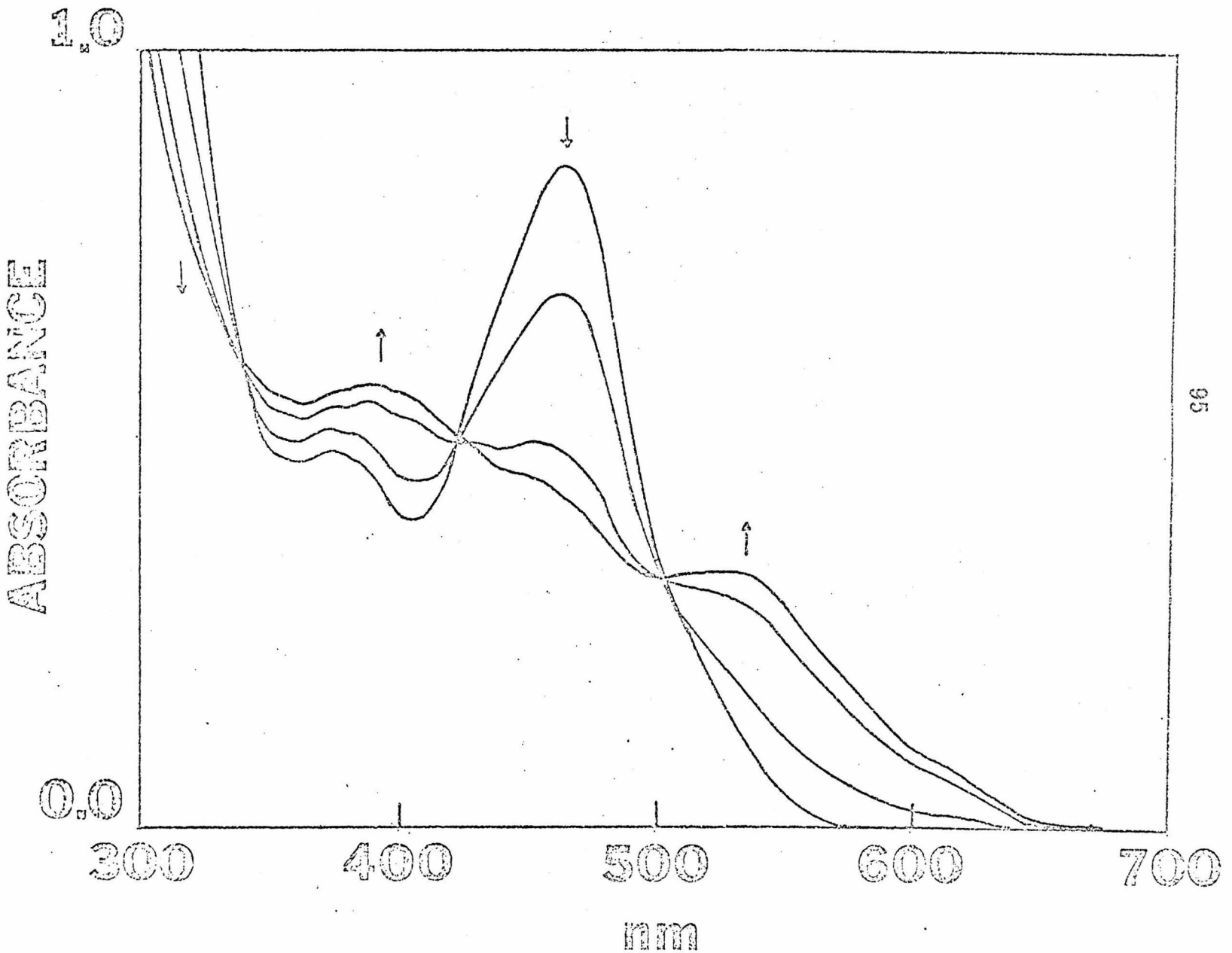
1.0
ABSORBANCE
0.0
300
400
500
600
700
nm

Table 19. Spectral Data for the Photochemical Substitution Reactions of $M(CNAr)_6$

Complex	uv-vis nm ($\epsilon \times 10^{-3}$)	$\bar{\nu}$(CN) in cm^{-1}
$Cr(CNPh)_5py$[a]	410 (37.8)	2080, 1940, 1730
$Mo(CNPh)_5py$	388 (41.8	--
$W(CNPh)_5py$	370 (41.0)	--
$Cr(CNIph)_5py$	320 (30.4)	1930, 2030
	372 (27.4)	
	461 (31.9)	
	568 (19.0)	
$Mo(CNIph)_5py$	405 (44.7)	--
	530 (30.0)	
$W(CNIph)_5py$	386 (57.5)	--
	452 (45.4)	
	630 (33.3)	
$Cr(CNIph)_5benz$[b]	318 (31.7)	1925
	428 (34.8)	
	475 (34.0)	
	610 (22.0)	
$Cr(CNPh)_5benz$	410 (35.1)	--
	550 (9.4)sh	
$Mn(pCNPhCH_3)_5py^+$	344 (45.1)	2075, 2160 wk
	410 (15.3)	

[a] py = pyridine.

[b] benz = benzylamine.

To confirm the fact that pyridine was indeed being introduced into the coordination sphere of the metal rather than the formation of a five coordinate species such as $M(CNAr)_5$, $Cr(CNPh)_6$, and $Cr(CNIph)_6$ were irradiated in benzylamine. Spectral changes in these cases are shown in Figures 30-31. Comparison of the spectral data for $Cr(CNAr)_5$benz with $Cr(CNAr)_5$py show similarities since both py and benzylamine are good N donors, but the peak positions are not in precisely the same place as they would be if a common product $M(CNAr)_5$ was formed, thus further supporting the formation of $M(CNAr)_5L$ rather than $M(CNAr)_5$.

Assignment of the $M(CNAr)_5$py UV-VIS spectra at this time would be premature, but the large values of the extinction coefficients for the bands suggests that they be considered LMCT or more likely MLCT bands. Although complexes such as $M(CO)_5$py have been made and the spectra assigned,[47-49] the analogous low energy peaks have been assigned as d-d transitions. Clearly, the high degree of similarity between the $M(CNAr)_5L$ and $M(CO)_5L$ spectra suggests that only by a careful study of both systems together can reasonable assignments be made.

Isolation of the $M(CNAr)_5$py complexes was attempted unsuccessfully. This is probably due to the high boiling nature of the CNAr ligands so that in a solution of $M(CNAr)_5$py in py one could pump off the pyridine but not the CNAr. (Isolation of the analogous $M(CO)_5$py complexes is much easier since the CO released on photolysis can be easily removed from the reaction mixture.) After photolysis

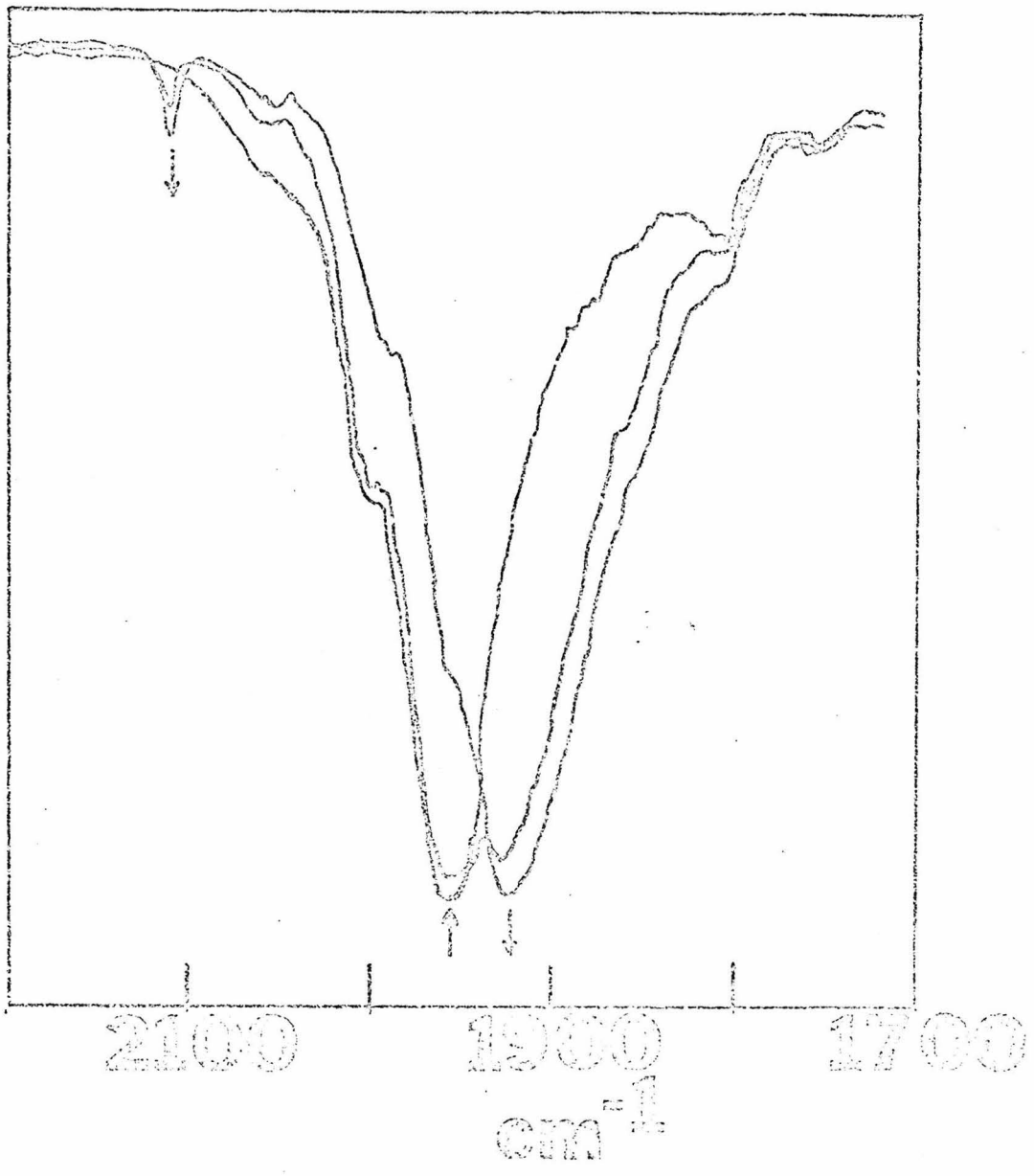

Figure 30. The photolysis of $Cr(CNIph)_6$ in neat benzylamine. Room light photolysis.

Figure 31. The photolysis of $Cr(CNIph)_6$ in neat benzylamine. Room light photolysis.

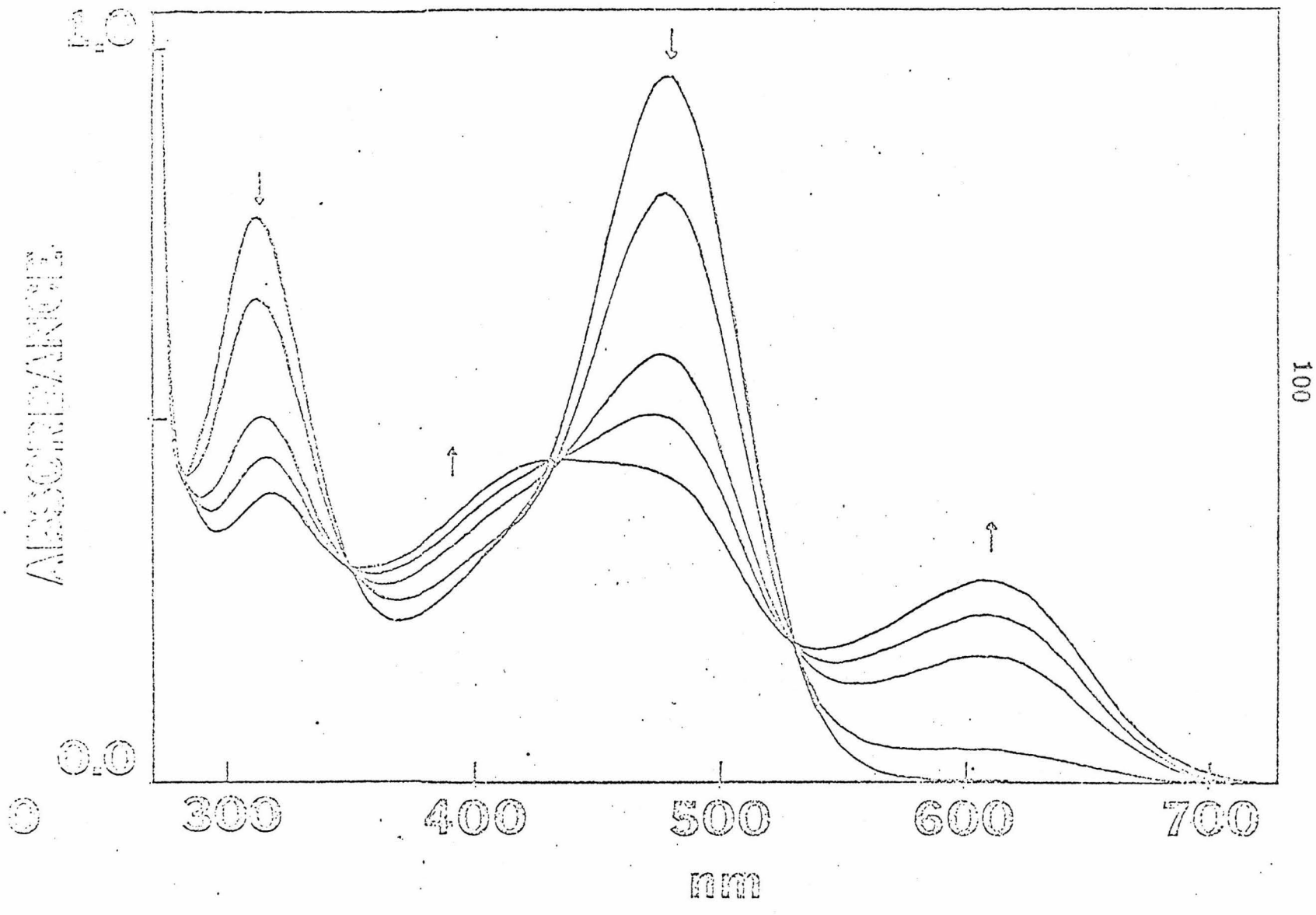
1.0
0.0
ABSORBANCE
0
300
400
500
600
700
nm
100

of $Cr(CNIph)_6$ in pyridine so as to obtain the IR shown in Figure 22 a brown solid was isolated by pumping of the excess pyridine under vacuum. This brown solid immediately decomposed on dissolving in undegassed chloroform. Over a period of months, the brown solid sample (which smelled the unique smell of CNIph) slowly changed to the red $Cr(CNIph)_6$ accompanied by the distinct odor of pyridine.

The Photochemistry of $Mn(pCNPhCH_3)_6ClO_4$

The UV-VIS (Figure 32) and IR (Figure 33) spectral changes which occur when $Mn(pCNPhCH_3)_6^+$ is irradiated in neat pyridine are very similar to those found for the chromium complexes. The infrared spectrum shows a band at 2125 cm^{-1} corresponding to released p-$CNPhCH_3$ and bands at 2160 and 2075 cm^{-1} which are attributable to $Mn(pCNPhCH_3)_5py^+$. The quantum yields for disappearance of $Mn(pCNPhCH_3)_6^+$ are 0.22 ± 0.01 and 0.21 ± 0.01 at 313 and 366 nm, respectively. These quantum yields are similar to the yield found on irradiating the analogous $Cr(CNAr)_6$ complexes.

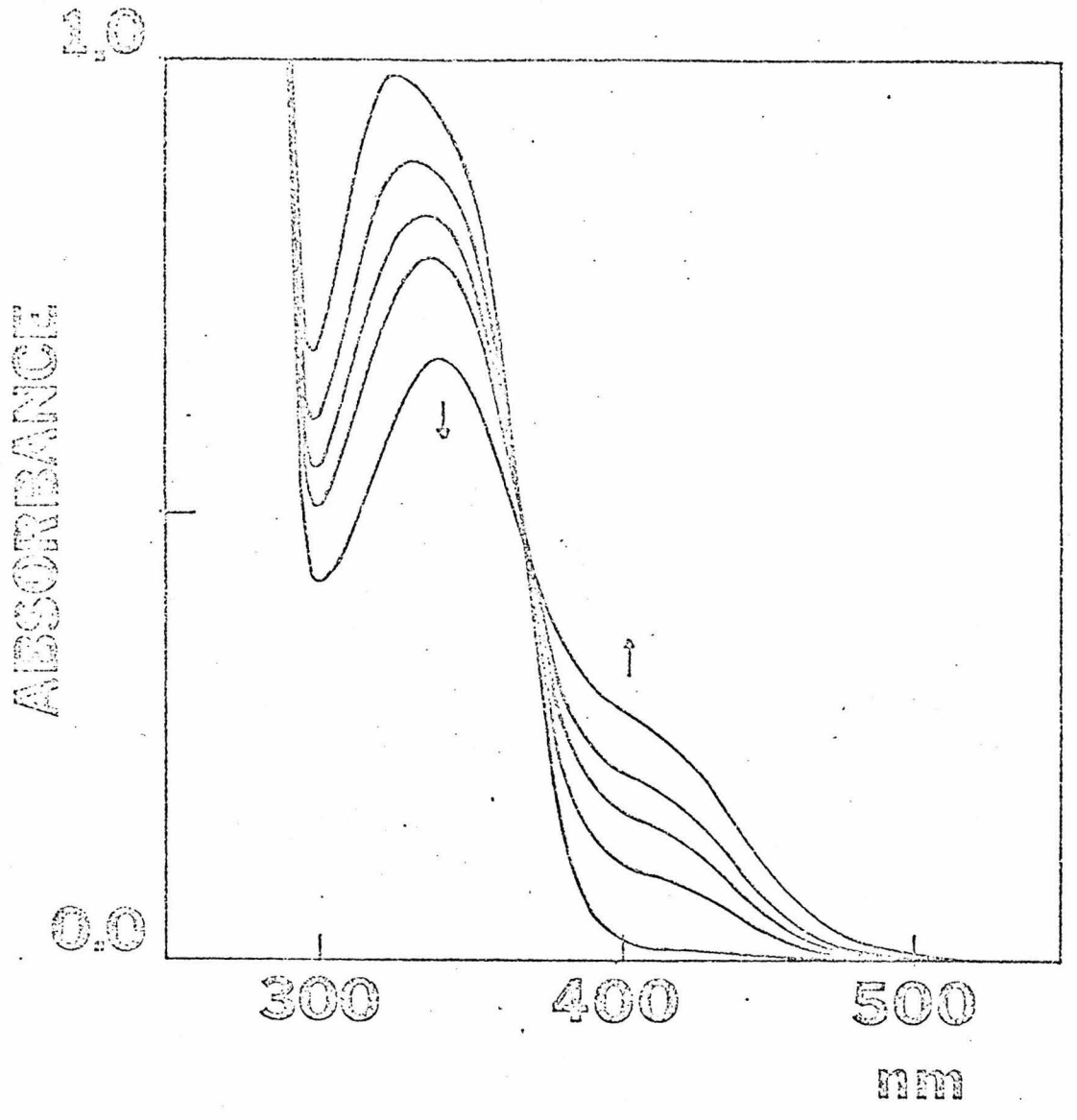

Figure 32. The photolysis of $Mn(pCNPhCH_3)_6ClO_4$ in neat pyridine ($\lambda > 313$ nm).

Figure 33. The photolysis of $Mn(pCNPhCH_3)_6ClO_4$ in neat pyridine ($\lambda > 313$ nm).

Mechanistic Considerations

Of primary interest is the large variation in the photochemical quantum yield of $M(CNAr)_5$ py obtained with changes in both the metal and the aryl group. Appearance quantum yields at 436 and 313 nm are given in Table 20 for M = Cr(0), Mo(0), W(0) and Ar =Ph and Iph. The mechanics of measuring the quantum yields are discussed in detail in the experimental section. At a given wavelength, the substitution quantum yield shows a large decrease in going to the heavier metals (Cr > Mo > W) and in the heavier metals, the complex of the more hindered ligand has a lower quantum yield. The substitution quantum yield is moderately wavelength dependent only for $Cr(CNPh)_6$, $Cr(CNIph)_6$, and $Mo(CNPh)_6$ the values being about a factor of two larger at 313 nm than at 436 nm.

The identical values for the quantum yields of $Cr(CNPh)_6$ and $Cr(CNIph)_6$, and their identical wavelength dependences suggest that these two complexes both substitute by the same mechanism. Since the complex with the hindered ligand has just as high a quantum yield as the unhindered complex, a standard dissociative mechanism is suggested, such as follows:

1) $ML_6 \xrightarrow{h\nu} ML_6^*$

2) $ML_6^* \rightarrow ML_5 + L$

3) $ML_5 \xrightarrow{L'} ML_5L'$

4) $ML_5 \xrightarrow{L} ML_6$ (free L in solution)

5) $ML_5 \cdots L \rightarrow ML_6$ (cage recombination)

Table 20. Quantum Yields for the Reaction $ML_6 \xrightarrow{py} ML_5py + L$ in Neat Pyridine

	313 nm	366 nm	436 nm
$Cr(CNPh)_6$	0.54 ± 0.01		0.23 ± 0.01
$Mo(CNPh)_6$	0.11 ± 0.001		0.055 ± 0.001
$W(CNPh)_6$	0.010 ± 0.001		0.011 ± 0.001
$Cr(CNIph)_6$	0.55 ± 0.01		0.23 ± 0.01
$Mo(CNIph)_6$	0.022 ± 0.01		0.022 ± 0.001
$W(CNIph)_6$	$<1\times10^{-4}$ ± 100%		$<3\times10^{-4}$ ± 100%
$Mn(pCNPhCH_3)_6ClO_4$	0.22 ± 0.01	0.21 ± 0.01	

Step (1) involves excitation of the complex to some reactive excited state either by direct irradiation or by some internal relaxation process from a higher excited state. Step (2) is a purely dissociative process which does not depend on the nature or concentration of the incoming ligand L' (pyridine). Step (3) is a rapid step in which the coordinatively unsaturated five coordinate intermediate is trapped by L' producing a product molecule of ML_5L'. Step (4) should also be a fast step but since the concentration of L' is at least 10^6 times greater than L should be negligible. A few words should be said about step (5), which is the rapid recombination in the solvent cage of the ML_5 species and L. This step could be an important one and tends to decrease the overall quantum yield for the reaction. Since all of the complexes are very similar in electronic properties and the solvent is the same in all cases, this process, if important, should tend to reduce the quantum yield of all the complexes reacting via a dissociative mechanism.

The quantum yields for the W complexes, however, show a marked dependence on the steric requirements of the isocyanide, decreasing by more than a factor of 100 in going from L = CNPh to L = CNIph. This behavior suggests that the substitution mechanism for the W complexes shows some associative character. Several mechanisms could be envisioned:

Scheme 1: Nucleophilic attack on the excited state forming an electronically excited seven coordinate intermediate

$$WL_6 \xrightarrow{h\nu} WL_6^*$$

$$WL_6^* + L' \rightarrow [WL_6L']^*$$

$$WL_6L'^* \rightarrow WL_5L' + L$$

Scheme 2: Similar to Scheme 1 except the seven coordinate intermediate has no excess electronic energy.

$$WL_6 \xrightarrow{h\nu} WL_6^*$$

$$WL_6^* + L' \rightarrow [WL_6L']^{\ddagger}$$

$$[WL_6L']^{\ddagger} \rightarrow WL_5L' + L$$

Scheme 3: Weak nucleophilic attack on the excited state by L', helping L to leave.

$$WL_6 \xrightarrow{h\nu} WL_6^*$$

$$WL_6^* + L' \rightarrow WL_5L' + L$$

The mechanism in Scheme 1 involves the formation of an exiplex with the incoming ligand L'. This type of intermediate with the seventh ligand bound only in the excited state might show up in an emission experiment as a very red shifted emission.[50] Experimentally, if the emission is shifted very much, it would occur in a spectral region (λ em $\geq$ 700 nm) which is very hard to

observe with a typical phototube. As previously discussed, the emission maxima of the W complexes are only slightly shifted in nucleophilic solvents (pyridine) from their position in p-xylene. Although exiplex formation might be occurring, it was not observed spectroscopically.

Schemes 2 and 3 are very similar, varying only in the lifetime of the seven coordinate intermediate. In Scheme 2, the seven coordinate intermediate is formed by attack of L' on the excited state of WL_6, but the seven coordinate intermediate has lost its excess electronic energy. Thus, it finds itself unstable with respect to both $WL_6 + L'$ and $WL_5L' + L$ but in a shallow potential well. This intermediate would be similar to one which could be envisioned in a thermal substitution reaction occurring via attack of L' on a ML_6 species. A species of this nature, seven coordinate, d^6 seems unlikely to have any sort of minimum in its potential surface since the only empty metal acceptor orbitals in a ML_6 low spin d^6 molecule are very high in energy.

Scheme 3, which is the most likely mechanism, is conceptually analogous to Scheme 2 except there is no minimum along the energy surface. The incoming nucleophile attacks the excited state causing a M--L bond to be broken as the nucleophile forms a bond to the excited state of ML_6. This mechanism extrapolates to a dissociative mechanism when the bond formation between the nucleophile and the electronically excited ML_6 molecule does not occur.

Electron Transfer Photochemistry

Characterization of Products

When $M(CNAr)_6$ complexes are photolyzed in chloroform, net oxidation of the metal occurs with concomitant formation of Cl^-. The extent of oxidation depends on the nature of the aryl group. In Figures 34-36, the spectral changes (UV-VIS and IR) are shown when $M(CNIph)_6$ complexes (M = Cr(0), Mo(0), W(0)) are irradiated. Irradiation of $Cr(CNIph)_6$ in CCl_4 produces a yellow solid which analyzes for $Cr(CNIph)_6Cl$ and has similar spectral properties to all the $M(CNIph)_6$/$HCCl_3$ products generated photochemically in solution. The IR data for the $M(CNIph)_6$ products show single $\bar{\nu}(CN)$ stretches at 2065 cm^{-1}, 2050 and 2040 cm^{-1} for M = Cr, Mo, and W, respectively. All the data, $\bar{\nu}(CN)$ positions and UV-VIS spectra suggest the common, $M(CNIph)_6^+$, formulation for these photoproducts (Table 21).

Further support of this formulation is the work of Triechel, et al.[12] in which complexes of the form $Cr(CNAr)_6PF_6$ have been synthesized from $Cr(CNAr)_6$ and $AgPF_6$. These complexes have been formulated as low spin d^5 systems on the basis of their magnetic moments. Since the crystal field splitting is usually much larger for the second and third row metal ions than for the analogous first row metal, it seems reasonable to also formulate the $M(CNIph)_6^+$ (M = Mo, W) complexes as low spin d^5. The IR spectral data in the $\bar{\nu}(CN)$ region for all the $M(CNIph)_6^+$ complexes are quite similar to the IR spectra of Triechel for the $Cr(CNAr)_6^+$ complexes.

If $M(CNPh)_6$ (M = Mo, W) complexes are photolyzed in degassed chloroform, the spectral changes shown in Figures 37-38 are observed.

Figure 34. The photolysis of $Cr(CNIph)_6$ in neat chloroform. Room light photolysis with about 5 sec. between spectra.

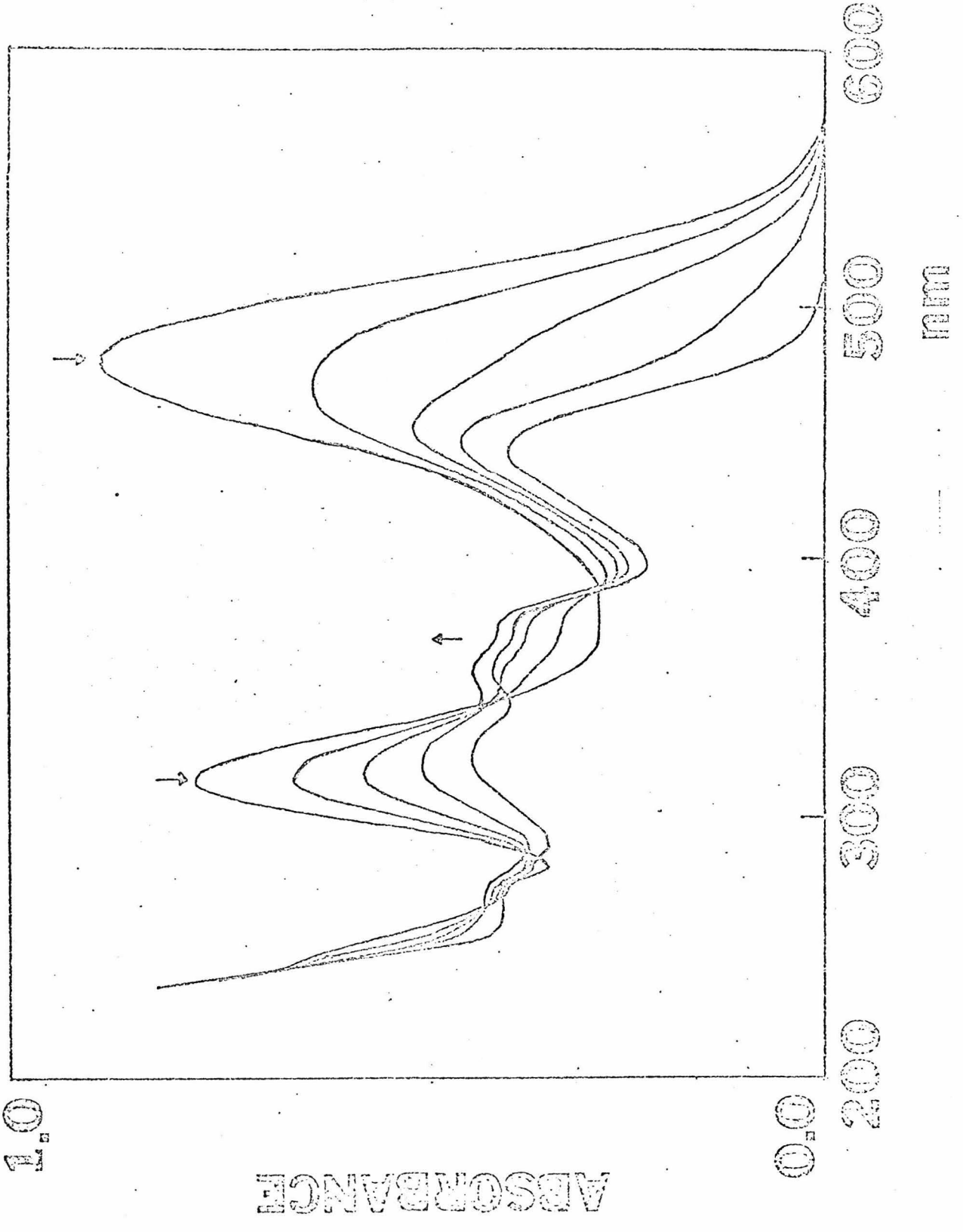
1.0
0.0
ABSORBANCE
200
300
400
500
600
nm

Figure 35. The photolysis of $W(CNIph)_6$ in degassed chloroform ($\lambda > 313$ nm). About 2 min. between spectra.

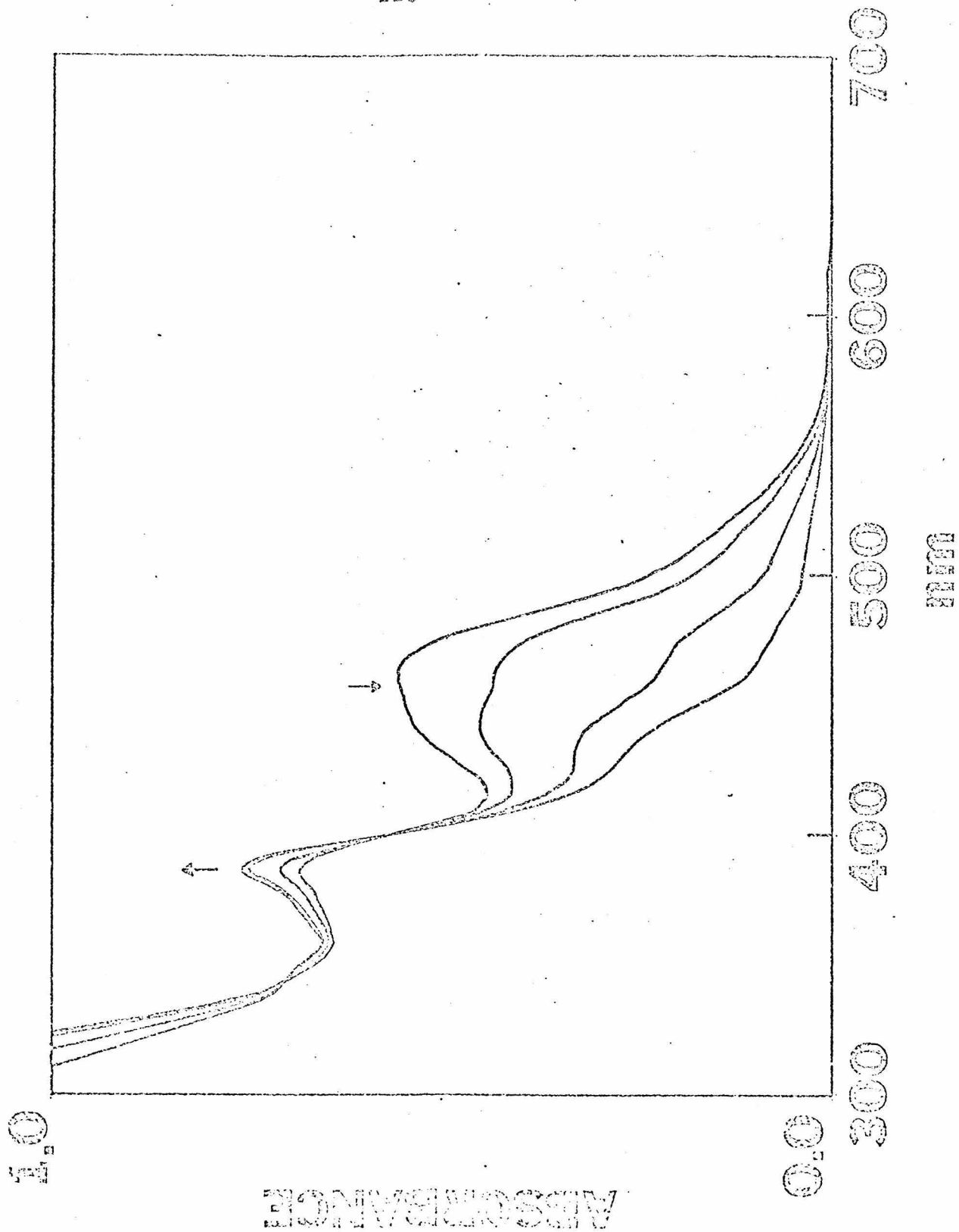
700
600
500
400
300
WAVELENGTH
WAVELENGTH

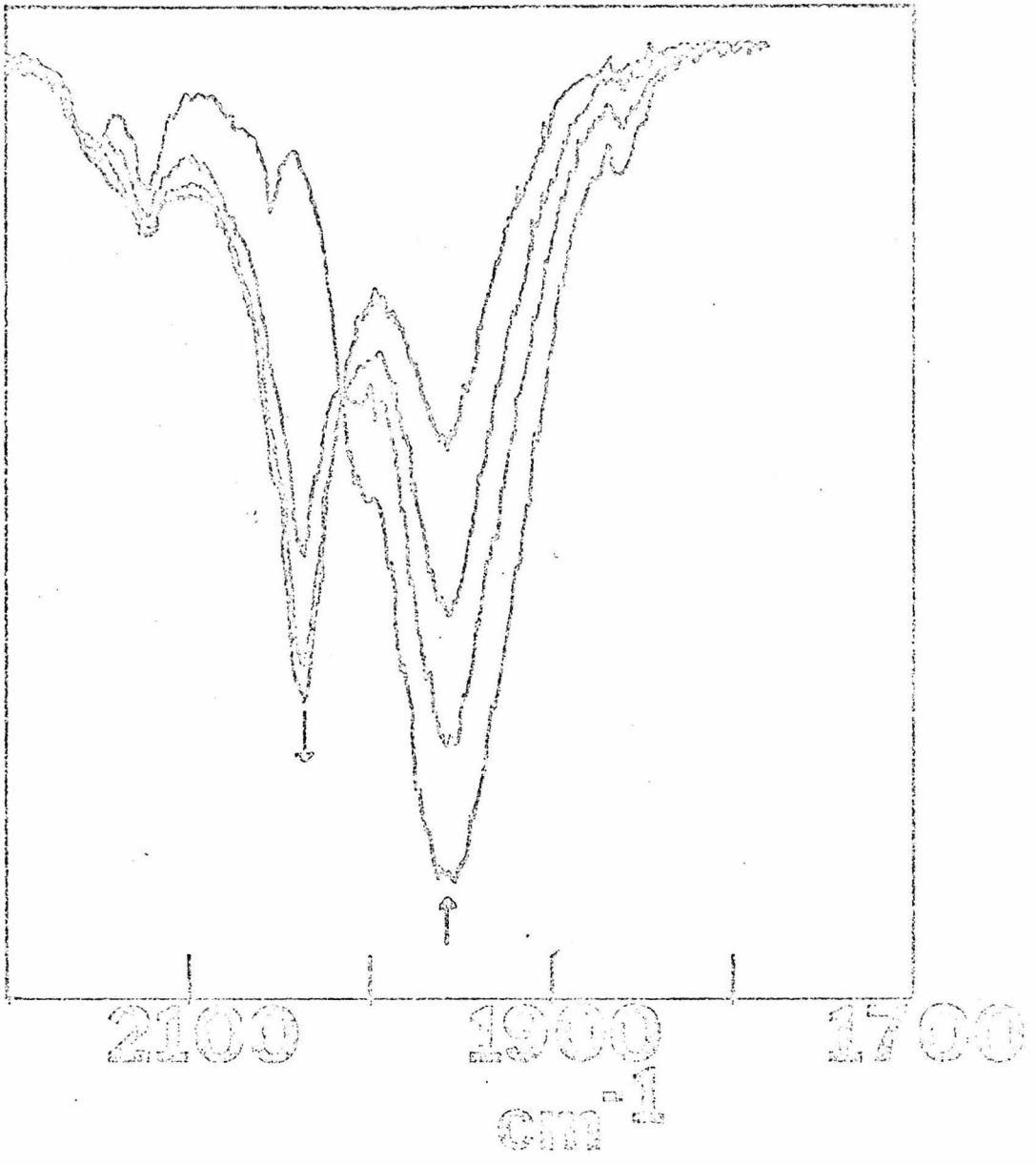

Figure 36. The photolysis of $W(CNPh)_6$ in undegassed CH_2Cl_2 ($\lambda > 313$ nm). 10 sec between spectra.

Table 21. Spectral Data for the Oxidation Products of $M(CNAr)_6$ Complexes

Complex	UV-VIS nm ($\epsilon \times 10^{-3}$)	$\bar{\nu}$(CN) in cm^{-1}
$Cr(CNPh)_6^+$	350 (44.5)	2065, 1985
	438 (34.0)	
"$[Cr(CNPh)_6Cl]^+$"	--	2115, 2125
$[Mo(CNPh)_6Cl]^+$	332 (43.8)	2100, 2130
$[Mo(CNPh)_6I]BPh_4$	--	2100, 2125
$Mo(CNPh)_6(PF_6)_2$	--	2135
$[W(CNPh)_6I]BPh_4$	--	2100, 2122
$Cr(CNIph)_6^+$	321 (49.6)	2065
	358 (46.4)	
	373 (44.0)	
	444 (45.6)	
$Mo(CNIph)_6^+$	380 (48.7)	2050
	430 (19.5)	
	465 (48.0)	
	480 (5.0)	
$W(CNIph)_6^+$	388	2040
	430 sh, wk	
	470 sh, wk	

Figure 37. The photolysis of $W(CNPh)_6$ in degassed chloroform ($\lambda > 313$ nm).


300
400
500
600
700
nm
ABSORBANCE
0.0
0.5

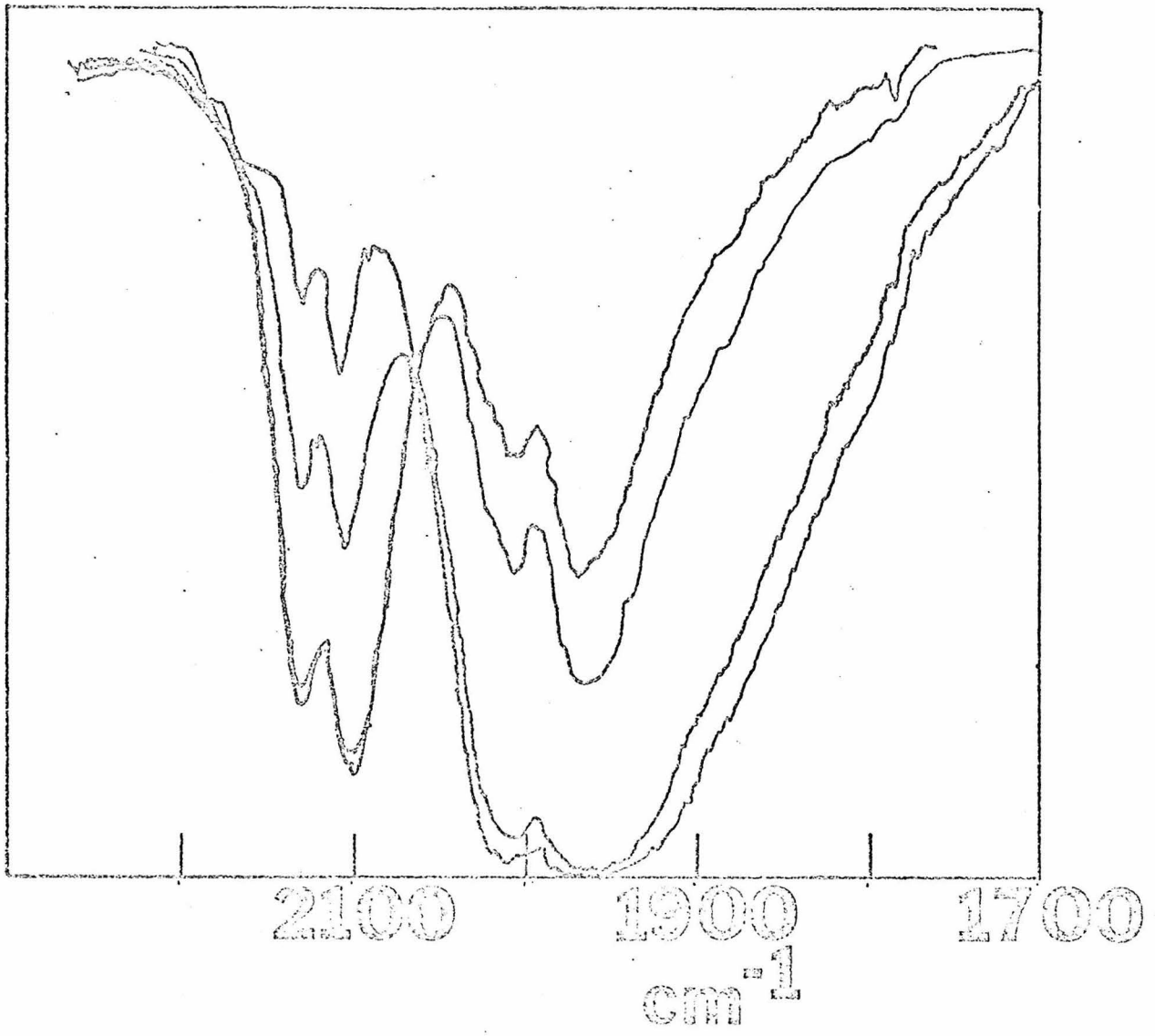

Figure 38. The photolysis of $Mo(CNPh)_6$ in degassed chloroform ($\lambda > 313$ nm).

New $\bar{\nu}$(CN) stretches grow in at 2130 and 2100 cm^{-1} for complexes of both metals, consistent with oxidation of the metal to the divalent state.

By adding $AgPF_6$ to a solution of $Mo(CNPh)_6$,[51] in acetone the only product obtained analyzed correctly for $Mo(CNPh)_6(PF_6)_2$. This product shows a single $\bar{\nu}$(CN) band at 2100 cm^{-1}. When Cl^- is added to a chloroform solution of $Mo(CNPh)_6^{2+}$ (Figure 39), an additional $\bar{\nu}$(CN) band is observed at 2130 cm^{-1}. The spectrum so obtained is very similar to the photolysis product obtained in chloroform, suggesting they are the same.

If I_2 is added to a dichloromethane solution of $M(CNPh)_6$ (M = Mo, W) and then $NaBPh_4$ is added, crystals which analyze correctly for $[M(CNph)_6I]BPh_4$ (M = Mo, W) are obtained. IR spectra of solutions of these complexes again show $\bar{\nu}$(CN) stretches at 2100 and 2130 cm^{-1} similar to the chloride containing photoproducts. By adding $NaPF_6$ to a HCl_3 solution of $Mo(CNPh)_6$ which has been photolyzed until the peaks at 2100 and 2130 cm^{-1} appear, a solid which has the same $\bar{\nu}$(CN) region IR as $Mo(CNPh)_6(PF_6)_2$ is obtained.

The above sequence of experiments is consistent with the existence of cations of the form $[M(CNPh)_6X]^+$ (M = Mo, W; X^- = I^-, Cl^-) which contain the divalent metal with seven ligands in the coordination sphere. A variety of seven coordinate complexes of Mo(II) containing isocyanide and halides are known.[51-55] The seven coordinate W(II) complexes have not previously been reported but the evidence suggests these should be formulated analogously to the Mo(II) compounds.

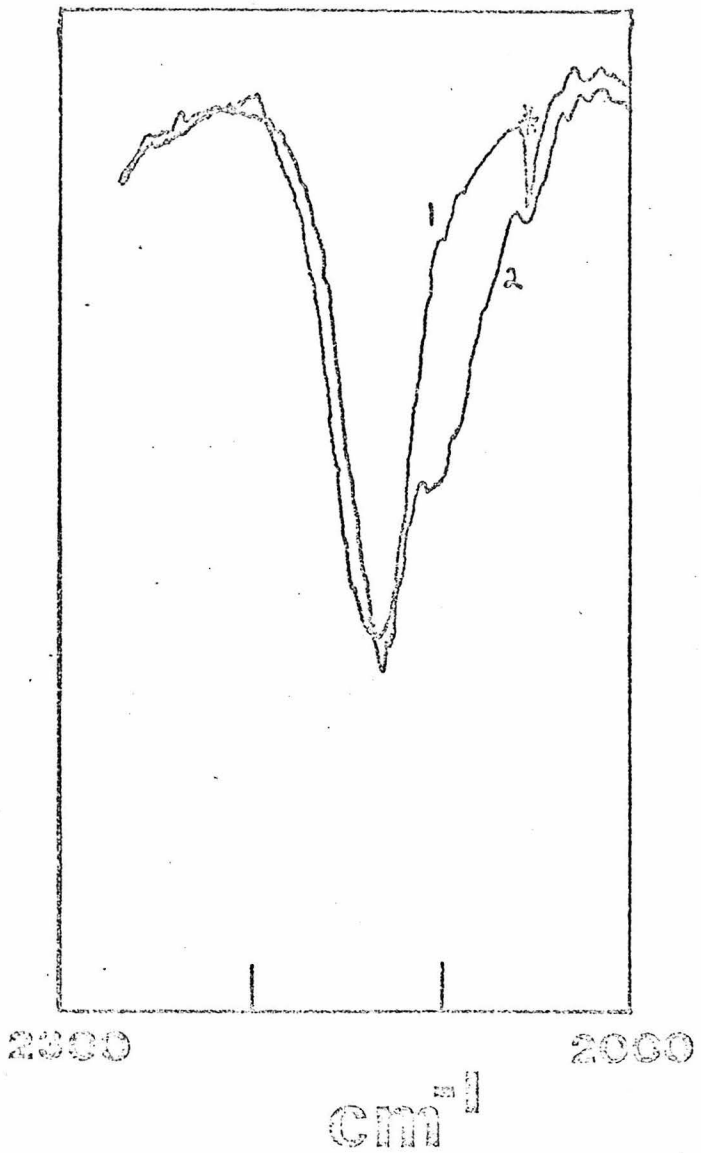

Figure 39. Curve 1: the $\bar{\nu}$(CN) IR spectral region of $Mo(CNPh)_6(PF_6)_2$ in chloroform.

Curve2: after addition of Et_4NCl.

The experiments also suggest that the halide ion can be removed from the seven coordinate cation by addition of a suitable halide scavenger,

$$[M(CNPh)_6X]^+ + AgPF_6 \rightarrow M(CNPh)_6^{2+} + PF_6^- + AgX\downarrow$$

generating the six coordinate $M(CNPh)_6^{2+}$ cations analogous to the $Cr(CNAr)_6PF_6$ compounds isolated by Triechel, et al.[12]

Photolysis of $Cr(CNPh)_6$ in degassed chloroform also leads to net oxidation, but the nature of the product formed is not as clear as in the Mo and W cases. Following the photolysis by IR (Figure 40) shows formation of a product which has $\bar{\nu}$(CN) at 2115 cm^{-1} and a shoulder at 2130 cm^{-1}. $Cr(CNPh)_6^+$ and $Cr(CNPh)_6^{2+}$ are reported to have $\bar{\nu}$(CN)'s at 2065 cm^{-1};1985 and 2161 cm^{-1}, respectively. The shoulder at 2130 cm^{-1} is in the precise position of the $\bar{\nu}$(CN) stretch of free CNPh, suggesting that this Cr photoproduct has lost at least one ligand. Most likely is the following thermal reaction which follows the photochemical reactions which generate the $Cr(CNPh)_6^{2+}$ cation:

$$Cr(CNPh)_6^{2+} + Cl^- \rightleftharpoons Cr(CNPh)_5Cl^+ + CNph$$

Addition of a large excess of Cl^- to a light yellow solution of $Cr(CNPh)_6^{2+}$ (Figure 41) results in formation of a transient brown color (similar to the color of $[M(CNPh)_6Cl]^+$ (M = Mo, W)) with immediate bleaching to a colorless solution which shows only the

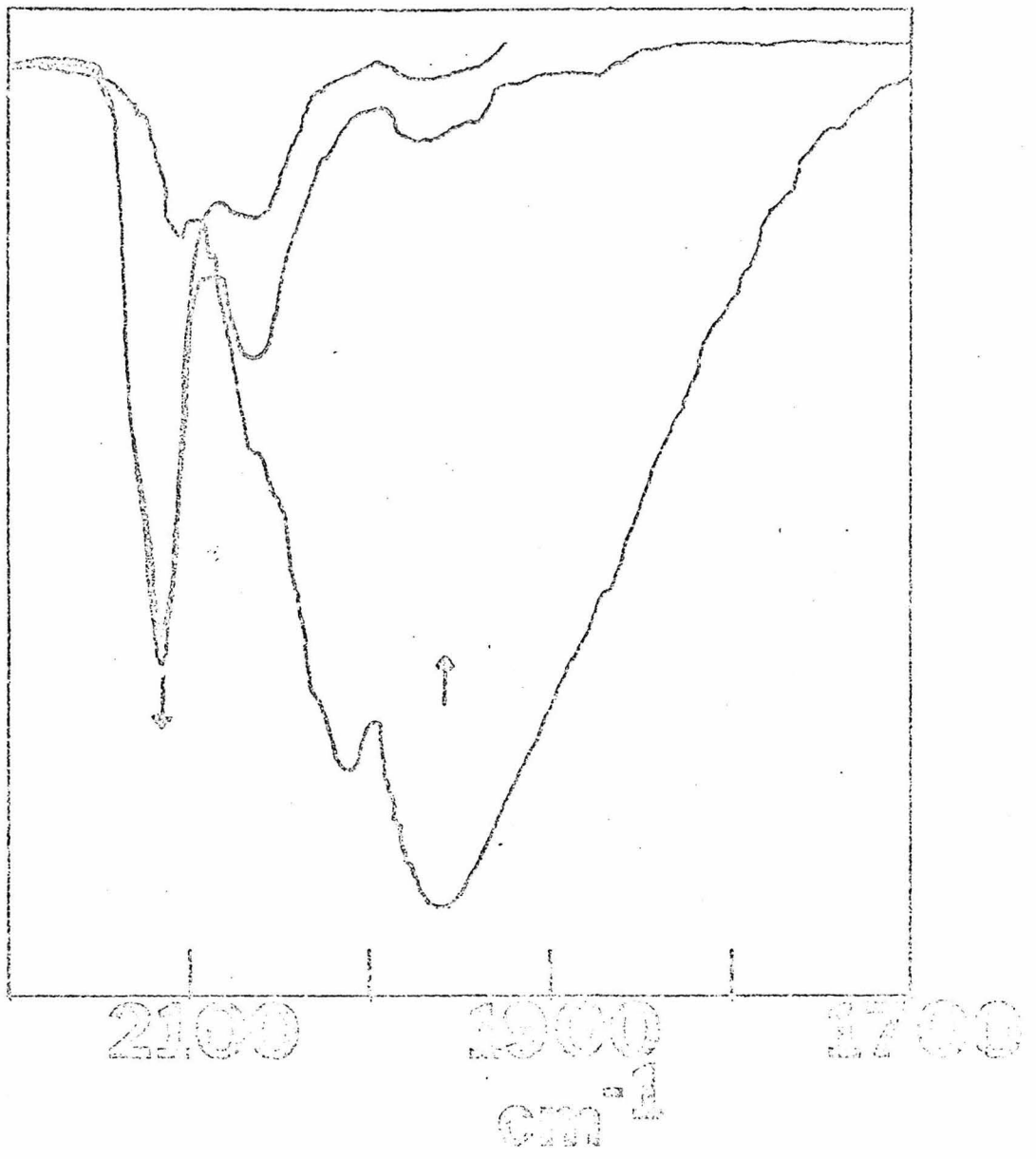

Figure 40. The photolysis of $Cr(CNPh)_6$ in degassed chloroform ($\lambda > 313$ nm).

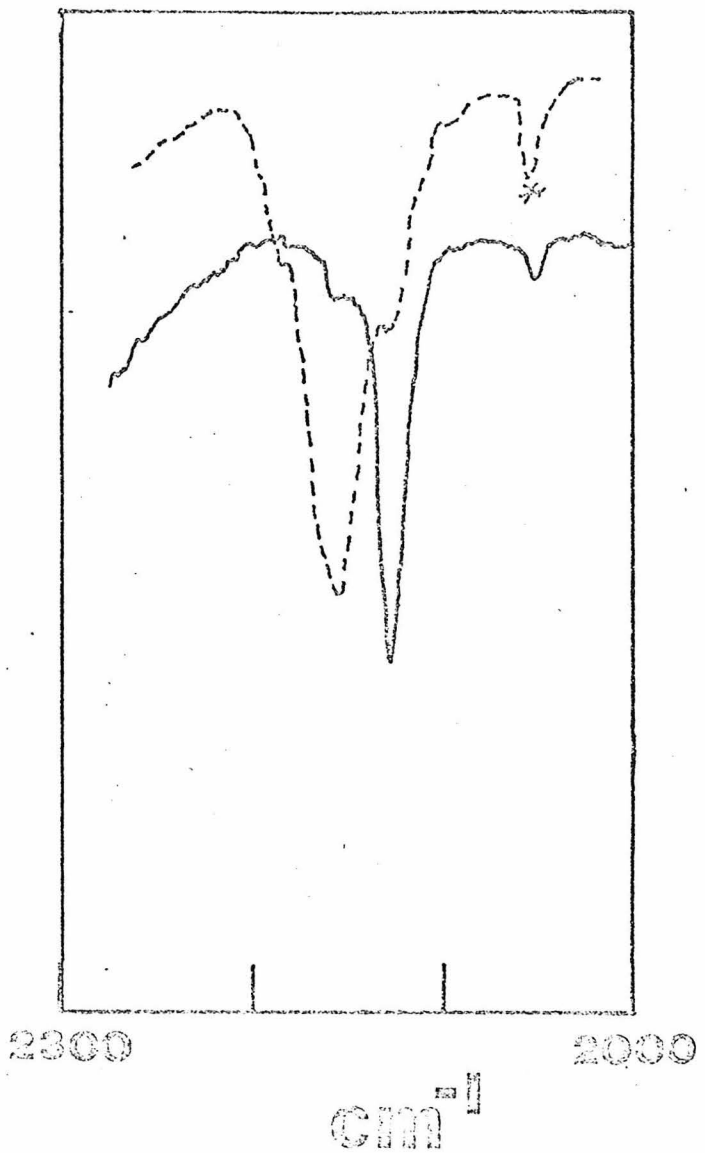

Figure 41. (---) spectrum of $Cr(CNPh)_6(PF_6)_2$ in chloroform;
(——) same sample after addition of Et_4NCl.

$\bar{\nu}$(CN) of free CNPh. This experiment is explained nicely by postulating unstable seven coordinate intermediates of the form $Cr(CNPh)_6Cl^+$ or $Cr(CNPh)_5Cl_2$ which lose CNPhin a stepwise fashion.

Further characterization of the solid and chloroform solutions of '$Cr(CNPh)_6Cl_2$' by magnetic susceptibility could determine the presence of $Cr(CNPh)_6^{2+}$, $Cr(CNPh)_5Cl^+$ and $Cr(CNPh)_6Cl^+$, the first two of these being paramagnetic with two unpaired electrons, while the third should be diamagnetic. The UV-VIS spectra of $Cr(CNPh)^{0,+1,+2}$ are shown in Figure 42.

Quantum Yields

The quantum yields for formation of $M(CNIph)_6^+$ from $M(CNIph)_6$ by photolysis at 436 nm in degassed chloroform were found to be 0.19 ± 0.01 for M = Cr, Mo, W (see Table 22). In air-saturated chloroform, the quantum yield for formation of $Cr(CNIph)_6^+$ was highly reproducible and considerably larger than that obtained under anaerobic conditions ϕ_{ox} = 0.70 ± .01. The formation of $[Mo(CNPh)_6Cl]^+$ and $[W(CNPh)_6Cl]^+$ in degassed chloroform were ϕ = 0.11 ± 0.01 and ϕ = 0.28 ± 0.02, respectively, at 436 nm. In degassed chloroform $Cr(CNPh)_6$ is smoothly converted to a Cr(II) species (see preceding discussion) while in oxygenated chloroform, $Cr(CNPh)_6^+$ is formed.

Mechanistic Considerations

The best mechanisms for the photochemical oxidation reactions of $M(CNAr)_6$ complexes which one could write should be able to explain the differences in the products $M(CNIph)_6^+$ vs.

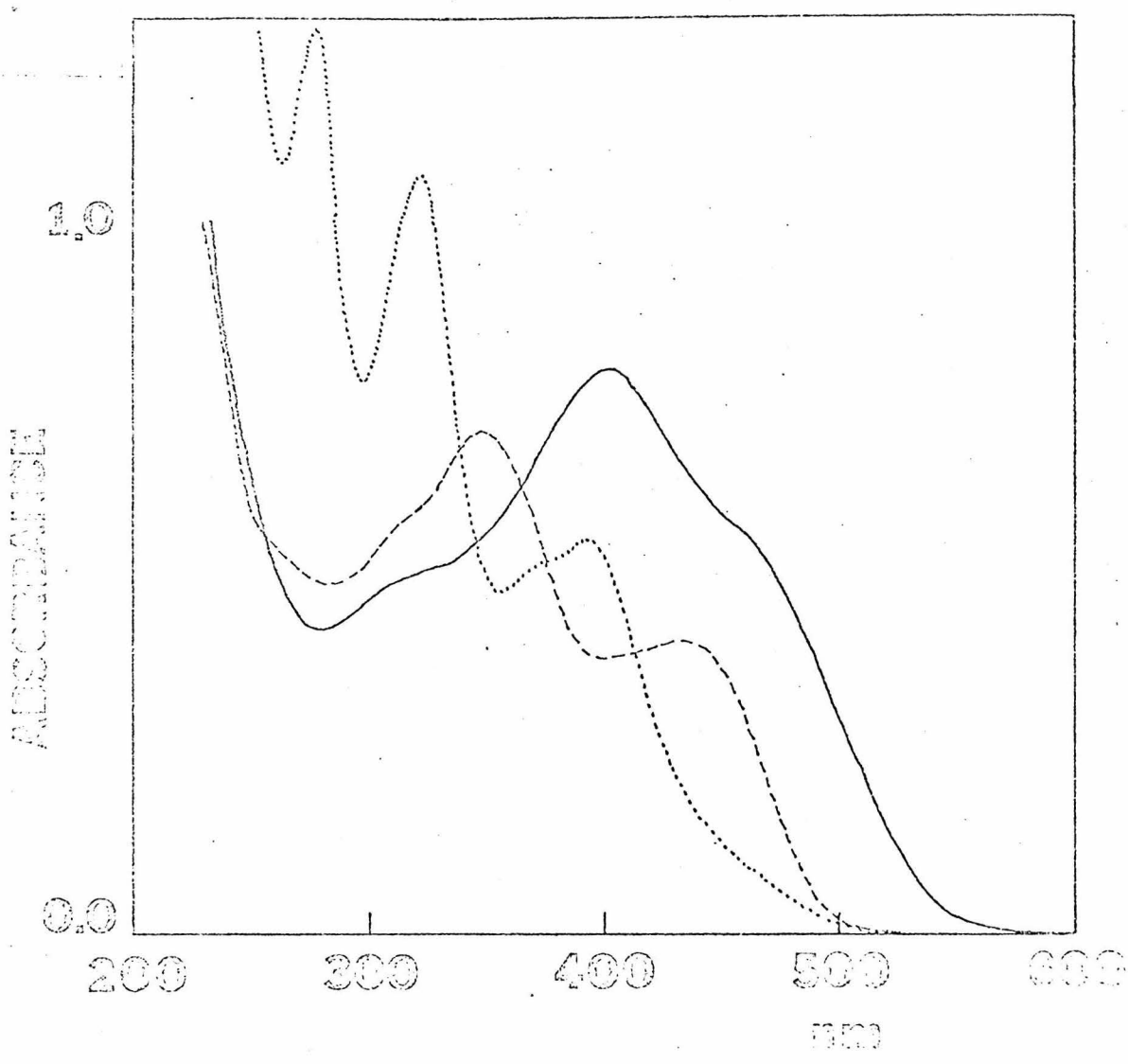

Figure 42. The visible spectra of $Cr(CNPh)_6$ (——), $Cr(CNPh)_6$-PF_6 (---), and $CrCNPh)_6(PF_6)_2$ (···) in CH_2Cl_2.

Table 22. The Quantum Yields for the Reaction of $M(CNAr)_6$ with Neat Chloroform

Complex	436 nm
$Cr(CNIph)_6$	0.19 ± 0.01
$Mo(CNIph)_6$	0.19 ± 0.01
$W(CNIph)_6$	0.19 ± 0.01
$Mo(CNPh)_6$	0.11 ± 0.01
$W(CNPh)_6$	0.28 ± 0.02

$[M(CNPh)_6Cl]^+$. Two mechanisms are reasonable, both having common intermediates for complexes of the hindered and unhindered ligands.

Mechanism 1: Charge transfer to solvent.

1) $M(CNAr)_6 + HCCl_3 \xrightarrow{h\nu} [M(CNAr)_6^+ \cdots HCCl_3^{\cdot -}]$

2a) $[M(CNAr)_6^+ \cdots H\dot{C}\bar{C}l_3] \rightarrow M(CNAr)_6^+ + Cl^- + H\dot{C}Cl_2$

2b) $[M(CNAr)_6^+ \cdots H\dot{C}\bar{C}l_3] \rightarrow M(CNAr)_6 + HCCl_3$

if Ar = Iph

3a) $M(CNIph)_6^+ + HCCl_2 \not\rightarrow [M(CNIph)_6Cl]^+$

4a) $HCCl_2 + HCCl_2 \rightarrow C_2H_2Cl_4$

if Ar = Ph

3b) $[M(CNPh)_6^+ \cdots H\dot{C}\bar{C}l_3] \rightarrow [M(CNPh)_6Cl]^+ + H\dot{C}\bar{C}l_2$

4b) $H\dot{C}\bar{C}l_2 + HCCl_3 \rightarrow Cl^- + C_2H_2Cl_4$

Mechanism 2: S_n^2 attack of excited state on $HCCl_3$

1) $M(CNAr)_6 \underset{h\nu \text{ or } \Delta}{\overset{h\nu}{\rightleftharpoons}} M(CNAr)_6^*$

2) $M(CNAr)_6^* + HCCl_3 \rightarrow [M(CNAr)_6^+ \cdots H\dot{C}\bar{C}l_3]$

from this step on the two mechanisms are identical.

Discussion

Mechanism 1 involves excitation of an electron from the metal to an orbital mostly based on a solvent molecule. This intermediate can then thermally return to reactants or can split out a chloride ion and a $HCCl_2$ radical. The following thermal reactions depend on the steric requirements of the ligands. If the complex is unhindered, the $H\dot{C}\bar{C}l_3$ radical anion can transfer a chlorine radical to the metal via an inner sphere attack on the $M(CNPh)_6^+$ species. If the complex is hindered, the $H\dot{C}\bar{C}l_3$ radical anion cannot oxidize $M(CNIph)_6^+$ and is destroyed.

Mechanism 2 involves excitation of an electron in a MLCT transition. This excited state has a long enough lifetime to then reduce a chloroform molecule to $HCCl_3$. This $H\dot{C}\bar{C}l_3$ radical anion can then either reduce $M(CNAr)_6^+$ back to $M(CNAr)_6$ or can difuse into the solvent, just as in Mechanism 1. From this point on, the two mechanisms are identical.

An example of Mechanism (1) is the photochemical oxidation of ferrocene by carbon tetrachloride:[56,57]

$$FeCp_2 + CCl_4 \xrightarrow{h\nu} [FeCp_2^+ \text{---} \bar{C}Cl_4] \xrightarrow{\text{products}}$$

Experimental data suggest that a new absorption band grows into the spectrum of ferrocene at 307 nm in chlorinated solvents which is not present in ethanol or hydrocarbons. This peak was suggested by Brand and Snedden[56] to be due to a metal to solvent charge transfer band.

Mechanism (2) has recently come into vogue with the ever-expanding amount of work on $Ru(bipy)_3^{2+}$, which in its lowest MLCT state has been shown to transfer an electron to suitable acceptor molecules.[45,58-63] This electron transfer mechanism has also been shown to be facile in the quenching of the emission fromthe lowest excited state.

Recently, work on $Ru(bipy)_3^{2+}$ [64] and the ferrocene/CCl_4 systems[57] have hinted that in neither case is the mechanism purely (2) (for Ru) or (1) (for ferrocene). This suggests that Mechanisms (1) and (2) are the two limiting mechanisms, while real systems seem to be best described by a mixture of the two, with one dominating.

In the case at hand, the absorption spectra of the $M(CNAr)_6$ complexes in chlorinated solvents show no obvious new absorption bands which could be assigned to metal to solvent charge transfer bands. This suggests but does not prove that Mechanism (2) is the more plausible. Gross similarities between the $Ru(bipy)_3^{2+}$ and the $M(CNAr)_6$ complexes also suggest that a mechanism similar to that found for excited state electron transfer in $Ru(bipy)_3^{2+}$ is also operative in the $M(CNAr)_6$ systems.

The constant value for the quantum yield for $M(CNIph)_6^+$ (M = Cr, Mo, W) even though there are large differences in the lifetimes of the lowest emitting states suggest that the actual electron transfer step is very fast, with the quantum yield being determined by either the diffusion rate of $HCCl_3$ or its decomposition rate. Emission at room temperature in air-saturated chloroform solution

was not observed. Emission does occur in other undeoxygenate solvents, suggesting that the emitting state in each case is efficiently quenched by chloroform.

The large increase in the quantum yield for formation of $Cr(CNIph)_6^+$ found in oxygenated chloroform (0.70 vs. 0.19) also fits in with a fast electron transfer step followed by another reaction which determines the actual quantum yield since O_2 may be the acceptor. The O_2^- formed being able to diffuse away before the back reaction can occur. Net oxidation of $Cr(CNPh)_6$ to $Cr(CNPh)_6^+$ has been observed in undegassed isooctane.

Although O_2 has been shown to thermally oxidize $Cr(CNAr)_6$ complexes to the analogous $Cr(CNAr)_6^+$ complexes, the thermal reaction with O_2 was slow enough so that the small amounts of $Cr(CNAr)_6^+$ formed thermally could be adequately corrected for.

Of interest is the fact that when $Cr(CNPh)_6$ is irradiated in undegassed chloroform (Figure 43), $Cr(CNPh)_6^+$ is formed while under anaerobic photolysis, Cr(II) products result. This suggests that O_2 acts as the acceptor when it is present rather than $HCCl_3$; termination of the oxidation at the Cr(I) stage is easily explained since O_2^- is not able to oxidize $Cr(CNPh)_6^+$ by transferring a chlorine atom in a subsequent oxidation step.

The quantum yields for formation of $[Mo(CNPh)_6Cl]^+$ and $[W(CNPh)_6Cl]^+$ are 0.11 ± 0.01 and 0.28 ± 0.02, respectively. The difference in these two values may be a consequence of slightly

Figure 43. The photolysis of $Cr(CNPh)_6$ in undegassed chloroform ($\lambda > 313$ nm).

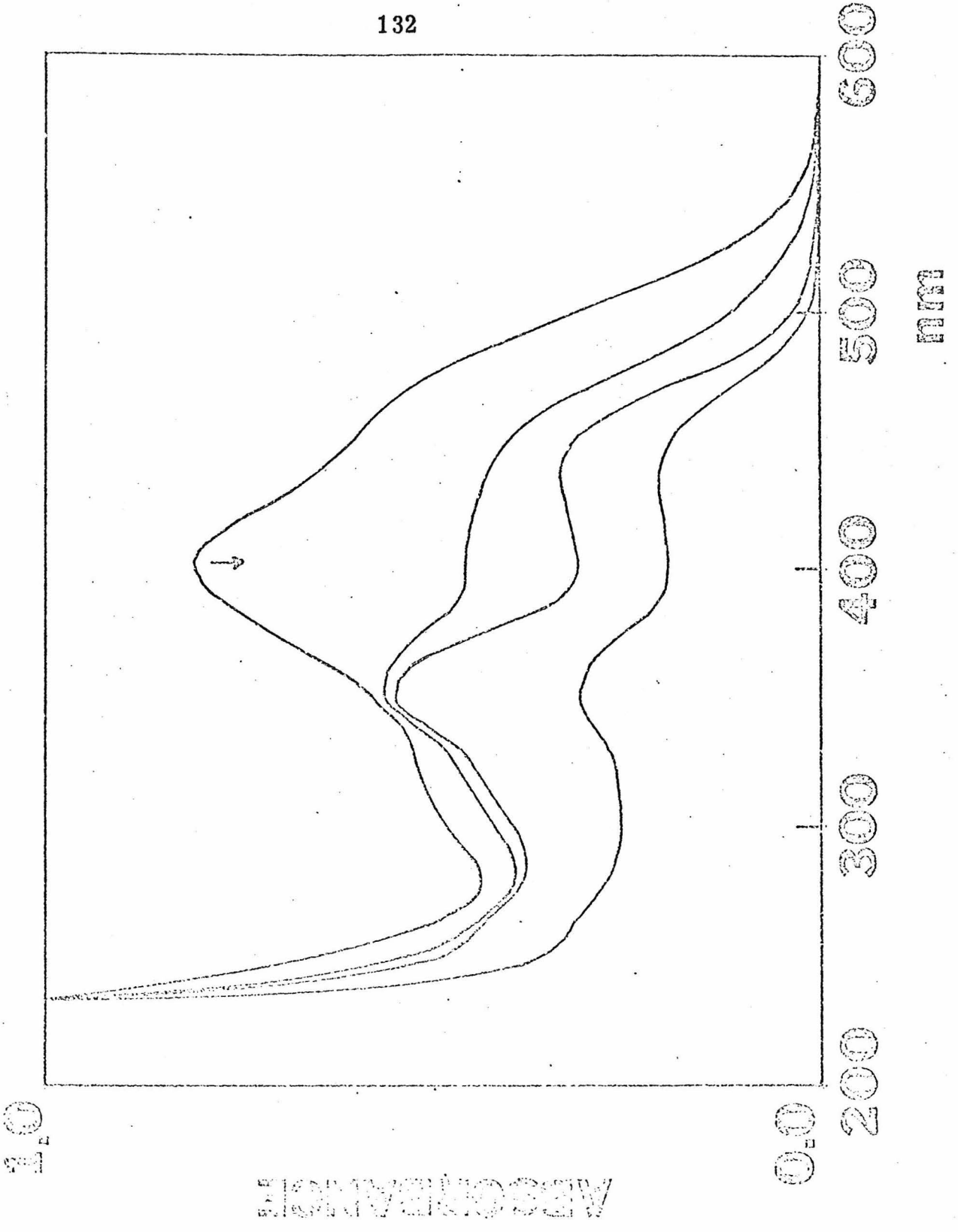
0.0
200
300
400
500
600
nm

different rate constants for the secondary oxidation of the metal center in these complexes.

Synthesis

Ligand Synthesis

The method of Ugi, et al.[65] was selected as the most convenient in terms of availability of starting materials and ease of workup. The method gives about a 50-70% yield of product depending on the particular isocyanide. The general procedure is as follows:

In a five liter, three-necked flask equipped with an overhead paddle stirrer and two efficient condensers were placed 500 ml dichloromethane, 1.1 moles of chloroform, 300 ml of saturated NaOH, 1 mole of the appropriate primary amine, and approximately 1 gram of the catalyst, benzyltriethylammoniumchloride. The resulting two-phase system was stirred vigorously. The exothermic reaction can be monitored by the dichloromethane reflux rate, which is maintained just into the condenser by adjusting the stirring rate. The use of the large flask is somewhat critical in that it allows good heat dissipation without which extremely strong pressure explosions result. The reaction, which makes NaCl in the form of a white precipitate, is usually over in 4 to 12 hours. The layers are then separated and the organic layer is washed with water several times and dri ed over $CaSO_4$. The dichloromethane is then pulled off under vacuum. The product can be distilled (phenyl, 2,6-diisopropylphenyl), recrystallized (2,6-dimethyl), or sublimed (4-chlorophenyl). The yield seems to be least for the 4-chloro substituted compound and best for the 2,6-diisopropyl phenyl. Characterization was by IR and NMR.

Synthesis of Metal Complexes

$Cr(CNR)_6$

The general method of synthesis used for these compounds was first described by Malatesta,[14] using $Cr_2(C_2H_3O_2)_4 \cdot 2H_2O$.[66] It was observed, however, that better yields were obtained if the reaction vessel was heated to 40°C. The complexes were recrystallized from hot toluene/ethanol in the dark. Crystals were obtained in all cases (Table 23).

$Mo(CNR)_6$

These compounds were obtained in about 30% yield as follows: To a stirred slurry of $Mo_2(C_2H_3O_2)_4$[67] in methanol under argon, an excess (10:1) of the appropriate isocyanide was added. The solution immediately turned red-brown and was warmed to 40°C on a hot plate for one hour. Upon cooling, filtration afforded the crude product which was recrystallized from hot toluene/ethanol. The compounds are slightly air sensitive, much more so in room lights. Solutions should be degassed and kept in the dark during recrystallization to avoid decomposition (Table 23).

$W(CNR)_6$

These compounds were prepared with difficulty in small yield (5-10%) by the following method (modification of Malatesta and Sacco[16]). A degassed slurry of absolute ethanol (80 ml) and magnesium powder (4g) in a three-necked flask (of at least 300 ml capacity) was prepared and cooled to 0°C with an ice bath. To this mixture 0.12 moles of isocyanide was added. Next 8g (~ 0.02 moles) of WCl_6 was added slowly along with 2 drops of acetic acid. Much heat is generated.

A large number of color changes occur during the reaction. After the reaction has proceeded to the point of controlled but sustained ethanol reflux, the ice bath is removed. As the reaction cools down, the product as red crystals is sometimes deposited. This procedure is rather tricky and at times the yield is zero. Variation of parameters such as temperature, solvent and reagent purification, and scale seemed to have a random effect on the yield. The perfect starting material for this reaction would be $W_2(C_2H_3O_4)_4$ which has not been made. The product is recrystallized from hot toluene/ethanol, preferably nitrogen, in the dark to minimize losses due to air oxidation (Table 23).

$[M(CNPh)_6I]BPh_4 (M = Mo, W)$

Complexes of this general form were obtained by adding an excess toluene solution of I_2 to $M(CNPh)_6$. The resulting precipitate was filtered and dissolved in dichloromethane. Excess solid $NaBPh_4$ was added and the resulting slurry was warmed, filtered, and diethylether was added. This crude product was recrystallized several times from dichloromethane/ether (Table 23).

$Cr(CNR)_6PF_6$

Complexes of this type were obtained as above, substituting KPF_6 for $NaBPh_4$. The BPh_4^- salt was also made by this method. These Cr(I) compounds, as well as the compounds containing $Cr(CNR)_6^{2+}$ have also been synthesized by the oxidation of $Cr(CNR)_6$ by $AgPF_6$ [12] (Table 23).

$[M(CNR)_6]Cl$

Complexes of this type were prepared from MnI_2 by the method of Sacco [17] (Table 23).

$[Mn(CNR)_6](PF_6)_2$

These complexes were obtained by oxidation of $Mn(CNR)_6Cl$ in glacial acetic acid with an equal volume of concentrated nitric acid. Addition of this solution to a saturated aqueous solution of $NaPF_6$ gave a red precipitate. The product can be recrystallized from hot ethanol (Table 23).

Table 23. Analytical Data for $M(CNR)_6$ Complexes

	C	H	N	M	Cl
$Cr(CNPh)_6$	75.21 calc	4.51	12.53	7.75	
	75.06 found	4.40	12.52	7.61	
$Mo(CNPh)_6$	70.59	4.23	11.76		
	70.89	4.23	11.62		
$W(CNPh)_6$	62.92	3.76	10.48		
	63.04	3.96	9.98		
$Cr(CNDph)_6$	77.30	6.487	10.002		
	76.70	6.53	9.51		
$Mo(CNDph)_6$	73.45	6.16	9.518	10.865	
	74.45	6.36	9.57		
$W(CNDph)_6$	66.80	5.61	8.662		
	75.85	5.65	8.58		
$Cr(CNIph)_6$	76.98	8.745	7.148		
	79.62	8.58	7.01		
$Mo(CNIph)_6$	76.81	8.43	6.89		
	76.84	8.35	7.04		
$W(CNIph)_6$	71.649	7.86	6.427		
	71.82	7.82	6.35		
Cr(pCNPhCl)	57.49	2.757	9.578		
	57.92	3.04	9.44		
$Mo(pCNPhCl)_6$	54.752	2.626	9.122		
	54.55	2.98	9.24		

	C	H	N	M	Cl
$W(pCNPhCl)_6$	49.983	2.397	8.327		
	48.15	2.55	7.97		
$Mn(CNPh)_6Cl$	71.14	4.26	11.85	6.90	5.00
	69.61	4.36	11.51	6.90	4.91
$Mn(CNPh)_6PF_6$	52.35	3.13	8.72	5.79	
	51.81	3.15	8.63	5.67	
$[Mo(CNPh)_6I]BPh_4$	68.29	4.34	7.24		
	68.35	4.52	7.21		
$[W(CNPh)_6I]BPh_4$	63.48	4.04	6.73		
	63.13	4.12	6.83		
$Cr(CNIph)_6PF_6$	70.94	7.79	6.36		
	70.57	7.78	6.22		
$Cr(CNPh)_6Cl_2$	75.15	8.25	6.74		
	75.09	8.26	6.67		
$Cr(CNPh)_6BPh_4$	80.08	5.10	8.49		
	79.21	5.26	8.35		
$Mo(CNPh)_6(PF_6)_2$	52.35	3.13	8.72	5.70	
	51.81	3.15	8.63	5.67	

Spectral Measurements

Infrared Spectra

Infrared spectra were recorded on a Perkin-Elmer 225 spectrometer as Nujol mulls, KBr pellets, or in 0.1 mm KBr solution cells. Spectra in pyridine and benzylamine were taken in a variable pathlength cell with neat solvent in the reference beam. Degassing of IR solutions was accomplished by bubbling argon through the compound dissolved in a small amount (1 ml) of the solvent. Standard syringe techniques were then used to fill the previously degassed cell.

Electronic Absorption Spectra

Electronic absorption spectra were measured using a Cary 17 spectrophotometer. Room temperature solution spectra were obtained in a 1 cm quartz cell with a quartz insert designed to decrease the pathlength to either 0.02 or 0.05 cm. This cell was calibrated[68] by using CrO_4^{2-}. Spectra at liquid nitrogen solution were obtained using a low temperature dewar fitted with Suprasil quartz windows and modified to hold a 0.1 cm cell. Solvents used in general were Spectro grade except for THF, 2-methylTHF, and Et_2O, 2-methyl pentane, which were reagent grade. Low temperature glasses used were EPA, 8:2:1 ethanol/methanol/diethylether, 1:1 isopentane/diethyl ether, 2 methylpentane, and 2 methyl THF. For the ionic compounds solutions were obtained by first dissolving the compound in a few drops of CH_2Cl_2 and then adding the glassing solvent. All solutions were made up in a dark room because of their extreme sensitivity to

light using solvent degassed by bubbling with argon. The solutions were either used immediately or frozen at liquid nitrogen temperature where photochemistry was observed to be slow. A few drops of nitric acid were added to each of the $Mn(CNAr)_6^{2+}$ solutions to prevent slow reduction to the Mn(I) complex.

Emission Spectra

Spectra

Emission spectra were obtained using a Perkin-Elmer MPF-3A fluroescence spectrometer. Low temperature measurements were made using an optical dewar. Samples were prepared by dissolving the appropriate compound in the solvent of choice spectrograde pyridine, p-xylene, or 2-methylTHF previously degassed by bubbling with argon. These solutions were then placed in Pyrex test tubes and freeze-thaw degassed on a vacuum line at least four cycles. The tubes were then sealed with a torch and kept at liquid nitrogen temperature until use. All the above operations were carried out under red light ($\lambda > 630$ nm). Room temperature spectra were measured (on concentrated solutions (10^{-3} M)) off the front face of the sample tube. Low temperature spectra were measured by the standard 90° to incidence technique.

Correction for Phototube and Monochrometer Response

All spectra in this thesis were corrected for phototube and monochrometer response in the following manner.

The intensity vs. wavelength response of a tungsten/halogen lamp was obtained by measuring the potential generated by directing the beam of the lamp through a 0.5 meter Jarrel-Ash monochrometer light onto a thermopile. Data points were taken every 10 nanometers from 300 to 800 nm. Then the same lamp was directed into the emission monochrometer and the lamp spectral output curve as a function of wavelength was obtained. Dividing this second curve by

the first curve in a point by point manner generates the correction curve. This smooth set of points was then fit to an eleventh order polynomial via computer fit.

$$\text{Corr}(\lambda) = a + bx + Cx^2 \ldots.$$

where

$a = 4.63990427 \times 10^{3}$	$g = -2.299848685 \times 10^{-14}$
$b = 4.706047370 \times 10^{0}$	$h = 2.963376321 \times 10^{-17}$
$c = -1.827965372 \times 10^{-2}$	$i = -7.061177302 \times 10^{-20}$
$d = 3.297836079 \times 10^{-5}$	$j = 1.955866691 \times 10^{-22}$
$e = 2.663711413 \times 10^{-8}$	$k = -2.259072966 \times 10^{-25}$
$f = 1.351673912 \times 10^{-11}$	$l = 8,928261361 \times 10^{-29}$

By digitalizing the experimental emission trace obtained from the instrument and then evaluating the above function at each data point, the corrected spectra were obtained by the use of eq. (1). These spectra were then plotted as desired.

eq. (1). Spectrum correct(λ) = Corr (λ). Spectrum uncorrected (λ).

Quantum yields

Low temperature emission quantum yields for the $M(CNAr)_6$ compounds in 2-methylTHF were obtained as follows: Dilute solutions of the complexes in 2-methylTHF were prepared as described, degassed by freeze-thaw degassing (4 cycles). Next reference solutions of $Ru(bipy)_3Cl_2$ which emits in the same general spectral region as the $M(CNAr)_6$ compounds were made up in EPA. The o.d. of each sample (≈ 0.2 absorbance units) was matched at liquid

nitrogen temperature as closely as possible to a reference solution. Emission spectra were then obtained for both sample and reference under precisely the same conditions. These spectra were corrected as above, plotted as a function of wavenumber, the area under the two peaks determined, and the ratio between them computed. The equation of Crosby, et al.,[69] was then used to compute ϕ sample assuming $n_x = n_s$. At least three determinations of each compound were made, the average taken as the quantum yield.

In Appendices 1 and 2 two computer programs are presented. The first OPTSPEC, written by Jeff Hare and modified by K.M., takes raw emission spectral data which has been converted to digital form , corrects the spectra for monochrometer response, and then plots it in terms of wavelength or energy. The second program (AREAKT) computes the area under a curve using the trapezoidal approximation for the area.

General Photochemical Measurements and Measurement of Quantum Yields

All actinometry was done using Ferrioxatate actinometry.[70-72] The yield for a 0.06 M solution at 436 nm was taken as 1.11. Irradiations were carried out in a block thermostatted with a large (~ 30 l) amount of distilled water.

The irradiation source was a 450 watt medium pressure Hanovia mercury lamp. The 436, 366, and 313 nm mercury lines were isolated using 5-74, 7-83, and 7-54 Corning filters, respectively. In addition to the glass filter for the 313 nm line, a 0.7 cm pathlength solution of 4.5 g K_2CrO_4 and 2.376 g K_2CO_3 in 4.5 l of water was used.[73] 3 ml aliquots of actinometer solution were irradiated under the same conditions as the samples. As a check, the quantum yield for aquation of $Cr(NH_3)_2(SCN)_4^-$ was checked at 436 nm against the ferrioxalate actinometer. Agreement at this wavelength with the literature value[74] was excellent.

Substitution Quantum Yields

Substitution quantum yields for the following reaction were measured in neat pyridine.

$$ML_6 + py \xrightarrow{h\nu} ML_5py + L$$

In every case, a long wavelength absorption band grew in for the ML_5py species. The appearance quantum yield was measured by measuring the increase in this longwavelength absorption absorption band as a function of irradiation time on a Beckmann D.U.

In Table 24 the wavelength monitored and the extinction coefficient of that wavelength for each complex are given. These extinction coefficients were measured by photolyzing solutions of each complex in pyridine to complete conversion. The extinction coefficients of the product was then obtained from the ratio of the absorbance of the reactant peak to the absorbance of the product peak assuming complete conversion. Due to slight photolysis of the product, ϵ's measured in this way are always slightly lower than the true value. Repeated measurements, however, gave highly reproducible values. The values given in Table 24 are at worst 10% low.

Sample Preparation

The compounds were all recrystallized at least twice before use. A small amount of complex (so that O.D. at λ ex $\gg$ 2) was placed in the mixing chamber of a cell which could be degassed on a vacuum line and then 3 ml of dry, spectrograde pyridine was pipetted in. This solution was then degassed by at least 3 freeze-thaw degassing cycles. All the above operations were carefully carried out in a dark room. Samples prepared in this manner were then photolyzed. Three independent determinations of each quantum yield were made, with at least 5 data points taken for each run. These values were then averaged. The precision of each quantum yield was very good, varying in somecases by less than $\pm$ 2%. Due to the large extinction coefficients at the monitoring wavelengths, conversion to products was on the order of 0.2%, thus avoiding problems caused by secondary photolysis and internal filtering effects.[75] All the quantum

Table 24. The Extinction Coefficients of ML_5py Used in Determining the Substitution Quantum Yields for

$ML_6 + py \rightarrow ML_5py + L$

	λ(nm)	ε
$Cr(CNPh)_6$	600	4,524
$Mo(CNPh)_6$	570	4,661
$W(CNPh)_6$	590	1,675
$Cr(CNIph)_6$	570	19,095
$Mo(CNIph)_6$	570	20,500
$W(CNIph)_6$	580	16,933
$Mn(pCNPhCH_3)_6ClO_4$	420	16,802

yields measured were reproducible only under rigorously deoxygenated conditions. The products generated are very air sensitive.

Oxidation Quantum Yields

The quantum yields for the oxidation reaction

$$M(CNIph)_6 + HCCl_3 \rightarrow M(CNIph)_6^+ + Cl^- + \text{organics}$$

were measured by following the disappearance of $M(CNIph)_6$ on the tail of the lowest energy absorption. A carefully weighted amount of complex (about 10 mg) was placed into the degassable cell described above. Then exactly 3 ml of carefully freeze-thaw degassed chloroform were distilled into the cell. These operations were carried out in the dark. The disappearance of absorbance was followed as a function of irradiation time, usually taking five or six points. Plots of A vs. irradiation time were linear out to 15% conversion. The quantum yield was then obtained directly from the slope. These yields were highly reproducible.

For $M(CNPh)_6$ (M = Mo, W), the absorbance was found to increase on the low energy tail so that these quantum yields were obtained by the same method as for the pyridine substitution reaction, product extinction coefficients again being determined in a separate experiment.

The quantum yield data for $Cr(CNIph)_6$ in chloroform need some further discussion. Initial irradiation at 436 nm in chloroform causes the absorbance at 574 nm to increase rapidly and then decrease linearly with time. A typical plot of A_{574} vs. irradiation

time at 436 nm in shown in Figure 44. Analysis of the linear decay portion of the data (after 9 minutes) is very reproducible and gives $\phi_{disappearance} = 0.19 \pm 0.01$. A likely cause of the initial increase in absorbance at 574 nm is photolysis of $Cr(CNIph)_6$ to a species of the form $Cr(CNIph)_5L$ where L is an amine impurity in the $Cr(CNIph)_6$. Assuming an ϵ of 19,000 for $Cr(CNIph)_5L$, the maximum amount of amine impurity is A = 0.275, A/ϵ = concentration $\times 10^{-5}$M of $Cr(CNIph)_5L = 1.45 \times 10^{-5}$M, $[Cr(CNIph)_5L]/Cr(CNIph)_6 = 0.44\%$.

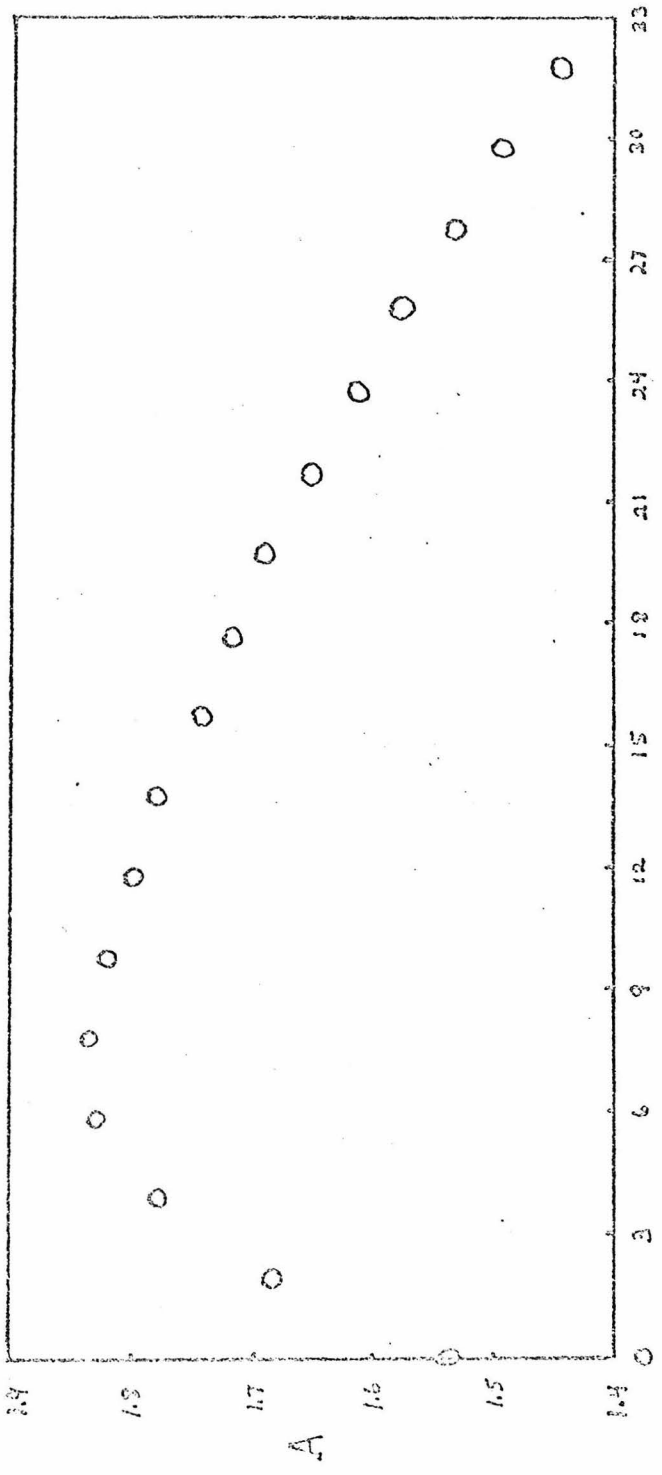

Figure 44. The absorbance at 574 nm as a function of time for the photolysis of a 3.246×10^{-3} solution of $Cr(CNIph)_6$ in degassed chloroform.

Appendix 1

Modified Version of OPTSPEC

(original version written by Jeff Hare)

```
      COMMON/DATBLK/WV(1000),AB(1000),BWV(1000),BAB(1000)
      COMMON/OPTBLK/SCALE,KK,NDATA,IT
      COMMON/COMPLO/ITEST,XLNGTH,YLNGTH
      NAMELIST/OPTION/IT,NTITL,NOPLT,NBASE,JLNTH,JNUM,KL,NABS,DELT,RHO,
     ZSCALE,KN
C     NN IS THE NUMBER OF DIGITIZED CARDS FOR THE SPECTRUM.  SCA IS
C     ABSORBANCE SCALE OF CARDS, SCW IS WAVELENGTH SCALE OF CARDS.
C     MM IS THE NUMBER OF DIGITIZED CARDS OF BASELINE.
C     NDAT IS THE NUMBER OF SETS OF DATA.
C     TO RETAIN OPTIONS FOR SUCCEEDING DATA DECK PUNCH SAME IN FIRST
C     FOUR COLUMNS OF CARD PRECEDING DATA DECK.  TO RETAIN THE
C     BASELINE, PUNCH SAME IN FIRST FOUR COLUMNS OF CARD FOLLOWING
C     DATA DECK.  THESE CARDS MUST NOT BE PRESENT IN INITIAL DATA DECK.
2     FORMAT(I3,F7.1,F5.1)
3     FORMAT((2X,7(F7.1,F7.3)))
5     FORMAT(2I3)
      READ(5,5)NDAT,NEMIT
      DO 12 IJ=1,NDAT
      READ(5,6) IKM
6     FORMAT(I3)
      IF(IKM.NE.0) GOTO 20
      GO TO 30
20    READ(5,OPTION)
30    READ(5,2) NN,SCA,SCW
      CALL DATRED(NN,SCA,SCW,WV,AB,N,NEMIT)
      WRITE(6,3) (WV(I),AB(I),I=1,N)
      IF(NBASE.EQ.0) GO TO 10
      READ(5,6)IKM
      IF(IKM.NE.0) GOTO 40
      GO TO 10
40    READ(5,2) MM,SCA,SCW
      CALL DATRED(MM,SCA,SCW,BWV,BAB,M,NEMIT)
      WRITE(6,3) (BWV(I),BAB(I),I=1,M)
10    IF(JLNTH.GE.1) CALL LINPLT(N,KL,NBASE,M,NABS,NP,NTITL,ND,&15,DELT,
     ZRHO,NOPLT,LDIF)
      IF(JNUM.GE.1) CALL NUMPLT(N,KN,NBASE,M,NABS,DELT,RHO,NOPLT,NP,ND,
     ZNTITL,&15,LDIF)
C     DATA HAS NOW BEEN PLOTTED ACCORDING TO OPTIONS GIVEN.
   12 CONTINUE
      STOP
15    WRITE(6,16) LDIF
16    FORMAT(2X,'YOU HAVE EXCEEDED THE MAXIMUM X-SCALE OF 50 INCHES.
     ZYOUR SCALE IS',2X,I3,2X,'INCHES')
      STOP
      END
      SUBROUTINE DATRED(IDR,SCA,SCW,Z,Y,J,NEMIT)
      DIMENSION Z(1000),Y(1000),IABZ(1000),IWAVE(1000)
      IDR=IDR*5
      READ(5,1102) (IWAVE(I),IABZ(I),I=1,IDR)
1102   FORMAT((1X,5(2I7),9X))
      J=0
      DO 1149 I=1,IDR
      IF(IWAVE(I).LE.0) GO TO 1149
      J=J+1
      Z(J)=0.0
```

```
      Y(J)=0.0
      Z(J)=FLOAT(WAVE(I))/SCW
      Y(J)=FLOAT(ABZ(I))/SCA
      IF(NEMIT.NE.0) GOTO2
      GOTO 1149
    2 X=Z(J)
      X1=2*(-463.993042*4.70604737*X-1.827965372E-02*X**2+3.297836079E-
     Z05*X**3-2.663711413E-08*X**4+1.351673912E-11*X**5-2.209848685E-14*
     ZX**6+2.963376321E-17*X**7-7.061177302E-20*X**8+1.955866691E-22*X**-
     Z9-2.259072966E-25*X**10+8.928261361E-29*X**11)
      Y(J)=X1*Y(J)
 1149 CONTINUE
      RETURN
      END
      SUBROUTINE LTHPLT(N,KL,NB,M,NABS,NP,NTITL,ND,*,DELT,RHO,NOP,LDIF
     Z)
      COMMON/DATBLK/WV(1000),AB(1000),BWV(1000),BAB(1000)
      COMMON/OPTBLK/SCALE,KK,NDATA,IT
      COMMON/DUMBLK/LDX(1000),AABS(1000)
      COMMON/COMPLO/ITEST,XLNGTH,YLNGTH
      DIMENSION BB(3),DD(3),FMT(2),WVLTH(2500),ABZ(2500),BABZ(2500)
      DATA BB/'DATA',0.0,1.0/
      DATA DD/2*0.0,1.0/
      DATA FMT/'(F6.','0)'/
      DATA LP/5/
      ITEST=1
      YLNGTH=10.0
      CALL SORTI2(WV,N,LDX)
      DO 109 I=1,N
      K=LDX(I)
  109 AABS(I)=AB(K)
      DO 119 I=1,N
  119 AB(I)=AABS(I)
      IF(NB.EQ.0) GO TO 100
      CALL SORTI2(BWV,M,LDX)
      DO 179 I=1,M
      K=LDX(I)
  179 AABS(I)=BAB(K)
      DO 189 I=1,M
  189 BAB(I)=AABS(I)
      LBMIN=IFIX(BWV(1))+1
      LBMAX=IFIX(BWV(M))
  100 LMIN=IFIX(WV(1))+1
      LMAX=IFIX(WV(N))
      IF(KL.EQ.1) SCALE=100.0
      IF(KL.EQ.2) SCALE=50.0
      IF(KL.EQ.3) SCALE=40.0
      IF(KL.EQ.4) SCALE=20.0
C     DATA HAS BEEN SORTED IN PROPER ORDER FOR SPLINE, AND PROPER PLOTTI
C     NG SCALE HAS BEEN ASSIGNED.
      IF(NB.EQ.0) GO TO 107
      IF(LBMIN.GT.LMIN) LMIN=LBMIN
      IF(LBMAX.LT.LMAX) LMAX=LBMAX
  107 WMIN=FLOAT(LMIN)
      WMAX=FLOAT(LMAX)
      AKK=50.0*(WMAX-WMIN)/SCALE
      KK=IFIX(AKK)
      SCC=SCALE/50.0
      WVLTH(1)=WMIN
      DO 149 J=2,KK
```

```
      I=J-1
      WVLTH(J)=WVLTH(I)+GCC
149   CONTINUE
      CALL DUPL(N,WV,AB,L)
      N=L
      IF(NB.EQ.0) GO TO 108
      CALL DUPL(M,BWV,BAB,L)
      M=L
108   CALL SPLINA(N,WV,AB,KK,WVLTH,ABZ)
      IF(NB.EQ.0) GO TO 110
      CALL SPLINA(M,BWV,BAB,KK,WVLTH,BABZ)
      DO 199 I=1,KK
      ABZ(I)=ABZ(I)-BABZ(I)
199   CONTINUE
110   IF(NABS.EQ.0) GO TO 101
      DO 209 I=1,KK
      ABZ(I)=DELT+RHO*ABZ(I)
209   CONTINUE
C     PLOTTING PARAMETERS ARE NOW CALCULATED
101   CALL MAXMIN(ABZ,KK,YMAX,YMIN)
      NSC=IFIX(SCALE)
      LLMIN=(LMIN/NSC)*NSC
      LLMAX=(LMAX/NSC)*NSC+NSC
      LDIF=(LLMAX-LLMIN)/NSC
999   IF(LDIF.GT.50) GO TO 102
      IF(YMIN.GE.0) GO TO 103
      DO 139 I=1,KK
      ABZ(I)=ABZ(I)-YMIN
139   CONTINUE
103   XLNGTH=17.0-1.00/SCALE
      LAB=-1
      LL=LDIF/15+1
      II=1
      JJ=1
      YMIN=0.000
      YMAX=2.000
      CALL LABEL(0.0,0.0,YMIN,YMAX,10.0,10,'ABSORBANCE',10,1)
      DO 159 MOX=1,LL
      ISTRT=LLMIN+17*NSC*(MOX-1)
      ISTOP=LLMIN+17*NSC*MOX
      IF(ISTRT.EQ.ISTOP) GO TO 112
      XMIN=FLOAT(ISTRT)
      XMAX=FLOAT(ISTOP)-SCALE
      XXMAX=FLOAT(ISTOP)-1.00/SCALE
      IF(ISTOP.GE.LLMAX) ISTOP=LLMAX
      IF(ISTOP.EQ.LLMAX) XMAX=FLOAT(ISTOP)
      SIZE=(XMAX-XMIN)/SCALE
      LDIF=IFIX(SIZE)
      NUM=(ISTOP-ISTRT)*50/NSC
      NWV=1+50*17*(MOX-1)
      IF(MOX.EQ.LL) LAB=0
      JAF=NWV+NUM
      IF(JAF.GT.KK) NUM=KK-NWV+1
      IF(NOP.GT.0) GO TO 104
      DO 169 I=II,N
      IF(WV(I).GT.WVLTH(NUM)) GO TO 106
169   CONTINUE
106   NN=I-1
      II=I
      CALL VLABEL(0.0,0.0,XMIN,XMAX,SIZE,LDIF,'WAVELENGTH (IN NM)',18,0,
```

```
     ZFMT,LF)
      CALL XYPLT(NN,WV(JJ),AB(JJ),XMIN,XXMAX,YMIN,YMAX,BB,LAB,12)
      JJ=NN
      IF(LAB.EQ.-1) GO TO 104
      IF(IT.GT.0) CALL TYPLT
      CALL LABEL(SIZE,0.0,YMIN,YMAX,10.0,10,'ABSORBANCE',-10,1)
      CALL SYSEND(-1,1)
104   CALL VLABEL(0.0,0.0,0.0,XMIN,XMAX,SIZE,LDIF,'WAVELENGTH (IN NM)',18,0,
     ZFMT,LF)
      CALL XYPLOT(NUM,WVLTH(NWV),ABZ(NWV),XMIN,XXMAX,YMIN,YMAX,DD,LAB)
      IF(LAB.EQ.-1) GO TO 159
      CALL LABEL(SIZE,0.0,YMIN,YMAX,10.0,10,'ABSORBANCE',-10,1)
      CALL SYSEND(-1,1)
      GO TO 112
159   CONTINUE
112   RETURN
102   RETURN 1
      END
      SUBROUTINE NUMPLT(N,KL,NB,NABS,DELT,RHO,NOP,NP,ND,NIITL,*,NDIF)
      COMMON/DATBLK/WV(1000),AB(1000),BWV(1000),BAB(1000)
      COMMON/OPTBLK/SCALE,KK,NDATA,IT
      COMMON/DUMBLK/LDX(1000),AABS(1000)
      COMMON/COMPLD/ITEST,XLNGTH,YLNGTH
      DIMENSION WVNBR(2500),ABZ(2500),BB(3),DD(3),FMT(2),IDX(2500),
     2XR(2500),BABZ(2500)
      DATA BB/'DATA',0.0,1.0/
      DATA DD/2*0.0,1.0/
      DATA FMT/'(F5.',' 1)'/
      DATA LF/5/
      ITEST=1
      YLNGTH=10.0
      DO 309 I=1,N
309   WV(I)=1.00E-07/WV(I)
      CALL SORTI2(WV,N,LDX)
      DO 319 I=1,N
      K=LDX(I)
319   AABS(I)=AB(K)
      DO 329 I=1,N
329   AB(I)=AABS(I)
      IF(NB.EQ.0) GO TO 300
      DO 389 I=1,M
389   BWV(I)=1.00 E-07/BWV(I)
      CALL SORTI2(BWV,M,LDX)
      DO 399 I=1,M
      K=LDX(I)
399   AABS(I)=BAB(K)
      DO 409 I=1,M
409   BAB(I)=AABS(I)
      NBMIN=IFIX(BWV(1))+1
      NBMAX=IFIX(BWV(M))
300   NMIN=IFIX(WV(1))+1
      NMAX=IFIX(WV(N))
      IF(KL.EQ.1) SCALE=2000.0
      IF(KL.EQ.2) SCALE=1000.0
      IF(KL.EQ.3) SCALE=500.0
      IF(KL.EQ.4) SCALE=200.0
C     DATA HAS BEEN CHANGED TO WAVENUMBER, SORTED PROPERLY FOR SPLINE
C     AND PLOTTING SCALE HAS BEEN ASSIGNED.
      IF(NB.EQ.0) GO TO 304
      IF(NBMIN.GT.NMIN) NMIN=NBMIN
```

```
      IF(NBMAX.LT.NMAX) NMAX=NBMAX
304   NMIN=FLOAT(NMIN)
      NMAX=FLOAT(NMAX)
      AKK=50.0*(NMAX-NMIN)/SCALE
      KK=IFIX(AKK)
      SCC=SCALE/50.0
      WVNBR(1)=NMIN
      DO 339 J=2,KK
      I=J-1
      WVNBR(J)=WVNBR(I)+SCC
339   CONTINUE
      CALL DUPL(N,WV,AB,L)
      N=L
      IF(NB.EQ.0) GO TO 305
      CALL DUPL(M,BWV,BAB,L)
      M=L
305   CALL SPLINA(N,WV,AB,KK,WVNBR,ABZ)
      IF(NB.EQ.0) GO TO 306
      CALL SPLINA(M,BWV,BAB,KK,WVNBR,BABZ)
      DO 419 I=1,KK
      ABZ(I)=ABZ(I)-BABZ(I)
419   CONTINUE
306   IF(NABS.EQ.0) GO TO 301
      DO 429 I=1,KK
      ABZ(I)=DELT+RMD*ABZ(I)
429   CONTINUE
301   CALL MAXMIN(ABZ,KK,YMAX,YMIN)
      NSC=IFIX(SCALE)
      NNMIN=(NMIN/NSC)*NSC
      NNMAX=(NMAX/NSC)*NSC+NSC
      NDIF=(NNMAX-NNMIN)/NSC
999   IF(NDIF.GT.50) GO TO 302
      IF(YMIN.GE.0) GO TO 303
      DO 379 I=1,KK
      ABZ(I)=ABZ(I)-YMIN
379   CONTINUE
      YMIN=0.000
303   YMAX=2.000
311   LAB=-1
      YMIN=0.000
      XLNGTH=17.0-1.00/SCALE
      LL=NDIF/15+1
      IT=0
      IF(IT.GT.0) CALL TIPLT
      CALL SORTD2(WVNBR,KK,IDX)
      DO 359 I=1,KK
      K=IDX(I)
359   XR(I)=ABZ(K)
      DO 369 I=1,KK
369   ABZ(I)=XR(I)
      CALL LABEL(0.0,0.0,YMIN,YMAX,10.0,10,LABSORBANCE1,10,1)
      DO 349 NOX=1,LL
      LLMAX=NNMIN
      ISTRT=NNMAX-17*NSC*(NOX-1)
      ISTOP=NNMAX-17*NSC*NOX
      IF(ISTRT.EQ.ISTOP) GO TO 310
      XMIN=FLOAT(ISTRT)
      XMAX=FLOAT(ISTOP)-SCALE
      XXMAX=FLOAT(ISTOP)-1.00/SCALE
      IF(ISTOP.LE.NNMIN) ISTOP=NNMIN
```

```
      IF(ISTOP.EQ.NNMIN) XMAX=FLOAT(ISTOP)
      SIZE=(XMIN-XMAX)/SCALE
      NDIF=IFIX(SIZE)
      NUM=(ISTRT-ISTOP)*50/NSC
      NWV=1+50*17*(MOX-1)
      IF(MOX.EQ.LL) LAB=0
      JAF=NWV+NUM
      IF(JAF.GT.KK) NUM=KK-NWV+1
      RMIN=XMIN/100.0
      RMAX=XMAX/100.0
      CALL VLABEL(0.0,0.0,0.0,RMIN,RMAX,SIZE,NDIF,'ENERGY IN KILOWAVENUMBERS
     $',25,0,FMT,LF)
      CALL XYPLOT(NUM,WVNBR(NWV),ABZ(NWV),XMIN,XXMAX,YMIN,YMAX,DD,LAB)
      IF(LAB.EQ.-1) GO TO 349
      CALL LABEL(SIZE,0.0,YMIN,YMAX,10.0,10,'ABSORBANCE',-10,1)
      CALL SYSEND(-1,1)
      GO TO 310
349   CONTINUE
310   RETURN
302   RETURN 1
      END
      SUBROUTINE DUPL(LNTH,WW,AA,J)
      DIMENSION WW(1),AA(1)
      J=1
      K=1
1500  DO 1509 I=2,LNTH
      X=10.0*WW(I)
      L=IFIX(X)
      IM1=I-1
      XX=10.0*WW(IM1)
      LM1=IFIX(XX)
      IF(L.EQ.LM1) GO TO 1501
      J=J+1
      WW(J)=WW(I)
      AA(J)=AA(I)
      K=1
      GO TO 1509
1501  AVM1=FLOAT(K)
      K=K+1
      AV=FLOAT(K)
      WW(J)=AVM1*WW(J)/AV+WW(I)/AV
      AA(J)=AVM1*AA(J)/AV+AA(I)/AV
1509  CONTINUE
1502  FORMAT(3X,'YOUR DATA IS ACCEPTABLE FOR SPLINA')
1503  FORMAT(3X,'DUPL HAS DELETED',I3,2X,'DATA POINTS'/)
      M=LNTH-J
      IF(M.GT.0) WRITE(6,1503) M
      WRITE(6,1502)
      RETURN
      END
      SUBROUTINE SPLINA(NN,X,Y,M,S,T)
C     SPLINE REVISED VERSION FOR OPTSPECT                              3
      DIMENSION X(1),Y(1),S(1),T(1),A(1000,3),B(1000),P(1000),H(1000)
      N=NN-1                                                           7
      NM1=N-1                                                          8
      DO 5 I=1,N                                                       9
5     H(I)=X(I+1)-X(I)
      DO 15 I=1,NM1                                                    11
      A(I,1)=H(I)/H(I+1)                                               12
      A(I,2)=2.0*(H(I+1)+H(I))/H(I+1)                                  13
```

```
      A(I,3)=1.0                                                          14
15    B(I)=6.0*((Y(I+2)-Y(I+1))/H(I+1)-(Y(I+1)-Y(I))/H(I))/H(I+1)
      A(1,1)=0                                                            16
      A(NM1,3)=0                                                          17
      CALL ALGEQQ(NM1,A,B,P)                                              18
      DO 35 I=1,M                                                         19
      IF(S(I).LT.X(1)) GO TO 10
      DO 25 J=1,N                                                         21
      IF(S(I).LE.X(J+1)) GO TO 20
   25 CONTINUE                                                            23
   10 WRITE (6,6)I                                                        24
    6 FORMAT('0   THE ',I5,'TH ELEMENT OF ARRAY S IS OUT OF RANGE ------  25
     CERROR MESSAGE FROM SPLINA')                                         26
      GO TO 35                                                            27
   20 IF(J .EQ. 1) GO TO 30                                               28
      IF(J .EQ. N) GO TO 40                                               29
      T(I)=(P(J-1)*(X(J+1)-S(I))**3+
     +      P(J)*(S(I)-X(J))**3+(6.0*Y(J+1)-H(J)**2*P(J))*(S(I)-X(J))+
     +(6.0*Y(J)-H(J)**2*P(J-1))*(X(J+1)-S(I)))/(6.0*H(J))
      GO TO 35                                                            33
30    T(I)=(P(J)*(S(I)-X(J))**3+(6.0*Y(J+1)-H(J)**2*P(J))*(S(I)-X(J))+
     +6.0*Y(J)*(X(J+1)-S(I)))/(6.0*H(J))
      GO TO 35                                                            36
40    T(I)=(P(J-1)*(X(J+1)-S(I))**3+
     +6.0*Y(J+1)*(S(I)-X(J))+
     +(6.0*Y(J)-H(J)**2*P(J-1))*(X(J+1)-S(I)))/(6.0*H(J))
   35 CONTINUE                                                            40
      RETURN                                                              63
      END                                                                 64
       SUBROUTINE ALGEQQ(N,A,B,Y)                                    AL    2
      DIMENSION A(1000,3),U(1000,3),D(1000,3),B(1),Y(1)              AL    4
      U(1,2)=A(1,2)                                                  AL    5
      U(1,3)=A(1,3)                                                  AL    6
      Y(1) = B(1)                                                    AL    7
      DO 10 I = 2, N                                                 AL    8
      I1 = I - 1                                                     AL    9
      D(I,2) = 1.                                                    AL   10
      U(I,3) = A(I,3)                                                AL   11
      D(I,1) = A(I,1) /U(I1,2)                                       AL   12
      U(I,2) = A(I,2) - D(I,1)*U(I1,3)                               AL   13
      IF (ABS(U(I,2)).LT.1.E-09) GO TO 35                            AL   14
   20 CONTINUE                                                       AL   15
   10 Y(I) = B(I) - D(I,1) * Y(I1)                                   AL   16
      Y(N) = Y(N) / U(N,2)                                           AL   17
      I = N                                                          AL   18
   25 I1 = I - 1                                                     AL   19
      Y(I1) = (Y(I1) - U(I1,3) * Y(I)) / U(I1,2)                     AL   20
      I = I - 1                                                      AL   21
      IF(I .EQ. 1) GO TO 15                                          AL   22
      GO TO 25                                                       AL   23
   15 RETURN                                                         AL   24
   35  WRITE (6,7)                                                   AL   25
    7  FORMAT (//5X'A IS A MATRIX WHICH REQUIRE PIVOTING OR IS SINGULAR'  26
     1)                                                             AL   27
      STOP                                                           AL   28
      END                                                            AL   29
      SUBROUTINE TIPLT
      DIMENSION BCD(2),BCE(2),BCF(4),BCG(4)
      DATA BCD/'GO S','IO'/
      DATA BCE/'  2 ','  4'/
```

```
      DATA BCF/'(0LI','VINE',' PHA','SE)'/
      DATA BCG/'**DE','TA**','    ',' LN'/
      CALL SYSSYM(12.0,9.0,0.5,BCD,6,0.0)
      CALL SYSSYM(12.0,8.75,0.5,BCE,7,0.0)
      CALL SYSSYM(12.0,8.0,0.25,BCF,15,0.0)
      CALL SYSSYM(12.0,7.5,0.25,BCG,15,0.0)
      RETURN
      END
//DATA   DD   *
```

Appendix 2

AREAKT

```
      DIMENSION IABZ(500),WAVE(500),ABZ(500),IWAVE(500),WNUM(500)
1     FORMAT(I3)
10    FORMAT(I5,2F10.5)
      READ(5,1) NSET
      DO 2 J=1,NSET
      READ(5,10) IDR,SCA,SCW
      IDR=IDR*5
      READ(5,3) (IWAVE(I),IABZ(I),I=1,IDR)
3     FORMAT((1X,5(2I7),9X))
      K=0
      DO 4 I=1,IDR
      IF(IWAVE(I).LE.0) GOTO 4
      K=K+1
      ABZ(K)=ABS(FLOAT(IABZ(I))/SCA)
      WAVE(K)=FLOAT(IWAVE(I))/SCW
      WNUM(K)=1.0 E07/WAVE(K)
      X=WAVE(K)
      X1=2*(-463.99302427+4.70604737*X-1.827965372E-02*X**2+3.297836079E-
     Z05*X**3-2.663711413E-08*X**4+1.351673912E-11*X**5-2.299848685E-14*
     ZX**6+2.963376321E-17*X**7-7.061177302E-20*X**8+1.955866691E-22*X**
     Z9-2.259072966E-25*X**10+8.928261361E-29*X**11)
      ABZ(K)=X1*ABZ(K)
      KSAVE=K-1
4     CONTINUE
      A=0.0
      DO 5 IJ=1,KSAVE
6     FORMAT(1X,F10.2,I10)
5     A=A+((ABZ(IJ   )+ABZ(IJ   +1))*(WNUM(IJ   )-WNUM(IJ   +1))/2.0)
      WRITE(6,6) A,J
2     CONTINUE
      STOP
      END
//DATA   DD    *
```

References

1. L. Malatesta and F. Bonati, "Isonitrile Complexes of Metals," Wiley, New York, 1969.
2. I. Ugi, ed., "Isonitrile Chemistry," Academic Press, New York, 1971.
3. P. M. Treichel, Adv. Organometal Chem., 11, 21 (1973).
4. F. Bonati and G. Minghetti, Inorg. Chim. Acta, 9, 95 (1974).
5. P. Fantucci, L. Naldini, F. Cariati, V. Valenti, and C. Brusseto, J. Organometal Chem., 64, 109 (1974).
6. A. C. Sarapu and R. F. Fenske, Inorg. Chem., 11, 3021 (1972); 14, 247 (1975).
7. Y. Dartiguenave, M. Dartiguenave, and H. B. Gray, Bull. Soc. Chim. France, 4225 (1969).
8. P. C. Fantucci, V. Valenti, and F. Cariati, Inorg. Chim. Acta, 5, 425 (1971).
9. J. M. Pratt and P. R. Silverman, J. Chem. Soc. (A), 1286 (1967).
10. V. Valenti, A. Sgamellotti, F. Cariati, and L. Naldini, Ric. Sci., 38, 1230 (1968).
11. A. Sacco and F. A. Cotton, J. Amer. Chem. Soc., 84, 2043 (1962).
12. P. M. Treichel and G. J. Essenmacher, Inorg. Chem., 15, 146 (1976).
13. G. Gondroelli, L. Giallongo, A. Giuffrida, and G. Romeo, Inorg. Chim. Acta, 7, 7 (1973).

14. L. Malatesta, A. Sacco, and S. Ghielmi, Gazz. Chim. Ital., 82, 516 (1952).

15. K. R. Mann, M. Cimolino, G. L. Geoffroy, G. S. Hammond, A. A. Orio, G. Albertini, and H. B. Gray, Inorg. Chim. Acta, 16, 97 (1976).

16. L. Malatesta and A. Sacco, Ann. Chim. (Italy), 43, 622 (1953).

17. A. Sacco and L. Naldini, Gazz. Chim. Ital., 86, 207 (1956).

18. P. Gans and S. M. E. Haque, Chem. Ind., 978 (1972).

19. Computer programs available through the CRYM crystallographic computing system on the IBM 370/158 computer at the California Institute of Technology. Scattering factors for Cr, C, and N were calculated by the method of D. T. Cromer and J. B. Mann, Acta Cryst., A24, 321 (1968). The scattering factor for H is that given in R. F. Stewart, E. R. Davidson, and W. T. Simpson, J. Chem. Phys., 43, 3175 (1965).

20. (a) G. Germain, P. Main, and M. M. Woolfson, Acta Cryst., Sect. A, 27, 368 (1972); (b) P. Main, M. M. Woolfson, L. Lessinger, G. Germain, and J. P. Delclercq, "Multan 74, A System of Computer Programes for the Automatic Solution of Crystal Structures from X-ray Diffraction Data," University of York, York, England and Laboratoire de Chemie Physique et de Cristallographie, Louvain-la-Neuve, Belgium, December 1974.

21. Least squares refinement was accomplished by the program UCIGLS which is derived from ORFLS, with substantial modifications and additions made at Brookhaven, Wisconsin, and Northwestern. The present UCI version is written in Fortran IV. See R. J. Doedens and L. F. Dahl, J. Amer. Chem. Soc., 88, 4847 (1966).

22. L. O. Brockway, R. V. G. Ewens, and M. W. Lister, Trans. Faraday Soc., 34, 1350 (1938).

23. D. S. Matteson and R. A. Bailey, J. Amer. Chem. Soc., 90, 3761 (1968).

24. W. D. Horrocks, Jr., and R. Craig Taylor, Inorg. Chem., 2, 723 (1963).

25. I. Ugi and R. Meyer, Chem. Ber., 93, 239 (1960).

26. N. A. Beach and H. B. Gray, J. Amer. Chem Soc., 90, 5713 (1968).

27. This complex was made by the method of D. S. Matteson and R. A. Bailey, J. Amer. Chem. Soc., 90, 376 (1968). The small amount of complex obtained was characterized by IR and used immediately, since it is quite unstable. Its UV-VIS spectrum is very similar to $Cr(CNPh)_6$ with bands occurring at 300 nm (sh), 370 nm, and 440 nm (sh).

28. R. W. Harrigan and G. A. Crosby, J. Chem. Phys., 59, 3468 (1973).

29. K. W. Hipps and G. A. Crosby, J. Amer. Chem. Soc., 97, 7042 (1975).

30. R. G. Pearson, J. Amer. Chem. Soc., 91, 4947 (1969).

31. M. D. Sturge, Solid State Phys., 20, 91 (1967).

32. J. W. Dawson, T. J. McLenan, W. Robinson, A. Merle, M. Dargiguenave, Y. Dartiguenave, and H. B. Gray, J. Amer. Chem. Soc., 96, 4428 (1974).

33. J. W. Dawson, H. B. Gray, J. E. Hix, J. R. Preer, and L. M. Venanzi, J. Amer. Chem. Soc., 94, 2979 (1972).

34. J. A. Alexander and H. B. Gray, J. Amer. Chem. Soc., 90, 4260 (1968).

35. M. K. Lloyd and J. A. McCleverty, J. Orgmet. Chem., 61, 261 (1973).

36. P. M. Triechel and G. E. Dineen, J. Orgmet. Chem., 39, C20 (1972).

37. R. A. Palmer and T. S. Piper, Inorg. Chem., 5, 864 (1966).

38. C. K. Jorgensen, Acta Chem. Scand., 11, 166 (1957).

39. F. E. Lytle and D. M. Hercules, J. Amer. Chem. Soc., 91, 253 (1969).

40. J. N. Demas and G. A. Crosby, J. Amer. Chem. Soc., 93, 2841 (1971).

41. G. A. Crosby, W. G. Perkins, and D. M. Klassen, J. Chem. Phys., 43, 1498 (1965).

42. D. M. Klassen and G. A. Crosby, J. Chem. Phys., 48, 1853 (1968).

43. R. W. Harrigan, G. D. Hager, and G. A. Crosby, Chem. Phys. Lett., 21, 487 (1973).

44. J. P. Paris and W. W. Brandt, J. Amer. Chem. Soc., 81, 5001 (1959).

45. C. Lin and N. Sutin, J. Phys. Chem., 80, 97 (1976).

46. C. S. Kraihauzel and F. A. Cotton, Inorg. Chem., 2, 533 (1963).

47. M. Wrighton, Inorg. Chem., 13, 905 (1974).

48. M. Wrighton, G. S. Hammond, and H. B. Gray, J. Amer. Chem. Soc., 93, 4336 (1971); Mol. Photochem., 5, 179 (1973).

49. M. Wrighton, Chem. Rev., 74, 401 (1974).

50. L. S. Forster, "Concepts of Inorganic Photochemistry," A. W. Adamson and P. D. Fleischauer, eds., Wiley-Interscience, p 31.

51. Personal communication from Steve Milder.

52. D. L. Lewis and S. J. Lippard, J. Amer. Chem. Soc., 97, 2697 (1975).

53. M. Novotny and S. J. Lippard, J. Chem. Comm., 2, 02 (1973).

54. F. Bonati and G. Minghetti, Inorg. Chem., 9, 2642 (1970).

55. D. F. Lewis and S. J. Lippard, Inorg. Chem., 11, 621 (1972).

56. J. C. D. Brand and W. Sneddon, Trans. Faraday Soc., 53, 894 (1957).

57. O. Traverso, M. A. Scandola, F. Scandola, Attidel II Convegno Nazionale di Chimica Inorganica, Bressanone, July 1969, p 157.

58. C. R. Bock, T. J. Meyer, and D. G. Whitten, J. Amer. Chem. Soc., 96, 4710 (1974).

59. G. Navon and N. Sutin, Inorg. Chem., 13, 2159 (1974).

60. G. S. Laurence and U. Balzani, Inorg. Chem., 13, 2976 (1974).

61. C. R. Bock, T. J. Meyer, and D. G. Whitten, J. Amer. Chem. Soc., 97, 2909 (1975).

62. C. T. Lin and N. Sutin, J. Amer. Chem. Soc., 97, 3543 (1975).

63. C. Creutz and N. Sutin, Inorg. Chem ., 15, 496 (1976).

64. J. Van Houten, R. J. Watts, J. Amer. Chem. Soc., 97, 3843 (1976).

65. W. P. Weber, G. W. Gokel, and I. K. Ugi, Angew. Chem. Internat. Edit., 11, 530 (1972).

66. W. L. Jolly, "The Synthesis and Characterization of Inorganic Compounds," Prentice-Hall, Englewood Cliffs, New Jersey, 1970.

67. A. B. Brignole and F. A. Cotton, Inorg. Syn., 13, 87 (1972).

68. G. W. Haupt, J. Optical Soc. of America, 42, 441 (1952).

69. J. N. Demas and G. A. Crosby, 92, 7262 (1970).

70. C. A. Parker, Proc. Roy. Soc. (London), A220, 104 (1953).

71. G. G. Halchard and C. A. Parker, ibid., A235, 518 (1956).

72. J. G. Calvert and J. N. Pitts,"Photochemistry," John Wiley and Sons, Inc., New York, 1966, pp 783-786.

73. G. Geoffroy, private communication.

74. E. E. Wegner and A. W. Adamson, J. Amer. Chem. Soc., 88, 394,(1966).

75. O. Kling, E. Nikolaiski, and H. L. S. Schlafer, Ber. Bunsenges. Physik. Chem., 67, 883.

CHAPTER 2

SPECTRAL CHARACTERIZATION OF Rh(I) ISOCYANIDE COMPLEXES

There has been considerable recent interest in the optical spectra and electrical conductivities of platinum compounds in which direct metal-metal interactions are present.[1-6] Perhaps the best known examples are the double salts, such as $[Pt(NH_3)_4]$-$[PtCl_4]$ (Magnus' green salt or MGS).[1] Low solubility of the double salts has generally restricted study to solid samples, although it should be noted that Isci and Mason have obtained electronic spectra for certain $[Pt(CNR)_4][Pt(CN)_4]$ complexes in ethanol solution.[6]

Many simple platinum salts also possess unusual properties.[2,3] The planar ions in these compounds, as in MGS, stack face-to-face in infinite columns. However, with the exception of one or two mixed-valence aggregates, notably $[Pt(C_2O_4)_2]_n^{1.6n-}$, complete dissociation to monomeric fragments occurs in solution. Even the copper-colored, mixed-valence Krogmann's salt, $K_2Pt(CN)_4Cl_{0.3}\cdot 3H_2O$, forms a nearly colorless solution containing discrete Pt(II) and Pt(IV) complex ions.[2]

We have begun a systematic investigation of metal ($\underline{d}^8$)-metal ($\underline{d}^8$) interactions in solution. Systems that appear to be highly promising are based on planar Rh(I) and Ir(I) arylisocyanides.[7] Here we report an electronic spectroscopic characterization of the oligomers formed in solutions of Rh(I) isocyanide complexes.

Experimental

The starting material $[Rh(COD)Cl]_2$ was prepared by the method of Chatt.[8] The isocyanides were prepared via the Hoffmann Carbylamine reaction[9] and were purified by vacuum distillation.

Table 1. Analytical Data

		C	H	N	Rh	$\bar{\nu}$(CN) cm^{-1}
$Rh(CNPh)_4BF_4$	calc	55.8	3.30	9.30	17.1	2160 CH_2Cl_2
	found	55.67	3.84	9.32	16.84	
$Rh(CNPh)_4BPh_4$	calc	74.85	4.80	6.72		2160 CH_2Cl_2
	found	74.59	4.82	6.76		
$Rh(CNPh)_4PF_6$	calc	50.92	3.03	8.49	15.59	2160 CH_2Cl_2
	found	50.66	3.22	8.39	14.58	
$Rh(CNi\text{-propyl})_4PF_6$	calc	36.65	5.38	10.69		2160 Nujol
	found	36.36	5.22	10.63		
$Rh(CNi\text{-propyl})_4BPh_4$	calc	68.79	6.93	8.02		2160 Nujol
	found	68.51	6.97	7.97		
$Rh(CNcyclohexyl)_4BF_4$	calc	53.69	7.08	8.94		2160 Nujol
	found	53.53	7.00	9.00		
$Rh(CNcyclohexyl)_4PF_6$*	calc	49.13	6.48	8.18		2160 Nujol
	found	43.84	5.75	7.16		
$Rh(CNPhCH_3)_4PF_6$	calc	53.65	3.94	7.82	14.36	2160 CH_2Cl_2
	found	53.79	3.80	8.03	14.06	
					Cl	
$Rh(CNt\text{-butyl})_4Cl$	calc	51.01	7.71	11.90	7.53	2160 CH_2Cl_2
	found	50.94	7.85	11.64	7.36	
$Rh(p\text{-}CNPhCl)_4BF_4$	calc	45.45	2.18	7.57		2165 Nujol
	found	45.46	2.19	8.10		

*Contaminated with KPF_6.

Spectrograde solvents (CH_3CN, $CHCl_3$, C_6H_6) were used for recrystalization and spectral measurements.

Synthesis

$Rh(CNR)_4Cl$.[10,11] An excess of the desired isocyanide was added slowly to a warm benzene solution of $[Rh(COD)Cl]_2$. The immediate precipitate was filtered, washed with cold benzene, ether and air dried. Complexes of phenyl, cyclohexyl, isopropyl, tert-butyl, p-methoxyphenyl, and p-chlorophenyl isocyanide were synthesized by this method.

$Rh(CNR)_4BF_4$. Crude $Rh(CNR)_4Cl$ obtained above was dissolved in the minimum amount of water, filtered and the resulting solution was then added to a saturated water solution of $NaBF_4$. The resulting precipitate was then recrystallized from acetonitrile. Similar methods were used to synthesize BPh_4^- and PF_6^- salts using $NaBPh_4$ and KPF_6, respectively.

Spectral Data

Absorption spectra were measured using a Cary 17 spectrophotometer. Spectra were obtained in 1.00, 0.1, and 0.006 cm cells, all of which were calibrated with K_2CrO_4 solutions.[12] Infrared spectra were measured using a Perkin-Elmer 257 infrared spectrometer. Emission and excitation spectra were obtained using a Perkin-Elmer MPF-3A fluorescence spectrometer equipped with a standard accessory which corrects excitation spectra for varying lamp intensity and monochromator efficiency from 200-600 nm and corrects emission spectra for varying photomultiplier tube response and monochromator

efficiency from 400 - 700 nm. The spectra reported here are corrected. Measurements at 77 K were performed using a specially constructed low temperature quartz dewar.

The absorption spectra for $Rh(CNPh)_4PF_6$ in 0.1 M $TBA^+PF_6^-$/acetonitrile at 25 °C and $Rh(CNt\text{-}butyl)_4Cl$ in 0.1 M NaCl/water at 25 °C were obtained as a function of monomer concentration, C°. The collected data at selected wavelengths are given in Tables 2 and 3. A_3 was taken at 750 nm rather than at the peak position, 727 nm, to avoid overlap with the tail of the 568 nm absorption.

Table 2. Absorption Spectra as a Function of Concentration for $Rh(CNPh)_4PF_6$ in 0.1 M $TBAPF_6$

c in moles/liter	A_1 (568 nm)	A_3 (750 nm)
0.0	0.0	0.0
0.00085589	0.239000	0.0
0.00130777	0.537500	0.0
0.00141355	0.626400	0.0
0.00203667	1.160000	0.0
0.00240491	1.629999	0.0
0.00253978	1.684999	0.0
0.00284890	2.299999	0.0
0.00315502	2.459999	0.0
0.00392480	3.669999	0.0
0.00436278	4.410000	0.0
0.00444007	4.580000	0.0
0.00611910	8.099999	0.750000
0.00714957	9.940000	0.940000
0.00856020	12.969999	1.480000
0.00926504	14.299999	1.780000
0.01256100	23.659988	3.889999
0.01266858	24.649994	4.303699
0.01459300	28.949997	4.911900
0.01538100	33.199997	6.160000
0.02077590	45.559998	9.370000
0.02101800	49.629990	10.384999
0.02338200	55.899994	11.629999
0.02469320	59.079987	13.940000
0.02585990	61.839996	15.219999
0.02635250	66.929993	15.500000
0.03315650	91.119995	23.109985
0.04400670	130.199997	43.619995
0.04861300	151.899994	56.859985
0.05803900	175.500000	67.199997

Table 3. Absorption Spectra as a Function of Concentration for $Rh(CNt\text{-}Butyl)_4Cl$ in 0.1 M NaCl/water

c in moles/liter	A_1 (371 nm)	A_2 (490 nm)
0.0	0.0	0.0
0.00016140	0.034000	0.486000
0.00043322	0.298000	1.613999
0.00091223	1.254999	3.299999
0.00175837	6.082000	9.352200
0.00424727	17.821487	14.011950
0.00829200	43.409241	22.309998
0.00791050	41.692490	22.399490
0.00832466	43.327499	22.889999
0.01157380	63.919998	29.099991
0.01320900	76.027495	32.209991
0.01228500	73.738495	33.026993
0.01348510	77.008499	33.026993
0.01537500	97.445999	37.929993
0.01926139	118.536987	43.979996
0.02325383	147.967499	50.349991
0.02672600	163.299988	54.118500
0.03073970	197.012497	63.269989

Results and Discussion

A simplified energy level diagram for a monomeric $\underline{d}^8$ complex of the form $Rh(CNR)_4^+$ is shown in Figure 1. The level ordering $b_{2g}(xy) < e_g(xz, yz) < a_{1g}(z^2) \ll a_{2u}\pi < b_{1g}(x^2 - y^2)$ is based on that found for alkyl isocyanide complexes of square planar $\underline{d}^8$ metal ions which have been recently studied[13] in detail. Ignoring spin orbit coupling, we expect three spin allowed and three spin forbidden transitions from the $^1A_{1g}$ ground state.

Spectra of dilute solutions of $Rh(CNAlkyl)_4^+$ are all very similar and agree with the spectrum of $Rh(CNEthyl)_4$. The band positions and the extinction coefficients depend only slightly on the nature of the alkyl group (Table 4).

Absorption, emission, and excitation spectra of $Rh(CNPh)_4^+$ monomer are shown in Figure 2. Band positions and assignments are given in Table 5.

It is interesting to note that all MLCT transitions in $Rh(CNPh)_4^+$ are red shifted relative to those found in the $Rh(CNAlkyl)_4^+$ ions.

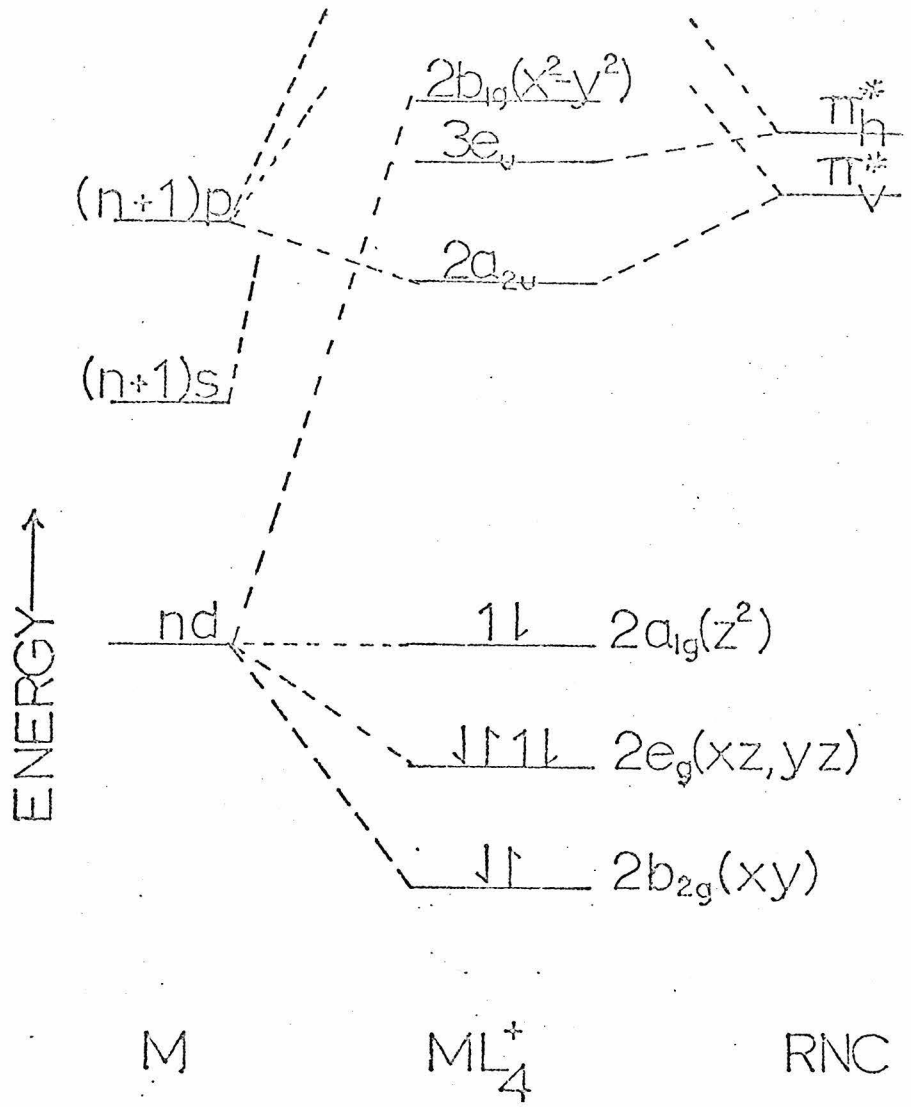

Figure 1. Molecular orbital diagram for $Rh(CNR)_4^+$ showing the spectroscopically important levels.

Table 4. Absorption Spectra of Alkyl Isocyanide Complexes of Rh(I)

Complex	$^1A_{1g} \rightarrow {}^1E_u$	$^1A_{1g} \rightarrow {}^3E_u$	$^1A_{1g} \rightarrow {}^1A_{2u}$	$^1A_{1g} \rightarrow {}^3A_{2u}$
$Rh(CNEthyl)_4^+$ [b]	307 (24.4)[a]	333 (3.45)	380 (8.40)	434 (0.26)
$Rh(CNi\text{-}propyl)_4BPh_4$ [c]	310 (28.0)	338 (3.80)	383 (11.2)	442 (0.34)
$Rh(CNcyclohexyl)_4BPh_4$ [c]	310 (32.8)	338 (4.20)	383 (11.8)	442 (0.39)
$Rh(CNt\text{-}butyl)_4Cl$ [c]	310 (25.5)	335 (3.40)	386 (9.90)	442 (0.30)

[a] nm ($\epsilon \times 10^{-3}$).

[b] Taken from reference 13.

[c] Determined at room temperature in CH_2Cl_2.

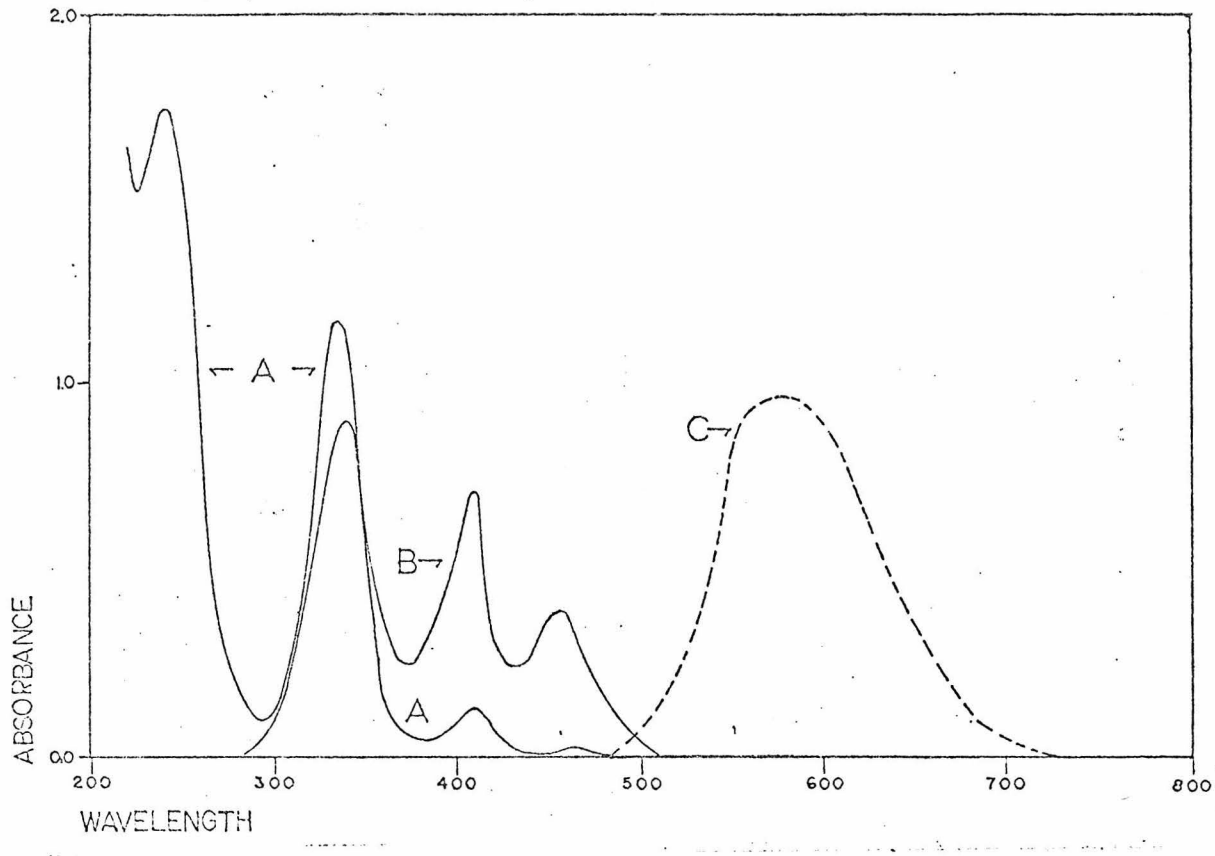

Figure 2. Curve A is the absorption spectrum at room temperature of $Rh(CNPh)_4BPh_4$ in acetonitrile, $C = 7.2 \times 10^{-6}$ M, 1 cm cell; Curve B is the excitation spectrum of $Rh(CNPh)_4BPh_4$ in an EPA glass at 77 K; Curve C is the emission spectrum of $Rh(CNPh)_3BPh_4$ in an EPA glass at 77 K.

Table 5. Absorption Spectra of Different Salts of the $Rh(CNPh)_4^+$ Cation

Compound[a]	Intraligand	$^1A_{1g} \rightarrow {}^1E_u$	$^1A_{1g} \rightarrow {}^1A_{2u}$	$^1A_{1g} \rightarrow {}^3A_{2u}$
$Rh(CNPh)_4BPh_4$	241 (60.5)	335 (40.2)	411 (5.00)	463 (0.63)
$Rh(CNPh)_4PF_6$	241 (59.2)	335 (49.1)	411 (5.94)	462 (0.67)
$Rh(CNPh)_4BF_4$	241 (59.4)	335 (41.7)	411 (5.71)	463 (0.66)

[a] Determined at room temperature in acetonitrile solution.

This shift is in line with the stabilization of the $a_{2u}\pi^*$ acceptor orbital via conjugation with the phenyl ring π system. This effect has previously been found to be important in other complexes of aromatic isocyanides.[14]

The shift for each band in $Rh(CNPh)_4^+$ relative to its counterpart in $Rh(CNAlkyl)_4^+$ is not constant from band to band, suggesting that slight energy shifts in the positions of the filled $e_g(d_{xy}, d_{yz})$ relative to the $a_{1g}(d_{z^2})$ orbital also occur.

The positions of the lowest spin allowed monomer band $^1A_{1g} \rightarrow {}^1A_{2u}$ in complexes of p-ClPhNC, p-MePhNC, and p-MeOPhNC are very close to those found for $Rh(CNPh)_4^+$, suggesting a very slight dependence of the band positions on phenyl ring substituents. This fact suggests that delocalization of the excited electron onto the phenyl ring is not a very important effect in these complexes.

$Rh(CNPh)_4^+$ was found to show strong emission in an EPA glass at 77°K. $Rh(CNAlkyl)_4^+$ complexes also emit under these conditions but were not studied.

The position of the emission which occurs at 580 nm in EPA glass at 77°K in $Rh(CNPh)_4^+$ is consistent with its assignment as $^3A_{2u} \rightarrow {}^1A_{1g}$. The red shift of the emission and the increase in the half width of the band relative to the corresponding spin forbidden absorbance band implies that the emitting state is somewhat distorted from the ground state's square planar geometry.[15] These effects have also been observed[16] in $[Rh(2\text{-phos})_2]Cl$ and $[Rh(2\text{-phos})_2]Cl$.

Such an effect may be caused by admixture of d-d states into the charge transfer excited state. The excitation spectrum in EPA at 77°K is very similar to the absorption spectrum revealing that relaxation processes from upper excited states to the $^3A_{2u}$ state are facile.

Representative absorption spectra for three different concentrations of $[Rh(CNPh)_4](PF_6)$ in acetonitrile solution are shown in Figure 3. The bands at 361, 411, and 468 nm dominate the low-concentration spectra and are logically due to monomeric $[Rh(CNPh)_4]^+$ as discussed previously. As the total Rh(I) concentration is increased, two new bands grow in, first at 568, then at 727 nm, while the higher energy bands decrease in relative intensity. Similar concentration dependences of the spectral charges are obtained with the BPh_4^- and BF_4^- salts (Figure 4), suggesting that the spectral changes are a property of the cation only. This behavior is interpreted in terms of an oligomerization equilibrium:

$$2M \overset{K_1}{\rightleftharpoons} D$$

$$D + M \overset{K_2}{\rightleftharpoons} T$$

where M = concentration of monomers, $Rh(CNPh)_4^+$,

D = concentration of dimers, $(Rh(CNPh)_4^+)_2$,

T = concentration of trimers, $(Rh(CNPh)_4^+)_3$.

Using the above equilibria expressions and the fact that the total concentration in terms of monomers must equal the weighted sum of all the species present, the following equations can be derived:

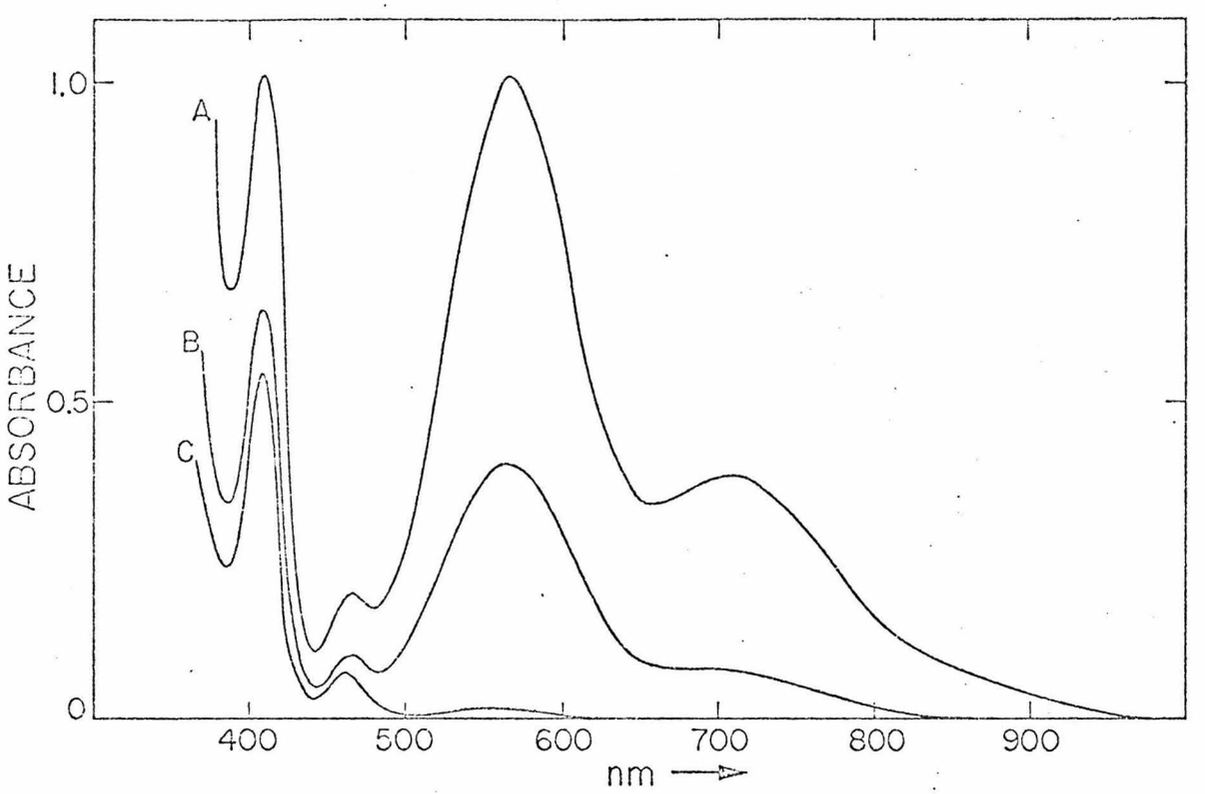

Figure 3. Absorption spectra of $Rh(CNPh)_4PF_6$ in acetonitrile at 25 °C. A; C = 5.7×10^{-2} M, path length = 0.06 mm; B, C = 2.7×10^{-2} M, pathlength = 0.06 mm, C, C = 6.3×10^{-4} M, pathlength = 0.75 mm.

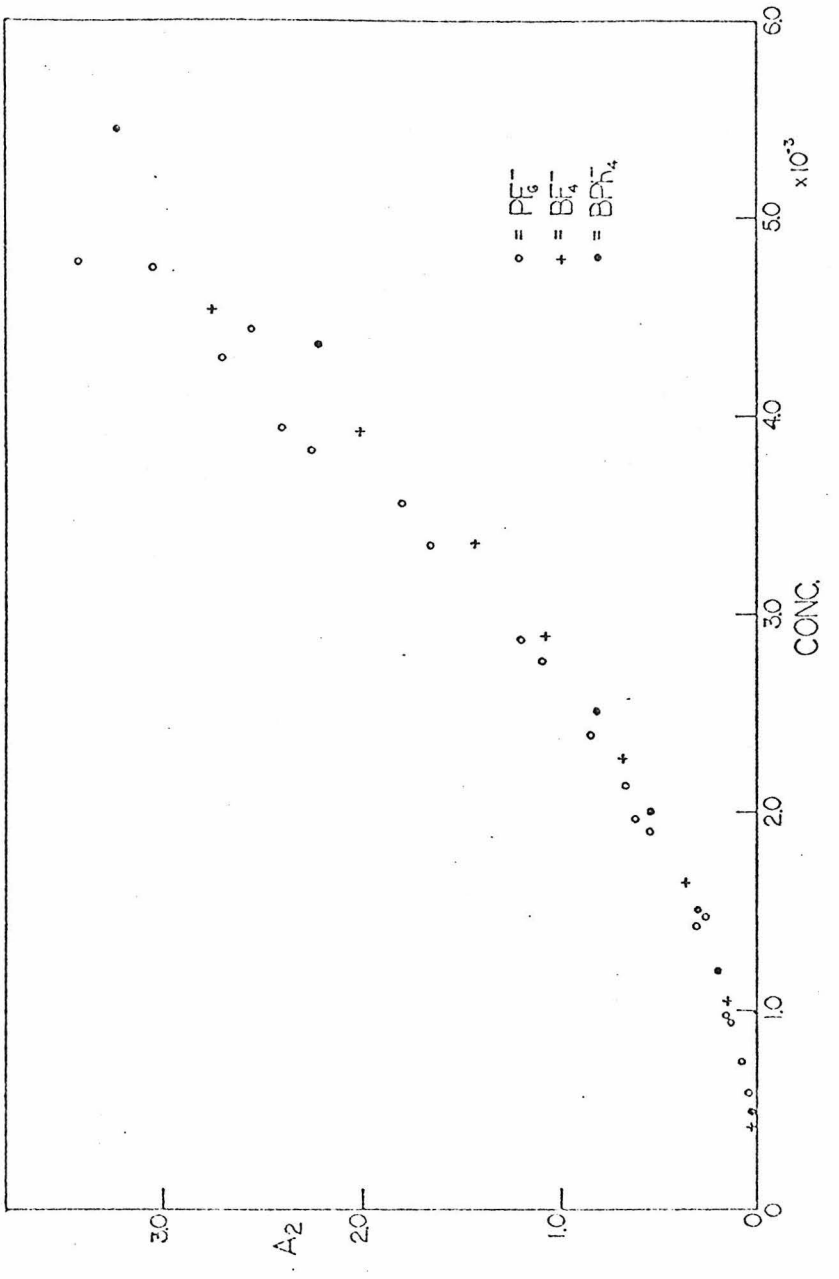

Figure 4. Plot of A_2 (568 nm) vs. stoichiometric Rh(I) concentration from 0 to 6×10^{-3} M for three different salts.

$$1)\quad \frac{c}{\sqrt{A_2}} = \frac{1}{\sqrt{\epsilon_2 K_1}} + \frac{2\sqrt{A_2}}{\epsilon_2} + \frac{3K_1K_2A_2}{\sqrt{\epsilon_2 K_1}\ \epsilon_2}$$

$$2)\quad A_3 = \frac{\epsilon_3 K_2 \sqrt{K_1}\ A_1^{3/2}}{\epsilon_2^{3/2}}$$

where c is the total Rh concentration in terms of monomer, A_2, A_3 are the absorbances due to only dimers and trimers; and ϵ_2, ϵ_3 are their corresponding extinction coefficients.

The band at 568 nm is logically assigned to the dimer (A_2) and the band which grows in more highly concentration solutions at 727 nm is assigned to a trimer absorption (A_3). These assignments are supported below.

A plot of $c/\sqrt{A_2}$ vs. $\sqrt{A_2}$ over the concentration range 5×10^{-2} M > c > 5×10^{-4} M in 0.1 M [(n-Butyl)$_4$N][PF_6] gives a straight line (Figure 5).

At the higher concentrations where the band at 727 nm (trimers) is present, this line still shows no deviation from linearity suggesting that the third term in equation (1) is much smaller than the first two terms. From the intercept ($1/\sqrt{\epsilon_2 K_1}$) and the slope ($2/\epsilon_2$) values for K_1 and ϵ_2, $K_1 = 35\ M^{-1}$ and $\epsilon_2 = 10,500$ are obtained. A plot of A_3 vs $A_2^{3/2}$ (eqn. (2)) (Figure 6) also gives a straight line with the slope equal to $\epsilon_3 K_1 K_2 / \sqrt{\epsilon_2 K_1}\ \epsilon_2 = 2.92 \times 10^{-2}$. Substituting in the values of K_1 and ϵ_2 from eqn (2) give $\epsilon_3 K_2 = 183,000$. Thus a value of ϵ_3 of 18,300 (a quite reasonable value) will give K_2 of 10 M^{-1}.

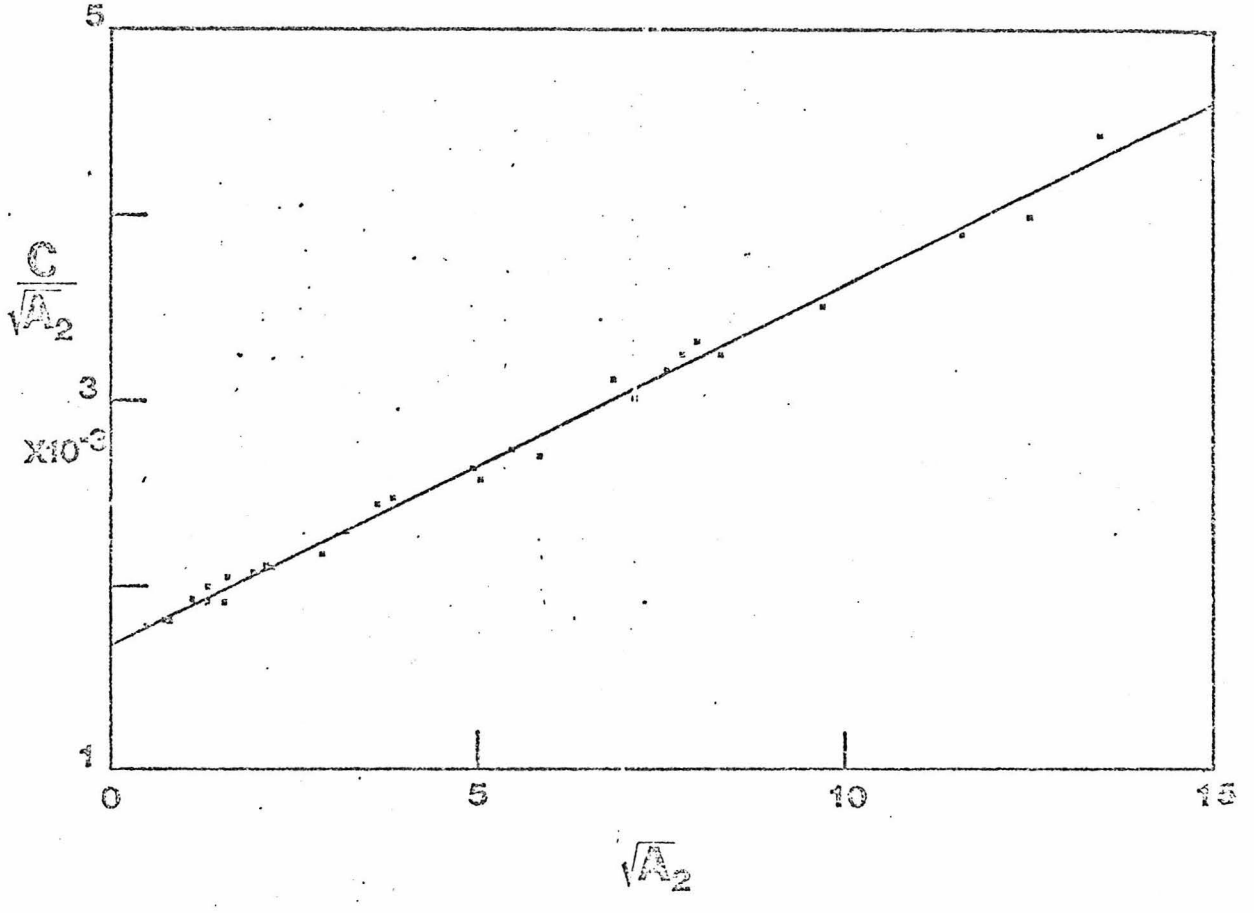

Figure 5. A plot of $C/\sqrt{A_2}$ vs. $\sqrt{A_2}$ for $Rh(CNPh)_4PF_6$ over the range 5×10^{-2} M > C > 5×10^{-4} M in 0.01 M $[(n\text{-Butyl})_4N][PF_6]/CH_3CN$.

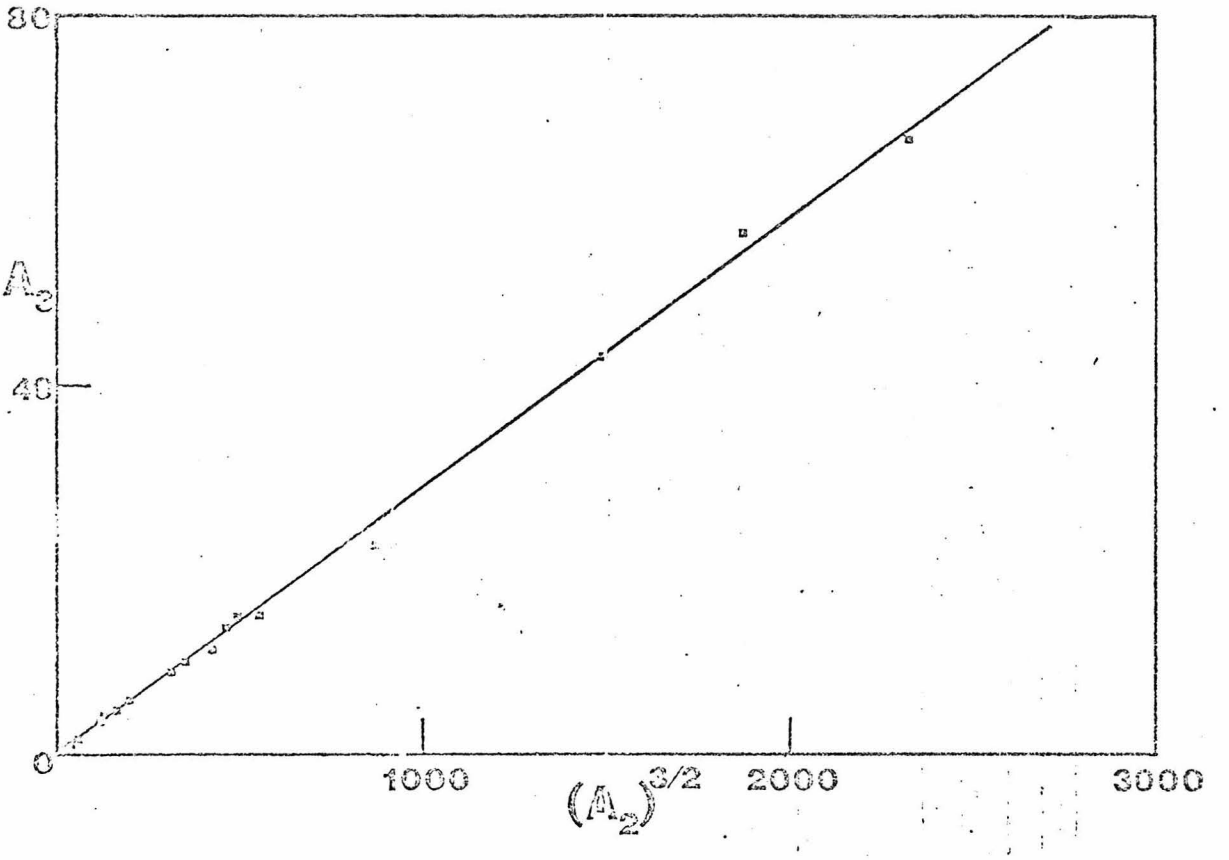

Figure 6. A plot of A_3 vs. $A_2^{3/2}$ for $Rh(CNPh)_4PF_6$ in 0.1 M $[(n\text{-Butyl})_4N][PF_6]/CH_3CN$.

The important information obtained from this equilibrium data is that it appears the equilibrium constant for adding another monomer unit to a dimer is similar to that for the initial formation of the dimer. Thus the interaction between two monomers and a monomer and a dimer appear to be of comparable magnitude. The nature of the interaction of the monomer units will be discussed in a later section.

Although no evidence for oligomerization of alkyl isocyanide complexes of Rh(I) in acetonitrile was found, $Rh(CNt\text{-}butyl)_4Cl$ was found to oligomerize in water solution. The absorption spectra show similar concentration effects.

The absorption due to the dimer was found at 490 nm with a band at 622 nm being assigned to a trimeric species. The band at 622 nm is present in solution only near the solubility limit of the complex. Concentration dependence data were not obtained for this absorption band. Data obtained in 0.1 M NaCl in water at 25 °C were obtained over the range $3 \times 10^{-2}\ M > C > 1.6 \times 10^{-4}\ M$. A plot of $c/\sqrt{A_2}$ vs. $\sqrt{A_2}$ (neglecting the third term in equation (1)) gives a straight line with $\epsilon_2 = 16,900$ and $K_1 = 251\ M^{-1}$ (Figure 7).

Since the data were not obtained in the same solvent, a direct comparison of the two equilibrium constants for $Rh(CNPh)_4^+$ and $Rh(CNt\text{-}butyl)_4^+$ cannot be made. The fact that dimer formation occurs in water but not in acetonitrile for $Rh(CNt\text{-}butyl)_4^+$ suggests that hydrophobic interactions of the large alkyl groups serve as part of the driving force for dimer formation in water. Also of importance

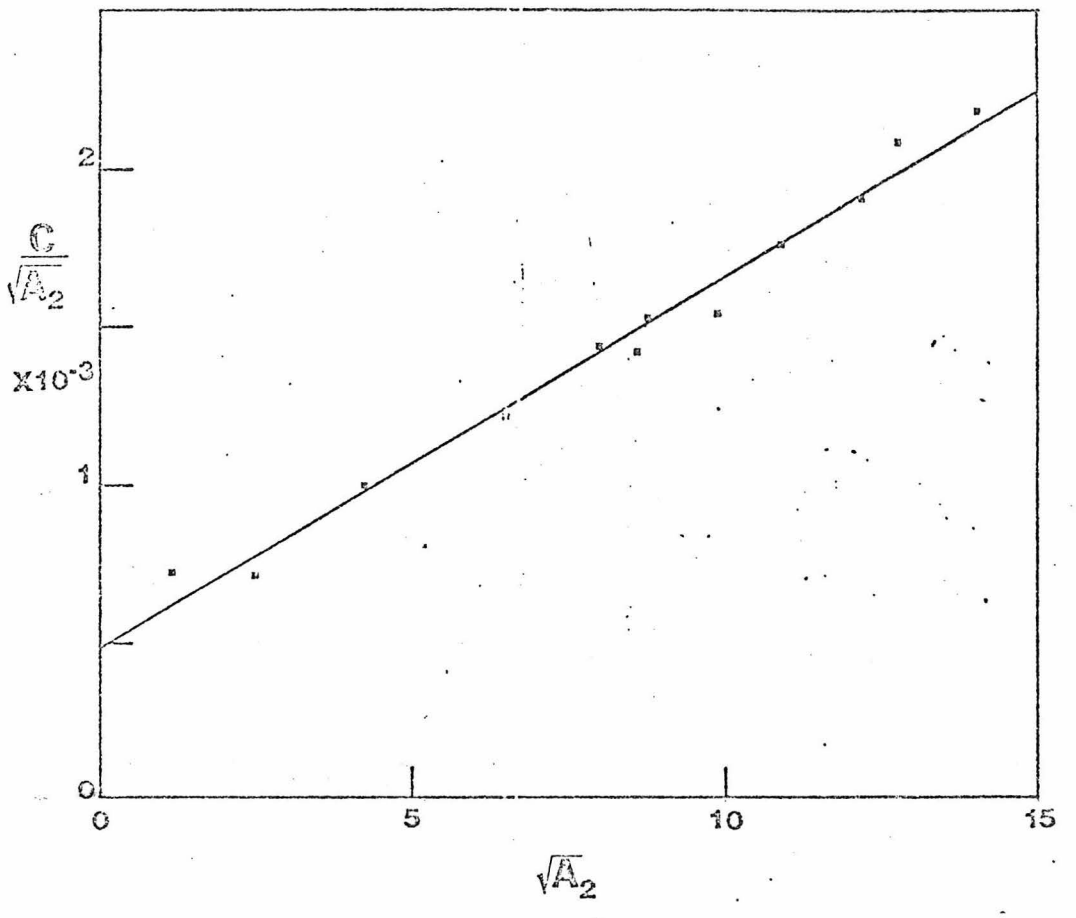

Figure 7. A plot of $C/\sqrt{A_2}$ vs. $\sqrt{A_2}$ for $Rh(CNt\text{-}butyl)_4Cl$ over the concentration range 3×10^{-2} M > C > 1.6×10^{-4} M in 0.1 M in 0.1 M $NaCl/H_2O$.

must be the ability of the higher dielectric medium, water (> 85) vs. acetonitrile (36.2) to stabilize the increase in charge density in going from two monopositive ions to one dipositive ion.

The electronic spectral properties of $[Rh(CNR)_4]_2^{2+}$ may be understood in terms of the orbital interactions diagrammed in Figure 8. As infrared spectral evidence rules out the involvement of bridging isocyanides,[17] the dimer is very probably bound through direct Rh---Rh interactions. These bonding interactions apparently are substantial, as they must overcome unfavorable coulombic forces between the cationic units. The orbitals that will interact most strongly are those that extend perpendicular to the molecular plane, namely the $a_{1g}(d_{z^2})$ and $a_{2u}[p_z, \pi^*(CNR)]$ functions. It is also important to note that a_{1g} is likely to be the HOMO, and a_{2u} the LUMO, in the monomeric units, as previously discussed.

It is not likely that there will be a significant energy difference between D_{4h} (eclipsed) and D_{4d} (staggered)rotameric configurations for the dimeric molecules where R = Ph, but the staggered configuration is much more likely for the dimer when R = t-butyl. The MO level scheme in Figure 2 gives symmetry labels for both possibilities. In both cases the upper and lower sets contain orbitals of the same symmetry, and as a result there will be considerable mixing, stabilizing the lower set ($1a_{1g}$, $1a_{2u}$, or $1a_1$, $1b_2$) and destabilizing the upper set ($2a_{1g}$, $2a_{2u}$, or $2a_1$, $2b_2$). As the lower set is filled, this stabilization must be the source of the intermonomer binding forces.

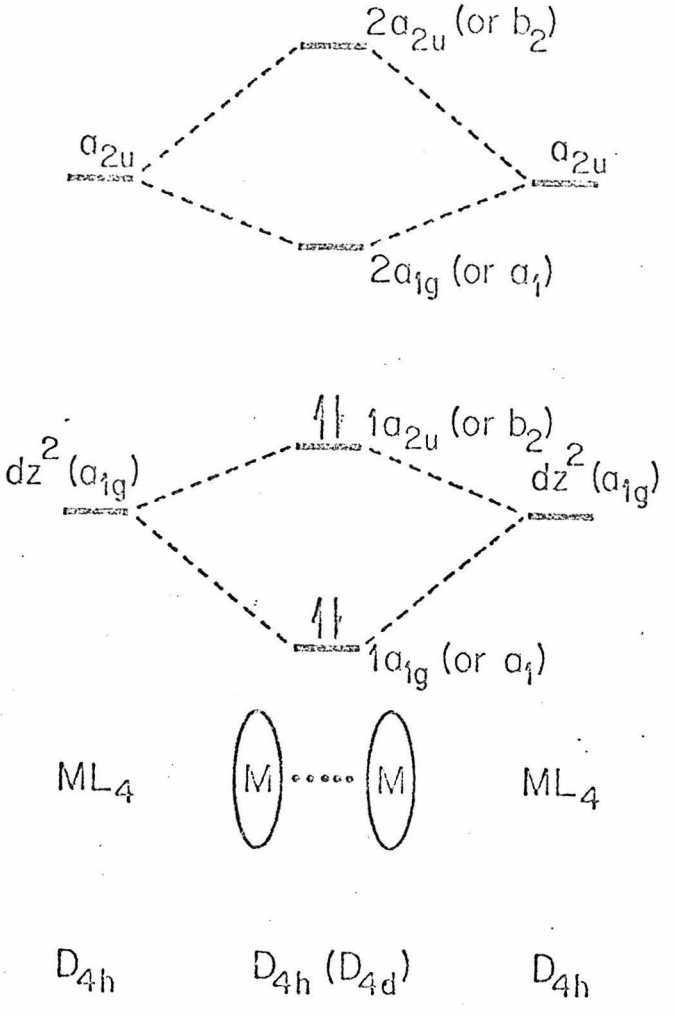

Figure 8. Relative energies of the molecular orbitals derived from $a_{1g}(d_{z^2})$ and a_{2u} monomer functions in D_{4h} (or D_{4d}) $[Rh(CNPh)_4]_2^{2+}$.

Two allowed electronic transitions are predicted for the dimer, one higher ($1a_{1g} \rightarrow 2a_{2u}$ or $1a_1 \rightarrow 2b_2$) and one lower ($1a_{2u} \rightarrow 2a_{1g}$ or $1b_2 \rightarrow 2a_1$) than the $a_{1g} \rightarrow a_{2u}$ excitation in the monomer. Thus the bands at 568 nm in $[Rh(CNPh)_4]_2^{2+}$ and at 490 nm in $[Rh(CNt\text{-}Butyl)_4]_2^{2+}$ are assigned to $1a_{2u} \rightarrow 2a_{1g}$ (or $1a_1 \rightarrow 2b_2$).

A similar analysis for a trimeric molecule predicts five allowed transitions, the lowest of which ($2a_{1g} \rightarrow 2a_{2u}$) is assigned to the 727 nm band in $[Rh(CNPh)_4]_3^{3+}$. The trimer band is observed for $Rh(CNt\text{-}Butyl)_4Cl$ at 622 nm.

In Table 6 are the locations of the lowest energy bands for the monomers, dimers, and trimers of several Rh(I) isocyanide complexes. According to simple Hückel theory, the dimer (E_D) and trimer (E_T) transition energies are given by: $E_D = E_M + \beta$; $E_T = E_M + \sqrt{2}\beta$; $E_M = E(a_{1g} \rightarrow a_{2u})$ in the monomer, and $\beta = \beta_{a_{1g}} + \beta_{a_{2u}}$.

The results for two of the complexes for which absorption data for monomers, dimers, and trimers are available (R = Ph and i-propyl) are given in Table 7.

The decreased value of β for the alkyl isocyanide vs. the aromatic isocyanide suggests a smaller interaction between the monomeric units.

Table 6. Band Positions for the Lowest Spin Allowed Band for Monomeric, Dimeric, and Trimeric Rh(I) Isocyanide Complexes

Complex	Monomer	Dimer	Trimer	Solvent
$Rh(CNPh)_4^+$	411[a]	568	727	CH_3CN
$Rh(p\text{-}CNPhCl)_4^+$	420	566	not observed	DMF
$Rh(CNt\text{-}butyl)_4^+$	371	490	622	H_2O
$Rh(CNi\text{-}propyl)_4^+$	383	495	610	H_2O
	383	505	not observed	CH_3CN
$Rh(CNcyclohexyl)_4^+$	383	516	not observed	CH_3CN

[a] Peak maxima in nm.

Table 7. Hückel analysis of $(Rh(CNPh)_4^+)_n$ and $(Rh(CNi\text{-}propyl)_4^+)_n$

Complex	E_M[a]	E_D[a]	E_T[a]
$Rh(CNPh)_4^+$	24.3[b]	17.2[b]	14.3[b]
	--	17.6[c]	13.8[c]
$Rh(CNi\text{-}propyl)_4^+$	26.1[b]	20.0[b]	16.4[b]
	--	19.6[d]	16.9[d]

[a] Values expressed in kK.

[b] Experimentally observed values.

[c] Calculated values taking $\beta = 7100\ cm^{-1}$.

[d] Calculated values taking $\beta = 6500\ cm^{-1}$.

References

1. D. S. Martin, Jr., R. M. Rush, R. F. Kroening, and P. E. Fanwick, Inorg. Chem., 12, 301 (1973).
2. K. Krogman, Angew. Chem. Internat. Ed., 8, 35 (1969).
3. T. W. Thomas and A. E. Underhill, Chem. Soc. Revs., 1, 99 (1972).
4. H. R. Zeller, Adv. Solid State Physics, 13, 31 (1973).
5. I. F. Shchegolev, Phys. Stat. Sol. (A), 12, 9 (1972).
6. H. Isci and W. R. Mason, Inorg. Chem., 13, 1175 (1974).
7. K. Kawakami, M. Haga, and T. Tanaka, J. Organometal Chem., 60, 363 (1973).
8. J. Chatt and L. M. Venanzi, J. Chem. Soc. (A), 4735 (1957).
9. W. P. Weber, G. W. Gokel, and I. K. Ugi, Angew Chem. Internat. Edit., 11, 530 (1972).
10. $[Rh(CNPh)_4]Cl$ has been prepared previously by reaction of $[Rh(CO)_2Cl]_2$ with CNPh (J. W. Dart, M. K. Lloyd, R. Mason, and J. A. McCleverty, J. Chem. Soc. Dalton, 2039 (1973)).
11. J. W. Dart, M. K. Lloyd, R. Mason, and J. A. McCleverty, J. Chem. Soc. Dalton, 2046 (1973).
12. G. W. Haupt, J. Opt. Soc. of Amer., 42, 441 (1952).
13. H. Isci and W. R. Mason, Inorg. Chem., 14, 913 (1975).
14. K. R. Mann, M. Cimolino, G. L. Geoffroy, G. S. Hammond, A. A. Orio, G. Albertin, and H. B. Gray, Inorg. Chim. Acta, 16, 97 (1976).

15. C. J. Ballhausen, N. Bjerrum, R. Dingle, K. Eriks, and C. R. Hare, Inorg. Chem., 4, 514 (1965).

16. G. L. Geoffroy, M. S. Wrighton, G. S. Hammond, and H. B. Gray, J. Amer. Chem. Soc., 96, 3105 (1974).

17. Solid samples of the PF_6^- and BPh_4^- salts of $[Rh(CNPh)_4]^+$ exhibit a single $\bar{\nu}(C\equiv N)$ ir absorption at 2150 cm^{-1}. A yellow CH_2Cl_2 solution of the PF_6^- salt which contains monomeric $[Rh(CNPh)_4]^+$, has $\bar{\nu}(C\equiv N)$ at 2160 cm^{-1}. Concentrated, blue solutions of the PF_6^- salt in acetonitrile also display a single $\bar{\nu}(C\equiv N)$ band at 2160 cm^{-1}. Neither the solids nor concentrated acetonitrile solutions exhibit any ir absorptions attributable to bridging isocyanides.

CHAPTER 3

THE PREPARATION, SPECTRAL PROPERTIES AND OXIDATIVE ADDITION REACTIONS OF A DIMERIC Rh(I) ISOCYANIDE COMPLEX $Rh_2(bridge)_4^{2+}$

Introduction

We have shown previously that cationic arylisocyanide complexes of rhodium(I) aggregate in solution through formulation of metal-metal bonds.[1] The chemical behavior of these oligomeric species should be quite interesting, as the opportunity for coupled electron transfer exists. In order to explore this possibility in a simple case, we have synthesized and characterized a dimeric Rh(I) complex containing four 1,3-diisocyanopropane (bridge) ligands. We have found that this dimer aggregates still further in solution to form higher oligomers, and that it undergoes two-center oxidative addition reactions with several substrates.

Experimental

$[Rh(COD)Cl]_2$ was synthesized by the method of Chatt, et al.[2] Solvents were spectrograde ($CHCl_3$, CH_3OH, CH_3CN).

1,3-diisocyanopropane, $C_5H_6N_2$, bridge. This ligand was synthesized using the method of Ugi, et al.,[3] and was purified by vacuum distillation. The PMR spectrum showed a complex multiplet at 3.68 δ and a broad peak at 1.98 δ which integrated in the ratio of 2:1. The infrared spectrum shows a very strong, narrow $\bar{\nu}$(CN) stretch at 2140 cm^{-1}. Other prominent peaks are located at 2930 m, 1660 m, and 1490 s.

$[Rh_2(bridge)_4]Cl_2$. This compound was obtained as a blue powder by adding a stoichiometric amount of bridge to a chloroform solution of $[Rh(COD)Cl]_2$.

$Rh_2(bridge)_4(BPh_4)_2 \cdot 2CH_3CN$. A stoichiometric amount of $NaBPh_4$ in methanol was added to a methanol solution of $Rh_2(bridge)_4Cl_2$. The purple solid was then recrystallized from acetonitrile. Calc: C, 66.37; H, 5.41; N, 10.75. Found: C, 65.59; H, 5.49; N, 10.24. $\bar{\nu}$(CN) 2172 cm^{-1} KBr pellet. PMR spectrum: broad singlets at 3.78 δ and 1.98 δ in 2:1 ratio in d^6DMSO. The peak due to acetonitrile was also observed.

$[Rh_2(bridge)_4I_2][I_3]_2$. Synthesis was accomplished by addition of I_2 to a warm acetonitrile solution of $Rh_2(bridge)_4(BPh_4)_2$. The product crystallized as red crystals on cooling. Calc: C, 15.0; H, 1.50; N, 7.05; I, 63.5. Found: C, 15.8; H, 1.65; N, 7.09; I, 62.2. $\bar{\nu}$(CN) 2227 cm^{-1} KBr pellet.

$[Rh_2(bridge)_4Br_2](Br_3)_3$. Synthesis was similar to I_2 adduct above. Cooling the solution gave yellow crystals. Calc: C, 19.67; H, 1.98; N, 9.17. Found: C, 19.97; H, 1.93; N, 9.06. $\bar{\nu}$(CN) 2230 cm^{-1} KBr pellet.

$[Rh_2(bridge)_4(CH_3)(I)](BPh_4)_2 \cdot 2CH_3CN$. A stoichiometric amount of CH_3I was added to a solution of $Rh_2(bridge)_4(BPh_4)_2 \cdot 2CH_3CN$ in acetonitrile. On slow addition of diethyl ether, reddish brown crystals were obtained. Calc: C, 60.66; H, 5.09; N, 9.69. Found: C, 58.74; H, 5.08; N, 9.29. $\bar{\nu}$(CN) 2183 and 2212 cm^{-1} (KBr pellet). PMR in d^6DMSO broad singlets at 4.08 δ (terminal CH_2), 2.18 δ (central CH_2), and a doublet at 1.38 δ (CH_3). Peaks were also observed for the acetonitrile protons and the tetraphenylborate protons.

Infrared spectra were obtained as KBr pellets on a Perkin-Elmer 225 spectrophotometer. Electronic absorption spectra were measured using a Cary 17 spectrophotometer. PMR spectra were recorded on a Varian A-60 spectrometer.

Absorption spectral data for different concentrations of $Rh_2(bridge)_4Cl_2$ were obtained in CH_3OH using a short pathlength cell calibrated[4] with CrO_4^{2-}.

Supplementary Data

Absorption at 555, 778 and 990 nm as a function of $Rh_2(bridge)_4Cl_2$ concentration in CH_3OH.

C	A_{555}	A_{778}	A_{990}
7.10 g/ℓ	35.97	81.75	79.40
2.84 g/ℓ	29.24	48.42	35.085
1.30 g/ℓ	18.01	15.90	7.02
1.04 g/ℓ	14.97	10.29	4.21
0.52 g/ℓ	9.82	2.34	0.58
0.13 g/ℓ	1.76	0	0

Results and Discussion

The chloride salt of the dimer, $[Rh_2(bridge)_4]Cl_2$, was obtained by addition of bridge to a stoichiometric amount of $[Rh(C_8H_{12})Cl]_2$ in chloroform solution. A blue precipitate was isolated and converted to a purple tetraphenylborate salt by metathesis in methanol. The BPh_4^- salt was recrystallized from acetonitrile. The infrared spectrum of a KBr pellet of the dimer exhibits one C≡N stretch at 2172 cm^{-1}. There are no bands in the IR attributable to bridging isocyanides. The

PMR spectrum of the dimer in DMSO displays broad singlets at 3.7 δ (terminal CH_2) and 1.9 δ (central CH_2). As steric considerations rule out bidentate coordination by bridge at a single Rh(I) center, we assume that the structure of $[Rh_2(bridge)_4]^{2+}$ is as shown in (I):

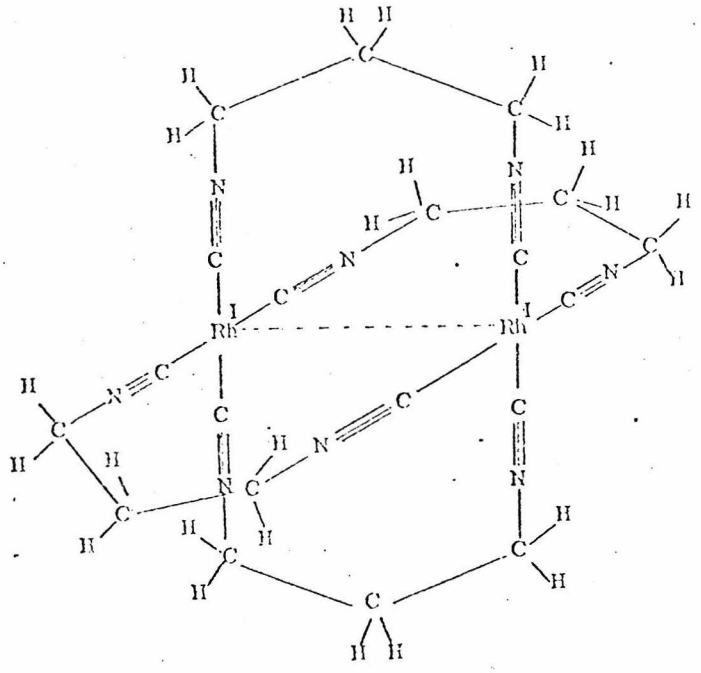

(I)

Electronic absorption spectra for three different concentrations of $[Rh_2(bridge)_4]Cl_2$ in methanol are shown in Figure 2. Absorptions at 318, 342, and 555 nm are the only bands observed at low concentrations of $[Rh_2(bridge)_4]Cl_2$, and are logically assigned to the dimer $[Rh_2(bridge)_4]^{2+}$, or D, itself. This assignment is supported by the

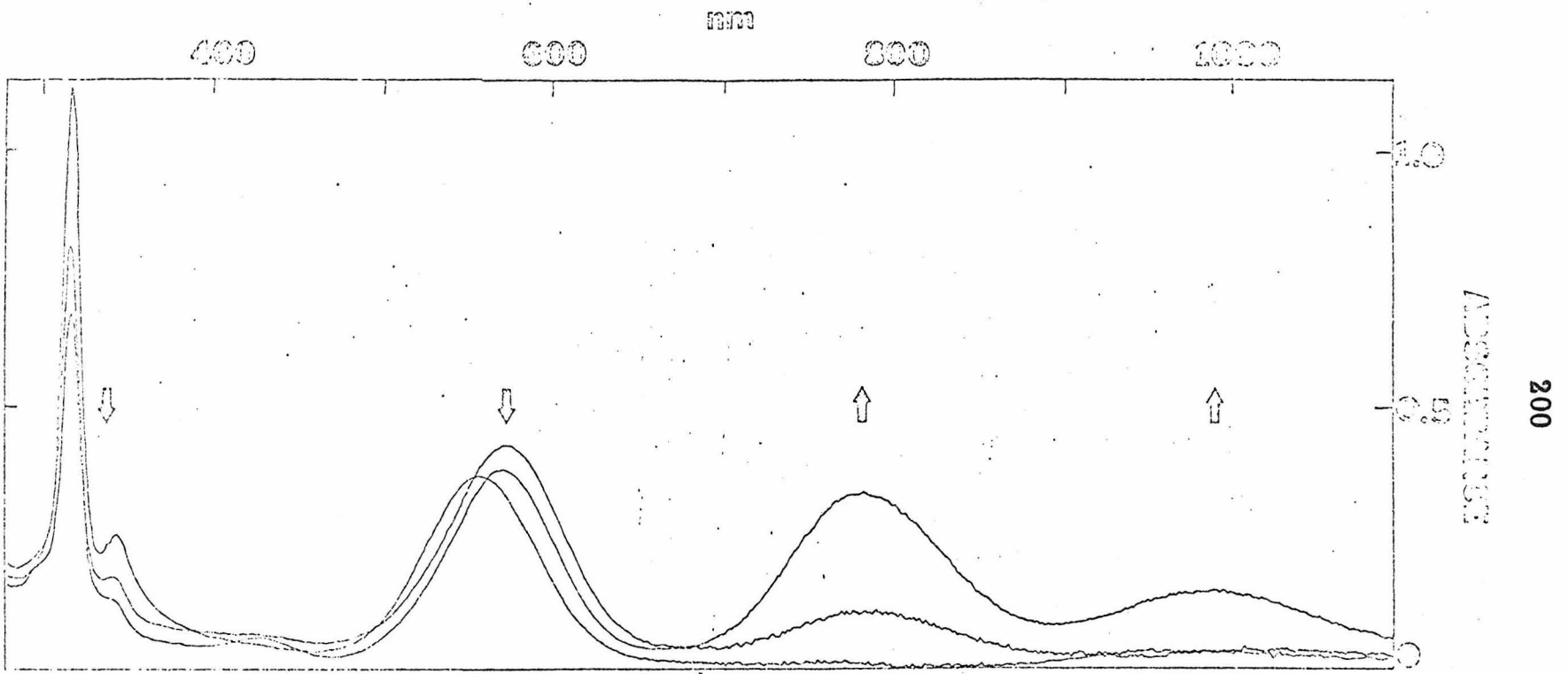

Figure 2. Absorption spectra of $Rh_2bridge_4Cl_2$ in methanol. Top curve C = 1.3 g/ℓ in 0.2 mm cell; middle curve 0.52 g/ℓ in 0.2 mm cell; bottom curve 0.13 g/ℓ ub 1 mm cell.

observation that absorptions owing to $[Rh(CNPh)_4]_2^{2+}$ and $Rh(CNPh)_4^+$ are reported, respectively, at 568 and 411 nm in acetonitrile solution.[1] As the solution becomes increasingly concentrated, principal low energy bands appear at 778, 990, 1140, and 1735 nm. The concentration dependence of the absorption spectra may be interpreted in terms of the following equilibria:

$$2D \overset{K_1}{\rightleftharpoons} D_2;\ D_2 + D \overset{K_2}{\rightleftharpoons} D_3;\ D_n + D \overset{K_n}{\rightleftharpoons} D_{n+1}$$

A plot of (A_{555}) vs. $\sqrt[2]{A_{778}}$ is a straight line, as is A_{555} vs. $\sqrt[3]{A_{990}}$, indicating that the bands at 778 and 990 nm be assigned to tetrameric and hexameric Rh(I) species. The bands at 1140 and 1735 nm are present only in the most concentrated solutions, and are logically attributable to higher oligomers ($n > 3$).

The observed spectroscopic behavior of the $[Rh_2(bridge)_4]^{2+}$ oligomers accords with simple MO theory (Figure 3). The 555 nm absorption may be assigned to the fully allowed $1a_{2u} \rightarrow 2a_{1g}$ transition, by analogy to the 568 nm band observed[1] in $[Rh(CNPh)_4]_2^{2+}$. Similar analysis of the tetrameric Rh(I) units suggests that the 778 nm bands be assigned to $2a_{2u} \rightarrow 3a_{1g}$, and the hexameric Rh(I) absorption at 990 nm be assigned to $3a_{2u} \rightarrow 4a_{1g}$. The band at 1140 nm is attributed to $4a_{2u} \rightarrow 5a_{1g}$ in an octameric species ($n = 4$).

The straight lines obtained for (A_{555}) vs. $\sqrt[2]{A_{778}}$ and (A_{555}) vs. $\sqrt[3]{A_{990}}$ (Figures 2 and 3) have slopes of 3.72 and 7.96, respectively, where the slope of the first line is equal to $\epsilon_{555}/\sqrt{K_1\epsilon_2}$ and the second equals $\epsilon_{555}/\sqrt[3]{K_1K_2\epsilon_3}$. ϵ_{555} is equal to 14,500 from measurements on dilute solutions of $Rh_2(bridge)_4BPh_4 \cdot 2CH_3CN$ in CH_3CN. Thus $K_1\epsilon_2 =$

1.52×10^7 and $K_1K_2\epsilon_3 = 6.04 \times 10^9$. Assuming reasonable values for ϵ_2 (29,000) and ϵ_3 (43,500) gives $K_1 = 524\ M^{-1}$ and $K_2 = 265\ M^{-1}$. These estimated values for ϵ_2 and ϵ_3 are reasonable since work on other similar systems[1,5] show that the extinction coefficient for the lowest band in the dimer is approximately the sum of the extinction coefficients for the monomers.

Because of the empirical nature of this approximation, these values should be viewed with caution. However, they are probably within ± 50% of the correct values. The equilibrium constants are also similar to those found in other Rh(I) systems where they have been measured.[6]

According to simple Hückel theory, the tetramer, hexamer, and actamer transition energies are given by: $E_{D_2} = E_D + \beta$; $E_{D_3} = E_D + \sqrt{2\beta}$; $E_{D_4} = E_D + \sqrt{5+1}/2$; $E_D = E(1a_{2u} \rightarrow 2a_{1g})$ and $\beta = \beta_1 a_{2u} + \beta_2 a_{1g}$. Theory and experiment accord closely for $\beta = 550\ cm^{-1}$: E_{D_2} (calcd) = 12,500, E_{D_2} (obsd) = 12,820; E_{D_3} (calcd) = 10,220, E_{D_3} (obsd) = 10, 080, E_{D_4} (calcd) = 9100, E_{D_4} (obsd) = 8770 cm^{-1}. The broad absorption system centered at about 1735 nm (5760 cm^{-1}) probably represents overlapping bands owing to oligomers with $n > 4$. For $N = \infty$, the calculated limit is $E_D + 2\beta$, or 7000 cm^{-1}.

The β internal (β between the two Rh atoms of the dimer) can be calculated from $E_D = E_M + \beta_{int}$, where E_M can be estimated from the monomer transition in $Rh(CNi\text{-}propyl)_4^+$ ($E_M = 26,100\ cm^{-1}$).[6] Since $E_D = 18,000\ cm^{-1}$, $\beta_{int} = 8100\ cm^{-1}$. Comparing this value

with the β between dimers (5500 cm^{-1}) suggests that the Rh atom interaction is stronger in the dimer unit than that between the units.

Oxidative Addition Reactions

Upon addition of I_2 to dilute acetonitrile solutions of $[Rh_2(bridge)_4](BPh_4)_2$, oxidation to a diiodo adduct, $[Rh_2(bridge)_4I_2]^{2+}$, takes place immediately. The product was isolated as a red triiodide salt. This oxidative addition product presumably contains two Rh(II)-I units connected by a single metal-metal bond. In terms of the MO formulation of the metal-metal interaction in $[Rh_2(bridge)_4]^{2+}$, the two electrons in the $1a_{2u}$ orbital are transferred to the two I atoms to give two I^- groups and a Rh(II)-Rh(II) bond $(1a_{1g})^2$. The infrared spectrum of a KBr pellet of $[Rh_2(bridge)_4I_2](I_3)_2$ exhibits a single C≡N stretching frequency at 2227 cm^{-1}, indicating trans I-Rh(II)-Rh(II)-(I) stereochemistry, as would be expected. The higher C≡N frequency observed for $[Rh_2(bridge)_4I_2]^{2+}$ as compared to that for $[Rh_2(bridge)_4]^{2+}$ is consistent with the Rh(II) formulation of the diiodo adducts.

When the I_2 oxidation was performed at high concentrations of $[Rh_2(bridge)_4]^{2+}$, a green intermediate species was observed (λ_{max} = 626 nm). The concentration of this intermediate was maximal for the stoichiometric ratio $2[Rh_2(bridge)_4]^{2+}$: I_2. Furthermore, the concentration of the intermediate was found to be proportional to $[[Rh_2(bridge)_4]^{2+}]^2$. The green species is formulated as $[I\text{-}D\text{-}D\text{-}I]^{4+}$.

Similar chemistry was observed when Br_2 was used as the oxidant yielding $[Rh_2(bridge)_4Br_2](Br_3)_2$. Interestingly, the Br_2 oxidative addition is thermally reversible in either acetonitrile or DMF-water solutions, and is thermally reversible in either acetonitrile or DMF-water solutions, and blue $[Rh_2(bridge)_4]^{2+}$ may be recovered or may be reoxidized with the addition of further bromine. A green species similar to that observed for the I_2 oxidation was also observed (λ_{max} = 595 nm in DMF) but no concentration dependence data were obtained. Addition of methyl iodide to $[Rh_2(bridge)_4](BPh_4)_2$ in acetonitrile solution, yields a yellow solution containing trans-$[Rh_2(bridge)_4(CH_3)(I)]^{2+}$. The CH_3I adduct was isolated as reddish brown crystals of a tetraphenylborate salt by slow addition of diethyl ether. The infrared spectrum of the trans-$[Rh_2(bridge)_4(CH_3)(I)]^{2+}$ exhibits C≡N stretches at 2183, and 2212 cm^{-1}, which is consistent with the structural formulation The PMR spectrum of the adduct exhibits broad singlets at 4.0, 2.1, and 1.3 δ. As the resonance at 1.3 δ does not correspond to any feature in unoxidized $[Rh_2(bridge)_4]^{2+}$, it is therefore attributed to a methyl group bonded directly to rhodium. The observation of a 1-2 Hz splitting of the 1.3 δ resonance owing to coupling to the ^{103}Rh nucleus confirms the assignment. Integration of the spectrum indicates that the compound contains only one methyl group per dimer, which is consistent with the proposed trans-$[Rh_2(bridge)_4(CH_3)(I)]^{2+}$ structure.

The electronic absorption spectrum of $[Rh_2(bridge)_4I_2]^{2+}$ in acetonitrile solution exhibits intense bands at 465 (ϵ 23,200) and 397 nm (ϵ 62,000). The very intense 397 nm band is logically attributable to the $\sigma \rightarrow \sigma^*$ transition ($1a_{1g} \rightarrow 1a_{2u}$) in the Rh(II)-Rh(II) single-bonded species. Similarly intense $\sigma \rightarrow \sigma^*$ bands in this energy region have been observed[7] for $Mn_2(CO)_{10}$ as well as numerous other $\underline{d}^7$-$\underline{d}^7$ metal-metal bonded complexes. The band at 465 nm could be due to one or more $d\pi \rightarrow \sigma^*(1a_{2u})$ transitions, again by analogy to $Mn_2(CO)_{10}$. Intense bands at 438 and 373 nm in $[Rh_2(bridge)_4Br_2]^{2+}$ and 470 and 397 nm in $[Rh(bridge)_4(CH_3)(I)]^{2+}$ (acetonitrile solution) presumably represent the $d\pi \rightarrow \sigma^*$ and $\sigma \rightarrow \sigma^*$ transitions, respectively, in these adducts. It is reasonable to expect that the $1a_{1g}$ orbital will be delocalized to some extent over the X-Rh-Rh-X unit, and as a result the $1a_{1g} \rightarrow 1a_{2u}$ in the $[Rh_2(bridge)_4Br_2]^{2+}$ complex is consistent with the proposed fractional charge transfer character.

The mechanism of oxidative addition to $[Rh_2(bridge)_4]^{2+}$ is under study. We have found that the rate of C_2H_5I addition to $[Rh_2(bridge)_4]^{2+}$ is comparable to that of CH_3I, and that CH_3OTs reacts extremely slowly. We suspect from these results that the initial step involves Rh(I) attack on a heavy atom in the substrate, yielding $[Rh_2(bridge)_4I]^{2+}$ and methyl radical in the case of CH_3I.

References and Notes

1. K. R. Mann, J. G. Gordon, II, and H. B. Gray, J. Amer. Chem. Soc., 97, 3553 (1975).

2. J. Chatt and L. M. Venanzi, J. Chem. Soc., 4735 (1957).

3. I. Ugi, ed., "Isonitrile Chemistry," Academic Press, New York, 1971.

4. G. W. Hampt, J. Opt. Soc. of America, 42, 441 (1952).

5. H. Isci and W. R. Mason, Inorg. Chem., 13, 1175 (1974).

6. This thesis, Chapter 2.

7. R. A. Levenson and H. B. Gray, J. Amer. Chem. Soc., 97, 6042 (1975).

8. Complexes of the type $[Rh_2(CNR)_2X_2]^{2+}$ obtained by mixing solutions of $[Rh(CNR)_4]^+$ and trans-$[Rh(CNR)_4X_2]^+$ (R = alkyl; X = halide) have been reported [A. L. Balch and M. M. Olmstead, J. Amer. Chem. Soc., 98, 2354 (1976)]. These adducts exhibit electronic spectral properties that are very similar to those of analogous $[Rh_2(bridge)_4X_2]^{2+}$ complexes. Of the two structures for $[Rh_2(CNR)_8X_2]^{2+}$ species suggested by Balch and Olmstead our results favor the one containing a direct Rh(II)-Rh(II) bond in preference to the Rh-X-Rh-X alignment. Balch and Olmstead also argued that their spectral data were more consistent with a Rh(II)-Rh(II) bonded species.